

**MULTI-AGENT SOURCE LOCALIZATION USING
PASSIVE SENSING**

MANSOOR SHAUKAT

*(B.E.), (M.S.), National University of Sciences & Technology
(NUST), Pakistan*

**A THESIS SUBMITTED FOR THE DEGREE OF DOCTOR OF
PHILOSOPHY**

**NUS GRADUATE SCHOOL FOR INTEGRATIVE SCIENCES &
ENGINEERING**

NATIONAL UNIVERSITY OF SINGAPORE

2015

DECLARATION

I hereby declare that this thesis is my original work and it has been written by me in its entirety. I have duly acknowledged all the sources of information which have been used in the thesis.

This thesis has also not been submitted for any degree in any university previously.

Mansoor Shaukat

22nd December 2015

ACKNOWLEDGEMENTS

In the name of Allah, the most beneficent, the most merciful.

I want to express my profound gratitude to the people who helped me complete my dissertation either technically, financially and/or emotionally. First, I would like to thank my advisor, Dr. Mandar Chitre who contributed significantly on all accounts. His guidance, patience, encouragement, easy accessibility and in-depth critical reviews helped me grow as an objective researcher.

I would also like to thank my co-supervisor, Prof. Ong Sim Heng, thesis advisory committee members, Prof. T. H. Lee and Prof. Marcelo H. Ang. Jr. for their precious suggestions and guidance throughout the tenure of my PhD.

I would also like to thank NUS Graduate School for Integrative Sciences and Engineering (NGS) and Acoustics Research Laboratory (ARL) for supporting my research work. In NGS, I would especially like to thank the Deputy Director, Prof. Tang Bor Luen for his guidance in multiple academic modules as an instructor. His mentorship was invaluable in helping me become a better researcher. Also, I would like to thank Ms. Chuan Irene Christina who always helped me patiently with sorting out my research-related reimbursement claims. In ARL, I would like to thank my dear friends Dr. Ahmed Mahmood and Mr. Prasad Anjangi for reviewing and proofreading my work along with random discussions as an antidote for boredom. Also, I am thankful to Mr. Tan Yew Teck, Mr. Ashish Raste, Dr. Hari Vishnu, Mr. Koay Teongbeng, Ms. Soo Peing, Dr. Bharath Kalyan, Mr. Harold Tay, Ms. Ong Lee Lin, Mr. Alex Kee, Mr. Mohan Panayamadam and Mr. Sivaraman Selvakumar for their support.

I would also like to thank my dear friends from NUS, Mr. Shahzor Ahmed, Dr. Qasim Mahmood, Ms. Saima Owais, Dr. Nick Bogard, Dr. Syed Rizwan Ahmed, Dr. Costas Pelekanakis, Mr. Kwok Jie Ming Jeremy, Mr. Kenry and Mr. Chengyao Shen for their moral support and fantastic time during the tenure of my PhD.

Lastly, I would like to end the acknowledgements by dedicating this dissertation to the people without whom none of this would have been possible. My late father who believed in me, my loving mother who lead a lonely life back home without ever complaining, my beautiful wife who sacrificed her career and moved to Singapore to support me, my lovely son whose never ending questions about sharks and dinosaurs got me going, my awesome sister who was always there to amuse me with her silly jokes and finally, my ever supportive in-laws.

Contents

Abstract	x
List of Acronyms & Abbreviations	xvii
List of Notation	xviii
1 Introduction	1
1.1 Motivation	1
1.1.1 Bio-inspiration	1
1.1.2 Explicit Communication vs. Implicit Communication . . .	2
1.1.3 Limitations of Explicit Communication	2
1.1.4 Implicit Communication: Stigmergy vs. Passive Sensing .	3
1.1.5 Instantaneous vs. Temporal Sampling for Gradient Sensing	4
1.1.6 Ambient Noise	4
1.1.7 Team Size	5
1.1.8 Robustness & Scalability	5
1.2 Research Scope	6
1.3 Related Work	6
1.3.1 Designing Collective Behaviour	6
1.3.2 Individualistic Behaviours	7
1.3.3 Social Behaviours	9
1.3.4 Social Behaviours using Passive Sensing	10
1.4 Thesis Outline & Research Contributions	11
2 Social Behaviours based on Passive Sensing of Neighbours	16
2.1 Background	16
2.2 Conventional Social Behaviours	17
2.2.1 Unit Vector based Long-Range Attraction and Short-Range Repulsion	18
2.2.2 Centroid based Long-Range Attraction and Short-Range Repulsion	19
2.2.3 The Neighbour Alignment	20
2.2.4 Fusion of Social Behaviours	20
2.3 Practicalities of the Long-range Attraction	20

2.4	Practicalities of the Short-range Repulsion	22
2.5	Practicalities of the Neighbour Alignment	22
2.6	The Alternative: Passive Sensing based Social Behaviours	24
2.7	Practicalities of the Passive Sensing Model	25
3	Problem Statement & Experimental Setup	28
3.1	Problem Statement	28
3.2	Simulation Setup	30
3.2.1	Sound Propagation	32
3.2.2	Evolutionary Optimization	33
3.2.3	Robustness Analysis	35
4	Static Temporal Sampling based Multi-Agent Source Localization	37
4.1	Background	37
4.2	Bio-CAST	38
4.2.1	Individualistic Behaviour: Target Drive	39
4.2.2	Group Cohesion	39
4.2.3	Collision Avoidance	41
4.2.4	Resultant Bio-CAST	42
4.3	Optimization Results	42
4.3.1	Arrival Time Optimization and Initialization Distance	44
4.3.2	Arrival Time Optimization and Limited Attraction Neighbourhood	47
4.3.3	Estimated Optimized Bio-CAST	52
4.4	Robustness Analysis	55
4.4.1	Arrival Time Performance	56
4.4.2	Trajectories and Expanse	57
4.4.3	Absence of Source	60
4.4.4	Neighbour-majority Detection Sensitivity	61
4.4.5	Initialization Distance Sensitivity	63
4.4.6	Agent Loss	63
4.4.7	Real-robot Analysis	65
4.4.8	Passive Sensing vs. Explicit Communication	67
4.5	Conclusion	68
5	Adaptive Temporal Sampling based Multi-Agent Source Localization	71
5.1	Background	71
5.2	Optimization Setup	72

5.3	Intensity based Adaptation	73
5.3.1	Optimized Shape for IbA	74
5.3.2	IbA-EXP Optimization for Infinite Attraction Radius	75
5.3.3	Optimization Results for Limited Attraction Radius	80
5.3.4	Estimated Optimized Behaviour for Individualistic Teams	85
5.3.5	Robustness Analysis	85
5.4	Connectivity based Adaptation	87
5.4.1	Optimization Results	89
5.4.2	Robustness Analysis	89
5.4.3	Passive Sensing vs. Explicit Communication	95
5.5	Conclusion	97
6	Adaptive Behaviours in Multi-Agent Source Localization	100
6.1	Background	100
6.2	Adaptive Cohesion based Localization Algorithm	101
6.2.1	Group Cohesion (GC)	101
6.2.2	Collision Avoidance (CA)	101
6.2.3	Adaptive Cohesion	101
6.2.4	Temporal Sampling	103
6.3	Optimization Results	103
6.3.1	Optimization for Infinite Attraction Radius	103
6.3.2	Optimization for Limited Attraction Radius	104
6.4	Robustness Analysis	107
6.4.1	Multipath Interference	109
6.4.2	Initialization Distance Sensitivity	111
6.4.3	Loss of Source Signal	113
6.4.4	Neighbour Detection Noise	114
6.4.5	Passive Sensing vs. Explicit Communication	115
6.5	Comparative Analysis	117
6.5.1	Emergent Source Localization Through Speed Variation	117
6.5.2	Speed Variation with a Self-sufficient Individualistic Behaviour	118
6.5.3	Bio-CAST	119
6.6	Conclusion	120
7	Conclusion & Future Research	123
7.1	Conclusion	123

7.2	Future Research	125
Appendix A Implementation Details		128
A.1	Sound Propagation Model	128
A.2	Evolutionary Optimization	129
A.3	Consistency Analysis for Number of Simulation Runs	131
Appendix B Supplementary Figures		134
B.1	Optimization Data for Varying Initialization Distances	134
Bibliography		140

Abstract

Purposeful collective behaviour in multi-agent systems can be achieved from a mix of simple individualistic and social behaviours of an agent. Social behaviours are the basis of cooperation in multi-agent systems and are fundamental in achieving collective behaviour. Practical implementation of conventional social behaviour models require explicit inter-agent communication, whereas in some environments, communication bandwidth and delays are critical constraints which may compromise the intended collective behaviour. This thesis introduces three source localization algorithms. Each algorithm is a set of individualistic and social behaviours, which do not require explicit inter-agent communication and rely solely on agent's passive sensing.

The first source localization algorithm is composed of static individualistic and social behaviours. The individualistic behaviour is inspired from a bacterium's random walk while performing chemotaxis and is self-sufficient in localizing sources of interest. Self sufficiency means that an agent can localize a source on its own using only its individualistic behaviour without any team cooperation via its social behaviours. However, better localization performance can be achieved when an agent uses an optimized weighted average of both individualistic and social behaviours. The social behaviours are inspired from the long-range attraction and the short-range repulsion behaviours of a fish. The second source localization algorithm assumes an adaptive individualistic

behaviour while keeping the social behaviours static. Finally, the third source localization algorithm is based on adaptive social behaviours without a self-sufficient individualistic behaviour and source localization is achieved as an emergent property of the social interactions between agents.

The agent behaviours for each source localization algorithm have been optimized using a Genetic Algorithm. Small homogeneous multi-robot systems are considered where neither the position information of the agents nor the position information of the source is available. An agent is assumed to have a single sensor to sense the source intensity and hence conducts temporal sensing to sense the gradient. For social interaction, an agent is assumed to have two sensors to detect the neighbour-majority either in its right or left sensing half. The behavioural optimization is carried out for a realistic underwater acoustic source in a range of initialization distances, neighbourhood radii and team sizes. The optimization data has been estimated by an analytical model for each localization algorithm. The performance of the collective behaviour resulting from the estimated model has been validated against agent's sensor and actuator noise along with strong multi-path interference due to variability of the environment.

Given the constraints of temporal sensing and loss of information due to noisy and simplistic passive sensing, the collective behaviours show remarkable robustness and scalability in terms of mean, median and variance of the arrival time distributions. Investigation of the team expanse in strong multi-path interference shows that team remains cohesive with minimal or no agent loss during the localization mission.

List of Tables

3.1	Symbols, Description and explored values of the mission variables in simulation.	31
4.1	Explored values of the parameters during the optimization process	44
5.1	Explored values of the parameters during the optimization process	77
5.2	Parameter and Root Mean Square Error (RMSE) values for respective equations	78
6.1	Explored values of the parameters during the optimization process	104
6.2	Parameter and Root Mean Square Error (RMSE) values for respective equations	105

List of Figures

2.1	Zonal model of fish interaction	18
2.2	Zones and behaviour models for Explicit Communication vs. Passive Sensing	24
3.1	A small team of four Swarmbots at Pandan Reservoir	29
3.2	Noise corrupted source-intensity spatial profile	33
3.3	A realization of the noise-corrupted spatial intensity levels	33
4.1	TD, GC and CA behaviours for Passive Sensing based Bio-CAST	40
4.2	Block diagram of Bio-CAST	43
4.3	Optimization results for varying initialization distances	45
4.4	Optimized uncertainty in decision making for varying initialization distances	47
4.5	Optimization results for varying attraction radii	48
4.6	Arrival time performance for initialization distance, r_0 of 1000 m and varying uncertainty in correction angle, σ_{θ_c}	51
4.7	The arrival time performance shown for initialization distance, r_0 of 1400 m and varying uncertainty in correction angle, σ_{θ_c}	51
4.8	Estimating optimized sampling time for infinite attraction radius	53
4.9	Estimating optimized parameters as function of the attraction radius	56
4.10	Comparative arrival performance for: (a) $\sigma = 1$ dB. (b) $\sigma = 6$ dB.	57
4.11	Trajectory of a random agent and the centroid of the team in varying noise conditions	58
4.12	Team expanse	59
4.13	Trajectories of all the agents over a time interval of 12h	61

4.14	Comparative arrival time performance for noiseless and noisy passive sensing of the neighbour-majority	62
4.15	Comparative arrival time performance for increasing initialization distances with optimized solution for 1000 m	64
4.16	The arrival time performance shown for initialization distance, r_0 of 1000 m and $\sigma = 1$ dB	65
4.17	Trajectories of 4 Swarmbots initialized 200 m away from the source	66
4.18	Comparative arrival time performance for passive sensing (PS) vs. explicit communication (EC) based social behaviours	68
5.1	Optimization results for IbA-NS	74
5.2	Estimated optimized shape for adaptive temporal sampling function	76
5.3	IbA-EXP Optimization for infinite attraction radius and varying initialization distances	77
5.4	IbA-EXP Optimization for limited attraction radius as a function of initialization distance, $r_0 = 1000$ m	81
5.5	Estimation of optimized adaptive sampling function and behaviour of optimized SD of correction angle	83
5.6	Estimation for optimized values of normalized adaptive sampling coefficient	84
5.7	Arrival time performance	86
5.8	Team expanse	87
5.9	Arrival time performance for CbA compensated IbA (IbA+CbA) vs. IbA arrival time performance for limited attraction radii	90
5.10	Arrival time performance for CbA compensated IbA (IbA+CbA) vs. SS arrival time performance for limited attraction radii	92
5.11	Expanse for CbA compensated IbA (IbA+CbA) during a localization mission for $N = 20$, varying attraction radii and noise levels	93
5.12	Number of agents breaking away from a team during a localization mission for $N = 20$, varying attraction radii and noise levels	94

5.13	Initialization distance sensitivity analysis for optimized solution for $r_0 = 1000$ m and $r_{GC} = 0.3r_0$	95
5.14	Neighbour majority detection sensitivity analysis for IbA+CbA with varying attraction radii as a function of r_0 and detection probability p where $r_0 = 1000$ m	96
5.15	Passive Sensing (PS) versus Explicit Communication (EC) implementation of IbA+CbA, $r_0 = 1000$ m	97
6.1	Optimization results for infinite attraction radius and varying initialization distances and team sizes	105
6.2	Estimation for optimized adaptive cohesion coefficient and the optimized adaptive sampling coefficient for infinite attraction radius	106
6.3	Optimization for limited attraction radius	108
6.4	Optimized CbA regulation for a team size of 10 agents and various limited attraction radii	109
6.5	Estimate for critical number of agents in limited attraction radii and associated mean arrival times	110
6.6	Arrival time performance for varying levels of ambient noise for the analytical model estimated for the optimized ACLA.	111
6.7	Failure rate analysis for ACLA for different attraction radii	112
6.8	Initialization distance sensitivity analysis for optimized solution for $r_0 = 1000$ m and $r_{GC} = 0.6r_0$ and noise levels: (a) $\sigma = 1$ dB. (b) $\sigma = 6$ dB.	113
6.9	Comparative team expanse for source signal vs. loss of source signal for $r_0 = 1000$ m and $r_{GC} = 0.6r_0$	114
6.10	Neighbour detection noise analysis for optimized solution for $r_0 = 1000$ m and $r_{GC} = 0.6r_0$ and noise levels: (a) $\sigma = 1$ dB. (b) $\sigma = 6$ dB.	115
6.11	Passive Sensing (PS) versus Explicit Communication (EC) implementation of ACLA with varying attraction radii as a function of initialization distance, $r_0 = 1000$ m	116
6.12	Mean arrival time comparison for ACLA vs. Bio-CAST for varying attraction radii and noise levels	120

A.1	Structure of the Evolutionary Algorithm	131
A.2	Vargha-Delaney's A-test for pair-wise stochastic equality	133
B.1	Optimization results for initialization distance, r_0 of 1400 m and varying attraction neighbourhood radii, r_{GC}	135
B.2	Optimization results for initialization distance, r_0 of 1200 m and varying attraction neighbourhood radii, r_{GC}	136
B.3	Optimization results for initialization distance, r_0 of 1000 m and varying attraction neighbourhood radii, r_{GC}	137
B.4	Optimization results for initialization distance, r_0 of 800 m and varying attraction neighbourhood radii, r_{GC}	138
B.5	Optimization results for initialization distance, r_0 of 600 m and varying attraction neighbourhood radii, r_{GC}	139

List of Acronyms & Abbreviations

SD	Standard Deviation
AUV	Autonomous Underwater Vehicle
UAV	Unmanned Aerial Vehicle
UGV	Unmanned Ground Vehicle
Bio-CAST	Bio-inspired Control Algorithm for Small Teams
TD	Target Drive module
GC	Group Cohesion module
CA	Collision Avoidance module
O	Orientation or Neighbour Alignment module
SS	Static temporal Sampling
IbA	Intensity based Adaptation
NS	Negative Sigmoid
EXP	Exponential
CbA	Connectivity based Adaptation
ACLA	Adaptive Cohesion based Localization Algorithm

List of Notation

$:=$	defined as
\leftarrow	replaced or substituted as
\approx	approximately equal to
\sim	distributed by
\diamond	Hadamard product of two vectors
\setminus	set difference
\mathbb{R}	set of real numbers
\mathbb{R}^N	set of N -tuples such that each element lies in \mathbb{R}
\mathbb{R}^+	set of positive real numbers
\mathbb{Z}	set of integers
\mathbb{Z}^+	set of positive integers
$\mathcal{N}(a, b^2)$	Normal distribution with mean a and standard deviation b
$\mathcal{U}(a, b)$	Uniform distribution with minimum value, a and maximum value, b
$\ \mathbf{x}\ $	L_2 norm of the vector \mathbf{x}
$\angle \mathbf{x}$	the phase of \mathbf{x} , i.e., $\angle \mathbf{x} = \tan^{-1}(\Im\{\mathbf{x}\}/\Re\{\mathbf{x}\})$
$\exp(x)$	exponential of x
$\text{sgn}(x)$	sign of x
$\log_{10}(x)$	logarithm of x to the base 10
\dot{x}	rate of change of x with respect to time

Chapter 1

Introduction

1.1 Motivation

Multi-agent systems have seen significant application in various fields of engineering [1–5]. In robotics, researchers have formulated multi-agent strategies for platforms such as Unmanned Aerial Vehicles (UAVs), Autonomous Underwater Vehicles (AUVs) and Unmanned Ground Vehicles (UGVs) [6–9]. Using such multi-robot platforms, efficiency of conducting search missions in large search spaces can be enhanced [10, 11]. An example of an extremely large search space is the Earth’s oceans, covering 71 % of the Earth’s surface; 95 % of which is still unexplored [12]. The recent events of aircraft crashes in the sea [13], algal blooms in water bodies [14] and oil spills undersea [15] have further underscored the importance of developing a large scale multi-robot system which can cooperatively localize sources of interest in real world. However, no such systems exist outside the laboratory environment [16].

1.1.1 Bio-inspiration

A large contribution to the literature on physical multi-agent systems is biologically inspired [17–19] from the collective behaviour in nature [20, 21]. Collective behaviour results from local and simple agent behaviours. The agent behaviours may either be individualistic or social. Individualistic

behaviours mean rules of agent's interaction with its environment, whereas social behaviours mean rules of agent's interaction with its neighbours. The field of robotics that studies the design of such interactions which can result in a desired collective behaviour is called swarm robotics [22]. In swarm robotics, foraging has been the main testbed application [16]. It has been used for investigating navigational behaviours such as collective exploration [23], collective transport [24] and collective decision making [25]. Source localization can be thought of as a subproblem of foraging where it benefits from collective exploration and collective decision making behaviours.

1.1.2 Explicit Communication vs. Implicit Communication

Any cooperative task requires some kind of information transfer which depends on the modality of a communication infrastructure, i.e., explicit or implicit [26]. Explicit-communication is defined as a deliberate act of invoking the signal transmission, whereas in implicit communication there is no such deliberate attempt [26, 27]. For example, an AUV sending out its position estimate in form of a data packet to another AUV is considered as an act of explicit-communication, whereas an AUV trying to estimate the position of its neighbour by analysing the neighbour's thruster noise is a form of implicit communication.

1.1.3 Limitations of Explicit Communication

Performance of explicit communication based strategies suffer substantially in environments with severely limited communication bandwidth and delays, e.g., undersea environments [28, 29]. In the range of hundreds of meters, undersea communication is restricted to the use of acoustic waves

[30]. Issues like propagation delay, time varying multi-path fading and frequency-dependent path-loss make the design of an acoustic communication system more complicated than the ground-based or airborne communication systems [31]. These phenomena also limit a team's capability to benefit from an effective distributed inter-agent communication [32]. Since the early days of swarm robotics, researchers have been interested in designing collective behaviour through implicit communication [33,34] and comparing the relative performance degradation to that of an explicit communication strategy [35,36]. However, it has been shown in [26] that a certain minimal communication pertaining to an agent's state is sufficient and more elaborate communication may not result in a significantly more efficient system. Nevertheless, if a purely implicit communication based approach is reasonably efficient for a particular task then having a minimal explicit communication based scheme may help improve the efficiency further. In cases where explicit-communication would fail, a system with an effective implicit-communication scheme will gracefully degrade in performance, avoiding a complete breakdown.

1.1.4 Implicit Communication: Stigmergy vs. Passive Sensing

Implicit communication can itself be classified into two types. The first one is stigmergy [37], referred to as *interaction via environment* [38] where the information is acquired through memory of the environment. Pheromone-trail deposition based collective behaviour of ants and termites has been a major inspiration in designing stigmergic multi-agent systems [39–41]. The other implicit communication approach is based on the interaction of an agent with its neighbours without using environment's memory, referred to as *interaction via sensing* [38]. In this thesis, we simply refer to agents using

implicit communication without stigmergy to interact with each other as social behaviours based on passive sensing. All the source localization strategies proposed in this thesis assume the same constraint on social behaviours. This limitation has been put in place because actively leaving a pheromone-like trail or modifying the environment so that other agents can use cues from the environment memory may not be desirable or even possible in many real world localization problems.

1.1.5 Instantaneous vs. Temporal Sampling for Gradient Sensing

Most of the source localization studies assume multiple sensors per agent for gradient detection [42]– [44]. However, the ability to sense the gradient instantaneously using multiple sensors is subject to the available intensity variations over the body length of an agent and the sensor or ambient noise levels. The *size-problem* discussed for the case of a bacterium performing chemotaxis in [45] relates well with a miniature agent sensing a gradient in real world. In case, an agent cannot detect the gradient instantaneously or is only equipped with one sensor, it resorts to temporal sampling to sense the gradient [46].

1.1.6 Ambient Noise

In most real world scenarios, instantaneous intensity values of the source are corrupted with high levels of ambient noise [47]. Especially in underwater environments, multipath constructive and destructive interference due to variability of the environment makes gradient sensing a hard problem to solve [30]. The phenomenon makes multiple sensor based instantaneous gradient

sensing almost impossible to achieve and underscores the need to have an efficient temporal sampling approach for a cooperative multi-agent system.

1.1.7 Team Size

Though there are examples of a massive swarm of real robots [48], their purpose is to support the collective behaviour research in a lab environment [49, p. 1302–1303]. There are no known examples of robotic swarms solving a real world problem [16, p. 31], mainly owing to the cost of fabricating a massive swarm of agents which have viable mission endurance for a real world problem. Hence from a practical standpoint and considering current state-of-the-art, it is important to investigate algorithms that can invoke collective behaviour in small multi-agent systems which is both robust and scalable.

1.1.8 Robustness & Scalability

Robustness and scalability are the most important desirable characteristics of a swarm robotic system. It is important to properly define both these terms owing to their extensive use in the following discussion in this thesis. Let us follow the definitions put forth by Erol Şahin in [22]:

Robustness: The property of a swarm robotic system where it is able to continue to operate, although at a lower performance, despite agent failures or ambient noise.

Scalability: The property of a swarm robotic system where it should be able to operate in a wide range of team sizes, i.e., the operation of the swarm should not be disturbed by change in the team size.

1.2 Research Scope

The scope of this thesis is to design simple source localization algorithms, i.e., a set of agent behaviours or interaction rules, that can invoke robust and scalable collective behaviours for multi-agent systems. Each source localization algorithm assumes constraints of temporal sampling for gradient sensing and social behaviours based on passive sensing.

1.3 Related Work

Nature has been a predominant source of inspiration for artificial multi-agent systems or swarm robotic systems [22,50], resulting in a significant number of bio-inspired contributions to the source localization problem [51–54].

1.3.1 Designing Collective Behaviour

In nature, complex collective behaviours emerge from agent's individualistic and social behaviours which are mostly based on some form of implicit communication [20]. Simple behaviours mean smaller, simpler and cheaper entities [38]. The challenge is to design the individualistic and social behaviours so that a desired collective behaviour emerges from them. The problem of source localization can be solved cooperatively by having a mix of individualistic and social behaviours [54]. An individualistic behaviour may either be self-sufficient to achieve the source localization such as a moth's casting behaviour [55] or it may not be, e.g., an agent changing its speed as a function of instantaneous intensity [56].

1.3.2 Individualistic Behaviours

1.3.2.1 *Random Walks*

Random walks are commonly used individualistic behaviours used in artificial multi-agent systems [57, 58]. Individualistic behaviours like Lévy walk and correlated random walk have long been representative of foraging patterns of many animal species [59, 60] and hence become a natural source of inspiration. However the application of random walk models for source localization is limited to a small and constrained search space where source intensities are unavailable or hard to detect. For a large and unconstrained search space where source intensity can be sensed, a biased random walk is a better alternative.

1.3.2.2 *Biased Random Walks*

There are many biased random walk implementations in the domain of chemical source localization [61, 62] where the researchers have designed behaviours inspired by a male moth finding a female moth via its pheromone trail [55]. The male moth travels upwind to localize a chemical source where the search space can span tens of meters [63]. Rapid upwind surge lasts for a short period of time (about four-tenths of a second) followed by a casting behaviour which lasts for a longer period of time (about four seconds) [64]. The casting behaviour refers to the turning back and forth behaviour of the moth perpendicular to the wind direction especially when it loses contact with the plume [65]. A similar behaviour is shown by the dung beetle, *Geotrupes stercorarius*, while searching for fresh cow pats [66]. Many biologically inspired chemotaxis implementations on robotic platforms exist in the literature, a

comprehensive review of which has been given in [67] and [44]. However, the implementations inspired from the casting behaviour assume two or more sensors per agent to localize the source.

Similarly, Valentine Braitenberg gave the idea of six very simple sensorimotor connections [68] that resulted in different agent responses towards the source such as attraction, repulsion and speed variability. As far as the proposed self-sufficient source localization behaviour is concerned, it localizes the sources by varying the speed of the left and the right motors driving the agent. However, this and similar other strategies [69, 70] assume more than one sensor per agent.

1.3.2.3 *E.coli's Temporal Sampling*

As we discussed, most of the source localization studies assume multiple sensors per agent for gradient sensing. The robotic implementations of a single sensor based gradient detection are generally inspired from the biased random walk of a bacterium, *Escherichia coli*, performing chemotaxis [67, 71, 72]. The bacterium has multiple chemoreceptors over its body, however, insignificant difference between concentration levels over its body length keeps it from instantaneous gradient sensing [45]. Hence, it resorts to temporal sampling to sense the gradient [46, 73]. The bacterium swims in a straight path interrupted by abrupt random turns at constant intervals [74, p. 225]. Increasing concentrations result in decreased frequency of abrupt turns and decreasing concentrations result in increased frequency, i.e., if a bacterium detects increasing concentrations then it swims relatively straight and takes random turns otherwise. A similar behaviour-based biased random walk was used to localize an underwater acoustic source [54, 75, 76]. However,

the randomness in the walk was because of the sensing noise and an agent's turn was deterministic – contrary to the bacterium model [77]. Since many bio-inspired robotic implementations use the bacterium's biased random walk model [67,71,72], it is worthwhile to investigate the role of randomness in an agent's turning decision. This thesis assumes a general biased random walk model inspired from *Escherichia coli* as an agent's individualistic behaviour, incorporating both the randomness from the agent's sensor noise as well as the randomness in its turns. It is interesting to note that the optimization data in Chapter 4 and Chapter 5 shows that randomness in an agent's decision making is not always the best strategy – especially in cooperative teams.

1.3.3 Social Behaviours

Many of the cooperative multi-agent approaches include an individualistic behaviour in addition to one or more social behaviours to invoke collective behaviour. For example, a modified version of Lévy Walk (LW) has been implemented for a team of miniature Autonomous Underwater Vehicles (AUVs) localizing multiple targets within a small search space ($8 \times 8 \times 1.5$ meters) [78]. In this research, a part of the CoCoRo project [79], the authors fuse an individualistic random walk model with a social firefly attraction behaviour that helps the AUVs to aggregate at the targets of interest. The aggregation is achieved by employing explicit communication between agents within a local neighbourhood where the exchange of information becomes the basis of a collective behaviour.

Similarly, school-of-fish social behaviours, i.e., short-range repulsion and long-range attraction [80] have been fused with a biased random walk to localize an underwater acoustic source using a team of AUVs [54]. Explicit

inter-agent communication of the position data was used to invoke cooperation in a small multi-agent system.

As far as the temporal sampling based multi-agent implementations are concerned, they either require centralized [81] or decentralized explicit inter-agent communication [54,82]. Most of the multi-agent source localization approaches, irrespective of the what individualistic model they use, are either scaled versions of the individualistic behaviour [83] or require explicit inter-agent communication for social behaviours [84]. Those which use implicit communication for social behaviours are inspired from ants' pheromone sensing and hence use stigmergy [40,41,85,86].

1.3.4 Social Behaviours using Passive Sensing

Implementation of social behaviours using strictly passive sensing is rare in the robotics literature. Even the strategies that assume passive sensing for one social behaviour, assume explicit communication for other social behaviours and hence can be categorized as hybrid strategies. For example, [35], uses a passive sensing based short-range repulsion behaviour, however, flocking behaviour requires explicit communication. In [87], some social behaviours are based on agent's capability of observing other agents via multiple sensors like stereo vision, proximity, force and touch etc. However, minimal explicit communication is used to exchange high level task goals and strategies.

There are no known cooperative source localization algorithms that use social behaviours under the constraints of passive sensing and individualistic behaviours under the constraints of temporal sampling. Recently, the author proposed a distributed source localization algorithm which addresses this gap [75]. The localization performance of the proposed algorithm was gauged

using a bio-inspired metric, i.e., in terms of localization time, the benefit a specific individual enjoys being in a team as compared to being alone. The primary focus of the study was to highlight the practical issues of implementing conventional bio-inspired models in multi-agent systems which require explicit inter-agent communication. Though it was shown that the proposed strategy works at par with its explicit communication based counterparts, it did not validate the robustness of the collective behaviour against different noise sources.

In [76], the author proposed an adaptive temporal sampling strategy where sampling time is a function of sensed intensity values. The adaptive temporal sampling strategy improved the performance of the localization algorithm proposed in [75] which was originally based on a static temporal sampling strategy. However, the performance of the localization algorithm against common noise sources was not validated and only a team size of 10 agents was considered.

1.4 Thesis Outline & Research Contributions

Practical implementation issues of conventional collective behaviour models, requiring social behaviours based on explicit inter-agent communication, are highlighted in Chapter 2. An alternative passive sensing model for each social behaviour is presented along with justifications for practical implementation. All the source localization algorithms presented in this thesis build on the same passive sensing models and their respective source localization performances have been compared against hypothetical counterparts based on lossless explicit communication channel without any communication delays.

The problem statement along with the experimental setup is presented in Chapter 3. The performance of the collective behaviours is validated against a conservative performance metric inspired by a real world source localization problem. The performance metric is the arrival time of the last agent inside a circular success zone defined around the source location. The experimental setup is based on a realistic underwater acoustic propagation model and can simulate a range of noise levels from sensing noise of a typical hydrophone to strong constructive and destructive multipath interference due to environment variability.

A distributed source localization algorithm is presented by the name of Bio-inspired Control Algorithm for Small Teams (Bio-CAST) in Chapter 4. The presented work is an extended version of the author's previously published work [75]. Bio-CAST has a self-sufficient individualistic behaviour under the constraints of static temporal sampling for gradient sensing and social behaviours based on the passive sensing models defined in Chapter 2. The individualistic behaviour is inspired by the biased random walk of a bacterium, *Escherichia coli*, performing chemotaxis [77]. This helps us investigate the role of uncertainty in decision making, both at the individualistic and the collective level. Extensive optimization of the individualistic and social behaviours is carried out on a range of initialization distances, team sizes and neighbourhood sizes which results in an estimated analytical model for optimized Bio-CAST. Simulated experiments validate the robustness and scalability of the collective behaviour against strong multipath interference in gradient sensing, initialization distance sensitivity, noise in passive neighbour detection and agent loss. Investigation of team's trajectories and expanse reveal that a cooperative team's cohesion is well regulated during the simulated

experiments and no agents break away from the team. Proof-of-concept real-robot experiment validates the optimized Bio-CAST against realistic noise patterns in sensors and actuators of the robots.

Bio-CAST with an adaptive temporal sampling approach is presented in Chapter 5 and is an extended version of the author's preliminary work in [76]. The adaptive temporal sampling approach is composed of Intensity based Adaptation (IbA) and Connectivity based Adaptation (CbA). IbA varies the agent's sampling time as a function of sensed intensity values and reports significant improvement over the static temporal sampling strategy in Chapter 4. In [76], IbA was assumed to be an arbitrary non-linear function of the sensed intensity values. The performance of the localization algorithm against common noise sources was not validated and only a team size of 10 agents was considered. In Chapter 5, these gaps are addressed where IbA is optimized along with other behaviours of an agent across a range of team sizes, initialization distances and neighbourhood radii. An optimized shape for the sampling function is identified which emerges from the optimization data. The robustness of the collective behaviour is validated against varying noise sources. It is revealed in the robustness analysis that IbA is sensitive to high noise levels such as strong multipath interference. To address the noise sensitivity of IbA, CbA is introduced which regulates IbA based on an agent's estimate of number of its neighbours within a local neighbourhood. Effectively, CbA regulates the expanse of the team by eliminating the number of agents breaking away from the team as a mechanism for robust behaviour. The resulting collective behaviour shows remarkable robustness to strong multipath interference as well as outperforms other temporal sampling strategies in all the considered scenarios.

In Chapter 6, an Adaptive Cohesion based Localization Algorithm (ACLA) is presented which does not require a self-sufficient individualistic behaviour to localize a source. Source localization is achieved as an emergent property through agent interactions. ACLA follows the same adaptive sampling strategy as given in Chapter 5. Given absence of a self-sufficient individualistic behaviour, CbA is crucial in controlling agent loss. Even a single agent breakaway would mean an increasing team expense in time. A two phase optimization strategy is introduced which is simpler than the previous optimization strategies of Chapter 4 and Chapter 5. In the first phase, IbA and an agent's cohesion behaviour are optimized for infinite neighbourhood and in the second phase CbA is optimized for limited neighbourhoods. It is in contrast to the earlier optimization strategies where the whole set of behaviours were optimized both for the infinite neighbourhood and the limited neighbourhood. The collective behaviour resulting from the estimated analytical model of optimized ACLA is validated against strong multi-path interference and other noise sources. Furthermore, the arrival time performance of ACLA has been compared against a similar emergent source localization algorithm and Bio-CAST. The emergent source localization algorithm is based on speed variation as a function of instantaneous intensity values. However, the algorithm fails to localize the source for the considered problem in this thesis. Against Bio-CAST, ACLA performs significantly better for low ambient noise, however, Bio-CAST shows more robustness than ACLA for high ambient noise levels.

Finally, a summary of the important findings of this thesis is provided in Chapter 7. Also, the chapter focuses on the current state-of-the-art in swarm robotics and the potential of the proposed strategies in making of a viable and a

reliable multi-agent system which is able to solve real world problems. Future work has also been proposed which highlights some of the points which can help in improving the proposed strategies further and gaining new insights.

Chapter 2

Social Behaviours based on Passive Sensing of Neighbours

The material in this chapter draws significantly on the author's previously published work [75].

2.1 Background

Social behaviours are the basis of cooperation in multi-agent systems and are fundamental in achieving collective behaviour. Conventional social behaviour models require explicit inter-agent communication. However in some environments, communication bandwidth and delays are critical constraints which may compromise the desired collective behaviour. This chapter introduces agent interaction models which do not require any explicit inter-agent communication and use only agent's passive sensing abilities to invoke collective behaviour in a multi-agent system. The chapter starts by reviewing the conventional social behaviour models followed by highlighting the implementation issues associated with these models in a real world scenario. The chapter concludes with proposing the passive sensing based social behaviours and substantiating their implementation viability. The three main source localization algorithms proposed in the following chapters assume the same passive sensing models for agent interaction as presented in this chapter.

2.2 Conventional Social Behaviours

In a school of fish, the collective behaviour is believed to emerge from an individual's social behaviours, i.e., its interaction with its neighbours [88, 89]. Many years of research [90–92] has classified three social behaviours as basis for complex collective behaviour in nature, i.e., the long-range attraction, the short-range repulsion and the neighbour alignment. An agent is attracted towards its neighbours unless it gets too close, in which case repulsion takes over attraction – a phenomenon jointly known as the long-range attraction and short-range repulsion. Also, an agent aligns its heading with some of its neighbours which is known as neighbour alignment. Current literature on animal collective behaviour shows a lack of consensus on whether these social behaviours are based on metric/zonal interactions [90, 92–94] or topological interactions [95–97]. By metric interaction, one assumes the interaction of the focal agent with its neighbours within a fixed radius. There are three distinct zones defined within the fixed radius of interaction as shown in Fig. 2.1. For a distance, $r \in \mathbb{R}^+$ (m), away from the focal agent, there exists a Collision Avoidance (CA) zone such that, $0 < r \leq r_{CA}$, within which short-range repulsion behaviour is active, an orientation (O) zone such that, $r_{CA} < r \leq r_O$, within which neighbour alignment behaviour is active and a Group Cohesion (GC) zone such that, $r_O < r \leq r_{GC}$, within which the long-range attraction behaviour is active. By topological interaction, one assumes that the focal animal interacts with a fixed number of nearest neighbours. However, these models are more restricted in explaining the collective behaviour in some flocks of birds and their generic application is rather debatable [56, 88].

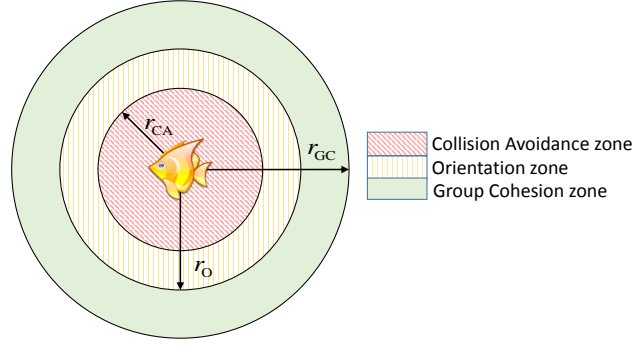


Figure 2.1. Zonal model of fish interaction.

2.2.1 Unit Vector based Long-Range Attraction and Short-Range Repulsion

For metric/zonal interaction, there are numerous models having some very subtle differences between them but many of them fit the experimental data quite well. A very simple model [56, 90] is based on the unit vector information of the neighbour positions. For example, in case the focal agent, i , with position, $\mathbf{x}_i(t)$, at time, t , detects any neighbour(s), j , inside its CA zone, i.e., the inter-agent distance, $r_{ij}(t) = |\mathbf{x}_j(t) - \mathbf{x}_i(t)| \leq r_{CA}$, it assumes heading according to the following unit direction vector

$$\mathbf{d}_{CA_i}(t + T_{CA}) = - \frac{\sum_{j \neq i}^{n_{CA}(t)} \frac{\mathbf{x}_j(t) - \mathbf{x}_i(t)}{r_{ij}(t)}}{\left\| \sum_{j \neq i}^{n_{CA}(t)} \frac{\mathbf{x}_j(t) - \mathbf{x}_i(t)}{r_{ij}(t)} \right\|} \quad (2.1)$$

where T_{CA} is the sampling time and $n_{CA}(t)$ are the number of neighbours in the CA zone. Similarly for any neighbour(s), j , in the GC zone such that $r_O < r_{ij}(t) \leq r_{GC}$, the focal agent, i , would assume heading according to the

following unit direction vector

$$\mathbf{d}_{GC_i}(t+T) = \frac{\sum_{j \neq i}^{n_{GC}(t)} \frac{\mathbf{x}_j(t) - \mathbf{x}_i(t)}{r_{ij}(t)}}{\left\| \sum_{j \neq i}^{n_{GC}(t)} \frac{\mathbf{x}_j(t) - \mathbf{x}_i(t)}{r_{ij}(t)} \right\|} \quad (2.2)$$

where T is the sampling time and n_{GC} are the total number of neighbours in the GC zone.

2.2.2 Centroid based Long-Range Attraction and Short-Range Repulsion

There are other collective behaviour models which build more directly on the significance of the centroid of the school's mass [98–101]. Some of these models assume a somewhat unrealistic notion that a focal agent has the knowledge of the global centroid and tries to bias itself towards that center. Nevertheless, there are models that only assume knowledge of the centroid of neighbour positions within a fixed radius [93, 102, 103]. In fact, we can write a very simple centroid model by slightly modifying (2.1) and (2.2) such as

$$\mathbf{d}_{CA_i}(t+T_{CA}) = -\frac{\sum_{j \neq i}^{n_{CA}(t)} (\mathbf{x}_j(t) - \mathbf{x}_i(t))}{\left\| \sum_{j \neq i}^{n_{CA}(t)} (\mathbf{x}_j(t) - \mathbf{x}_i(t)) \right\|} \quad (2.3)$$

and

$$\mathbf{d}_{GC_i}(t+T) = \frac{\sum_{j \neq i}^{n_{GC}(t)} (\mathbf{x}_j(t) - \mathbf{x}_i(t))}{\left\| \sum_{j \neq i}^{n_{GC}(t)} (\mathbf{x}_j(t) - \mathbf{x}_i(t)) \right\|} \quad (2.4)$$

respectively. By limiting the r_{GC} in the centroid model, we can mimic knowledge of the local centroid and by increasing it to a very large number, we can mimic knowledge of the global centroid.

2.2.3 The Neighbour Alignment

As for the orientation zone, the focal agent, i , with velocity, $\mathbf{v}_i(t)$, at time, t , aligns itself with the orientation of its j neighbour(s) by assuming heading according to the following unit direction vector

$$\mathbf{d}_{O_i}(t + T) = \frac{\sum_{j \neq i}^{n_O(t)} \frac{\mathbf{v}_j(t)}{|\mathbf{v}_j(t)|}}{\left\| \sum_{j \neq i}^{n_O(t)} \frac{\mathbf{v}_j(t)}{|\mathbf{v}_j(t)|} \right\|} \quad (2.5)$$

where T is the sampling time and $n_O(t)$ are the number of neighbours in the orientation zone.

2.2.4 Fusion of Social Behaviours

Conventionally, the repulsion behaviour holds the highest priority and in case a neighbour is found inside the CA zone, the attraction and orientation behaviours are suspended [90]. Attraction and orientation behaviours are active at the same time and are generally given equal weights in calculating the resultant heading of the agent.

2.3 Practicalities of the Long-range Attraction

Long-range attraction contributes towards the cohesion and compactness of a group. It is interesting to investigate the advantages of having an attraction behaviour in multi-agent systems for some real world problem. It has been shown that the long-range attraction behaviour without aid of any other collective behaviours (repulsion or orientation) can contribute towards increasing the efficiency of a source localization problem [54]. However, the implementation cost of behaviours given by (2.2) and (2.4) is in terms

of an agent acquiring its own reliable position estimate and to establish communication with other agents to exchange the position information. Acquiring a reliable position estimate and/or communication with acceptable delays and bandwidth in certain environments is a hard and an expensive problem to solve [30, 104].

Having a small attraction radius may alleviate the communication issues to some extent [105, 106]. However from the perspective of a source localization problem, having a small attraction radius may consequentially require a very large team of agents [107]. For example, a small team with agents having small attraction radius will be potentially sampling a strong spatially-correlated cue which may have detrimental effects on its collective decision making in noisy environments [108]. Fishes are known to have small neighbourhoods but some schools of fish undertaking distant migration are composed of several million individuals connected through small neighbourhoods over several kilometers [109, 110]. It is highly unlikely in the present times to build such a massive swarm of autonomous agents with sufficient mission endurance to solve a real world problem. Especially in the case of an agent using temporal sampling for gradient estimation, we investigate the dependence of initialization distance, attraction radius and team size in Chapter 4. We show that a smaller attraction radius requires a larger cooperative team to invoke collective behaviour, i.e., performing significantly better than an individualistic team. It is intuitive if we imagine reducing the attraction radius of a small team while demanding the team remains cohesive, we are approaching the case of a single individual. The team members in such a case would have very small sampling times to alleviate the risk of an agent breaking away from the team and hence very poor gradient estimates.

2.4 Practicalities of the Short-range Repulsion

Repulsion allows more volume to a school allowing it to span more space. Also, increasing r_{CA} results in decreasing cohesion in a school [92]. There is also a difference of opinion on the effect of repulsion on the overall schooling, e.g., some studies report that removing the CA zone causes school disintegration [91, 111], whereas some report that removal of the CA zone has insignificant effect on schooling [92, 112, 113]. Nevertheless, the short-range repulsion allows sophisticated multi-agent systems such as land robots, UAVs or AUVs to avoid collisions with their peers during a cooperative mission. From the perspective of an agent safety, collision avoidance control is indispensable in most multi-robot setups.

Short-range repulsion suffers from the same issues as discussed in the preceding section for the long-range attraction. Models defined in (2.1) and (2.3) also require the focal agent to acquire the position information of all the neighbouring agents.

2.5 Practicalities of the Neighbour Alignment

The neighbour alignment model in (2.5) serves the purpose of mimicking the *polarization* of a school, i.e., the mean of the angle deviation of each agent to the mean swimming direction of the fish group [92]. School polarization increases as degree of alignment among individuals in a school increases and decreases otherwise. It is generally measured as a normalized parameter varying between 0 (maximally confused state) and 1 (optimally parallel state) as defined in [90]. The long-range attraction and the short-range repulsion models without the orientation model account well for the *expansive* of a school, i.e., the

mean distance of all the fish from the school's centroid, but not so much for the polarization [88]. It is also known that the phenomenon of alignment is dependent on the radial neighbour density. For example, a low density would result in a disordered orientation and only for a certain threshold of density, order emerges and increases thereafter as a function of group size [114, 115]. Such a transition from disorder to order (alignment) is seen in a group of locusts [116] where for small populations, there was no significant alignment among individuals. Similar transitions are observed in a school of fish [117]. These observations also hint towards the possibility of alignment being an emergent property that is a consequence of the long-range attraction and the short-range repulsion phenomenon in a high density group.

From the perspective of source localization, there is a high chance that alignment may result as an implicit consequence of following a certain cue. For example, a recent study has shown that alignment emerges from the long-range attraction and short-range repulsion phenomenon when agent speeds are varied as a function of instantaneous cue intensities [80]. Working with a small team of autonomous agents, it is interesting to investigate if alignment would be of any help, especially in the source localization problems. Recently, the author showed that the alignment behaviour only helps marginally over the long-range attraction and short-range repulsion behaviours in a source localization problem [118].

As far as the implementation issues are concerned, the orientation model requires the focal agent to have a good estimate of the velocity vectors of each of its neighbours. In addition to the knowledge of the position coordinates of all the neighbours as in the case of the long-range attraction and the short-range repulsion, this would require agent memory to compute velocities of their

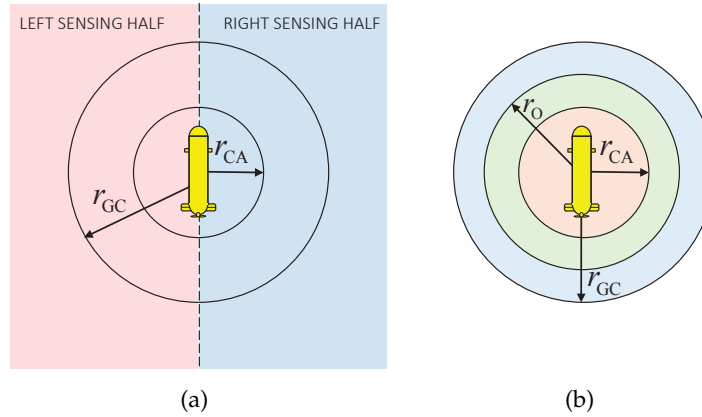


Figure 2.2. (a) Passive sensing based interaction zones for CA and GC. (b) Explicit communication based interaction zones for CA, GC and O.

neighbours from the past and present position coordinates. Alternatively information regarding neighbours' range and heading can help in achieving the alignment behaviour [23, 119]. However in most real world environments, acquisition of the heading information is not possible over large distances without explicit communication. This is also reflected in [23, 119] where a virtual sensor comprising of a compass and a communication unit was assumed to exchange the heading information between robots.

2.6 The Alternative: Passive Sensing based Social Behaviours

As discussed earlier, the conventional social behaviour models require explicit inter-agent communication. Our focus is to adopt an alternative set of social behaviours that build on the conventional counterparts but only require passive sensing to achieve similar characteristics and performance.

We assume that each agent is equipped with two passive sensors, one on its right side and one on its left side. This effectively partitions the two-dimensional sensing world of an agent as shown in Fig. 2.2(a) into a right and a left half plane. Now, there are two interaction zones, i.e., the CA and the

GC zone as compared to the three zones of the conventional case in Fig. 2.2(b). As discussed in the preceding section, given the neighbour alignment requires an agent to acquire neighbours' heading information [23,119], we have ignored the orientation zone as acquiring such an information is not possible without explicit communication. Moreover, it is also important to note that even if we had the resources to implement explicit inter-agent communication, the role of the neighbour alignment behaviour is controversial in the biological world [75] and the performance benefits of its addition to the other two behaviours is marginal [118] as discussed in the preceding section.

The following information is required for the passive sensing based social behaviours:

1. Where is the majority of neighbours in my GC zone? Either to my right or to my left?
2. Are there any neighbours inside the CA zone? If so, what is the estimated range to the closest one and which half is it located in?

Based on this information an agent exercises short-range repulsion and long-range attraction behaviours. We discount the neighbour alignment behaviour following the discussion in the preceding section.

2.7 Practicalities of the Passive Sensing Model

Here we provide some examples of using the dual sensor topology from the perspective of practical implementation. A very simple scenario is using two microphones or hydrophones per agent where the focal agent can *listen* for the presence of its neighbours. In most of the situations the drive or propulsion systems of land robots, UAVs or AUVs make a significant amount of noise

which can be sensed easily by the focal agent within some local neighbourhood. Using the time-of-arrival analysis on the sensors' data can help the focal agent detect where the majority of neighbours is located. In harsh environments such as undersea environments, where communication bandwidth is severely limited, low frequency sound signals like the thruster noise can travel several hundreds of meters [47, 120, 121]. The thruster noise of a typical AUV or a ROV is in the range of 120 dB to 160 dB re¹ 1 μ Pa at 1 m [122, 123]. AUVs can also be mounted with locator beacons which emit an acoustic pulse at a fixed rate in time. For example, a 20 kHz pinger with a source level of 180 dB re 1 μ Pa at 1 m can be heard over several kilometers undersea. In environments where light can travel, e.g., clear waters, the two sensors can simply be light detectors. For example, in the case of CoCoRo project, the researchers use small AUVs which can emit light [78]. Comparing the mean value of light intensity sensed by each sensor over some time window can give a good estimate of where the majority of the neighbours are. Cameras can also be an option as two passive sensors in environments where robots can detect the neighbour majority using simple image processing techniques.

Where an estimate of the neighbour majority completely defines the long-range attraction behaviour, the short-range repulsion behaviour requires the estimated range from the nearest neighbour. We can think about the neighbour as an additional source. Given an agent has some prior knowledge of the source (neighbour in this case) intensity and its propagation model, it can obtain a good estimate of the range in a close proximity. This is especially true for sources which follow the inverse square law, i.e., the intensity is inversely proportional to the distance squared. Since the repulsion radius is generally

¹an abbreviation of 'reference to'

small, the assumption pertaining to the knowledge of the estimated nearest neighbour distance is practically valid.

Chapter 3

Problem Statement & Experimental Setup

3.1 Problem Statement

Let us say that we have a team of homogeneous, miniature and simple robots such as shown in Fig. 3.1, called Swarmbots. An agent cannot explicitly communicate with other agents, however, it can detect the majority of neighbours in either its left or right half within some local neighbourhood using two sensors. Each agent is also equipped with one sensor to sense the signal of the source and hence conducts temporal sampling to sense the gradient. Note that neighbour-majority detection and gradient sensing may require two separate sensing mechanisms. For example, a team of agents localizing a chemical source where each agent senses the gradient via a single chemical sensor and its neighbours via two acoustic sensors. The whole team needs to travel a certain distance in an unconstrained search space and arrive at the source location. In a GPS denied environment where the robots do not have a sense of their own position or of the source location, this becomes a challenging task. We can have a single point-source such as a Radio Frequency (RF) beacon (on land) or an Underwater Locator Beacon (ULB) (in sea) installed at the source location, the signal strength of which can help the robots to localize the target.

We can also flip the notion. For example, when a team consisting of miniature and simple robots is employed for a certain task, it is natural to consider its post-mission retrieval. Assuming the same constraints on the team

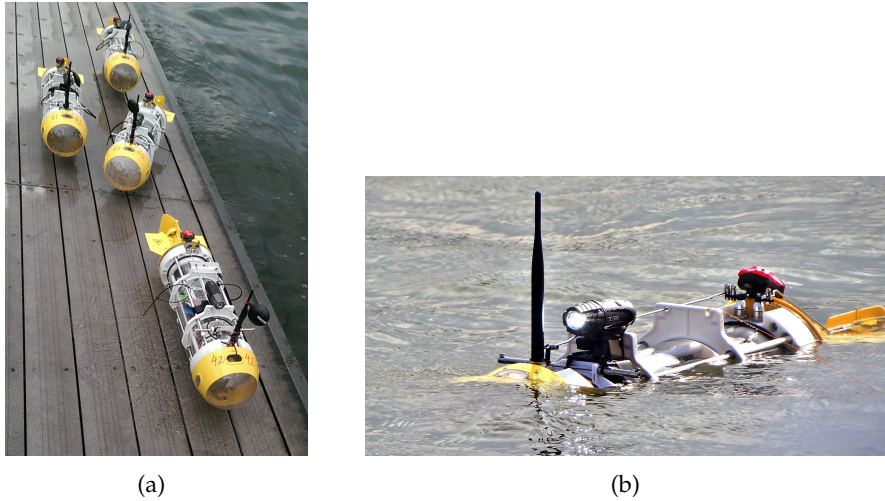


Figure 3.1. (a) A small team of four Swarmbots at Pandan Reservoir. (b) A Swarmbot during a mission in the lake.

and knowledge of the positional data, team retrieval is a challenging task. For example, a team of Swarmbots is exploring a certain area cooperatively. After some desired period of exploration time, the team needs to be retrieved. Assuming each agent has a single hydrophone to sense the gradient of an acoustic source, a ULB may be suspended from a surface vessel to aid in the team retrieval. Though the idea of having a huge number of inexpensive units is to have some tolerance of losing a few during a mission, it is important to have retrieval algorithms that are robust in maximizing the percentage of retrieved units – ideally to 100%.

We define *arrival time* as the time taken by the last agent in a team to enter a success zone of radius, r_s , centered around the point-source where each agent that enters the success zone does not diverge from the source afterwards.

To substantiate that a specific source localization algorithm is invoking collective behaviour, the localization performance in terms of the mean, median and the variance of the arrival time distribution of a cooperative team (using

individualistic and social behaviours) needs to be significantly better than a non-cooperative team (using only individualistic behaviours).

3.2 Simulation Setup

A team of $N \in \{1, 2, \dots, 20\}$ homogeneous agents is considered. Simulated model of an agent follows the kinematics of Swarmbot where each agent is assumed to be of length, l , has its turning rate, $\dot{\theta}$ and speed, s . A constant speed operation with non-holonomic constraints has been assumed and both the turning rate and the speed have been further corrupted with additive Gaussian noise for each agent to simulate the effects of turbulence in the medium. The compass reading, θ , has also been corrupted with additive Gaussian noise, ε_θ which follows the empirical characterization of the sensor, i.e., Ocean Server's OS5000. A simplistic motion model is meant to keep the model-specific artifacts resulting from a more realistic dynamical model from affecting the results of the collective behaviours we study in this thesis.

The attraction radius, r_{GC} , i.e., the maximum size of an agent's neighbourhood in which it interacts with its neighbours, is expressed as a fraction of the initialization distance, i.e., $r_{GC} = \gamma r_0$ where $\gamma \in [0, 1]$. The repulsion neighbourhood radius (see Section 2.2), r_{CA} , has been set to twice the minimum distance, $r_{\min} = 2sT_{CA} + \frac{l}{2}$. Note that r_{CA} needs to be greater than $2sT_{CA} + \frac{l}{2}$ for an agent to detect all the potential collisions. The constraint, $r_{\min} = 2sT_{CA} + \frac{l}{2}$, has been calculated assuming the worst case scenario of a head-on collision between two agents travelling at speed, s , where the sensor is assumed to be mounted at the center of each agent's body length, l . Since the formulation for r_{\min} makes sense if both the agents are travelling at the same speed, r_{CA} needs to be sufficiently larger than r_{\min} to compensate for any noise

Table 3.1. Symbols, Description and explored values of the mission variables in simulation.

Sym.	Description	Value(s)
N	Total number of team members	1 to 20
r_0	Initialization distance	$\{200, 600, 1000, 1400\}$ m
r_s	Radius of the success zone	50 m
r_{GC}	Attraction radius	$\{0.1r_0, 0.2r_0, \dots, 0.6r_0, \infty\}$
r_{CA}	Repulsion radius	7.6 m
T_{CA}	CA sampling time	1 s
r_{\min}	Minimum radius of the repulsion zone	3.8 m
l	Length of an agent	0.8 m
s	Speed of an agent	$\sim \mathcal{N}(1.5, 0.15)$ m s ⁻¹
ε_θ	Compass heading error	$\sim \mathcal{N}(0, 1)$ °
$\dot{\theta}$	Turning rate of an agent	$\sim \mathcal{N}(35, 3.5)$ ° s ⁻¹
σ	Noise in received intensity level	$\{1, 2, \dots, 6\}$ dB

in speed regulation. The sampling time for the collision avoidance module, T_{CA} , is arbitrarily fixed at 1 s.

Each of N agents is assumed to be deployed with a random pose in a circular area of radius 10 m centered around the initialization point. The initialization distance, r_0 , i.e., the distance of the initialization point from the source is varied in a range to simulate different Signal to Noise Ratio (SNR) conditions. The radius of the success zone centered around the source, r_s , is set to 50 m.

All the values for the variables with their description have been listed in Table 3.1.

3.2.1 Sound Propagation

The acoustic source is assumed to be a Dukane DK-180 ULB with a frequency of 8.8 ± 1.0 kHz and an effective bandwidth of 100 Hz [124]. The Source sound-Level, SL , is set to 180 dB re 1 μ Pa at 1 m. The assumed ambient Noise Level, NL , is set corresponding to the pressure spectral density level of 52 dB re 1 μ Pa² Hz⁻¹ pertaining to sea state 3 [47]– [120] which is equal to a sound level of 84 dB re 1 μ Pa in the operating frequency band of the ULB.

We adopt a simple incoherent model for sound propagation taking into account the transmission losses due to spherical spreading and absorption in seawater [125] (see Appendix A.1). Spatial profiles of a realization of received source-intensity, I , are shown in Fig. 3.2. Intensity levels have been corrupted with additive Gaussian noise of zero mean and equivalent dB-scale standard deviation of $\sigma = 1$ dB in Fig. 3.2(a) and of $\sigma = 6$ dB in Fig. 3.2(b). Assuming the noise of a typically calibrated sensor, $\sigma = 1$ dB of noise in received intensity levels is a valid assumption given a sufficiently long sampling window. However, in dynamic environments where there is a strong constructive and destructive multipath interference [126], the variation in received intensity levels can be estimated by setting σ within the range of 3 dB to 6 dB. We will consider the more conservative case of $\sigma = 6$ dB in conjunction with $\sigma = 1$ dB to validate the robustness of the source localization algorithm against noise.

For reference, a realization of noise-corrupted source-intensity as a function of distance from the source is shown in Fig. 3.3 for $\sigma = 1$ dB and $\sigma = 6$ dB.

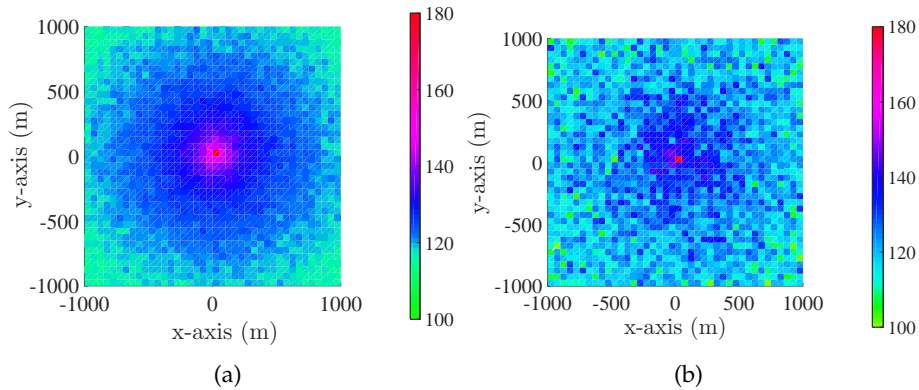


Figure 3.2. (a) A realization of source-intensity spatial profile for $\sigma = 1$ dB. (b) A realization of source-intensity spatial profile for $\sigma = 6$ dB.

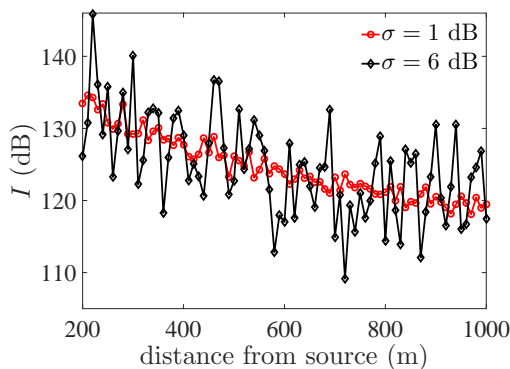


Figure 3.3. A realization of the noise-corrupted spatial intensity levels.

3.2.2 Evolutionary Optimization

The parameters of the individualistic and social behaviours of each localization algorithm discussed in this thesis are optimized using a Genetic Algorithm (GA) [127]. According to the classification given in [16], agent behaviours can be designed by either *behaviour based design* or *automatic design*. Behaviour based design involves manually developing the individual behaviors of the agents which result in a desired collective behavior. It is generally a trial and error procedure where iterative tuning of the individual behaviors is carried out until the desired collective behavior is achieved. On the other hand, automatic design for multi-robot systems is mainly based on

the evolutionary robotics approach. In evolutionary robotics approach, initially a population of individual behaviors is generated at random. In each iteration, a certain number of experiments or simulations for each individual behavior are conducted. In each iteration, a fitness function is used to evaluate the collective behavior resulting from the individual behavior. Individual behaviors with a good fitness value are modified by genetic operators and then used for the subsequent iterations. Once no improvement is seen in the fitness value of the best individual behaviour for a specific number of iterations, the evolutionary process is ended.

In this thesis, we have a fixed general structure of the individualistic and social behaviours. Let us take the example of the individualistic behaviour where an agent would move for some time in a straight path and then take a random turn. However, the optimal values of the sampling time and turn's probability distribution parameters are found through GA. The process is identical to that of the evolutionary robotics approach where each behaviour in a population would be a different set of values of the sampling time and the turn's probability distribution parameters. Our approach differs from a purely evolutionary robotics approach since the search space has been constrained by an already fixed behavioural structure. Hence our approach can be seen as a hybrid of behaviour based design and automatic design. However, note that GA itself is not critical in the design process since any optimization strategy that is suitable for a high-dimensional, nonseparable and nonlinear problem without any guarantees of convexity can be used to find the optimal parameter values.

The GA has been implemented using NVIDIA[®] CUDA[™] computing platform and employing three NVIDIA[®] Tesla[®] K20 Graphical Processing Units

(GPUs) in parallel [128]– [129]. The GPU-based architecture enables us to have 48 individuals in a single generation of the GA and all of the individuals to be evaluated in parallel. The GA structure and implementation details have been given in Appendix A.2.

The GA's fitness function is the mean arrival time (defined in Section 3.1) over 1024 simulated source localization missions. The number of simulated missions have been calculated using the Vargha and Delaney's A-measurement test [130] to ensure similar distributions for the entire GA population. The justification of using the particular number of simulated missions is given in Appendix A.3.

When dealing with the evolutionary optimization techniques, it is important to ascertain that the optimized solution is not exploiting any specific information that is local to the particular environment or any initial condition, which would not hold in general [131]. For this reason, measures are taken to ensure that no artifacts make their way into the optimization process, e.g., when initializing from a constant distance we ascertain the reported solution to be the same even if the multi-agent system is initialized from different quadrants of the search space relative to the source location. Also, the trajectories of the agents during a mission, both in the simulation environment and real-world experiments, are carefully studied to rule out any artifacts.

3.2.3 Robustness Analysis

A general trend in this thesis is to optimize the behaviours of a certain collective behaviour for an ambient noise level of 1 dB, followed by estimation of the optimized behaviours with an analytical model. The collective behaviours based on these analytical models are then validated against varying

degrees of ambient noise in the range of 1 dB to 6 dB. The validation is mainly based on the statistical analysis of the arrival time distributions via box-plots where each plot represents 5×10^4 simulated experiments, a band represents the median of a distribution, a box delineating the 25th to the 75th percentile, the whiskers show the lowest datum still within 1.5 Inter Quartile Range (IQR) of the lower quartile, and the highest datum still within 1.5 IQR of the upper quartile. Wherever comparisons between different localization algorithms have been made, significance of comparative medians has been tested using the Mann-Whitney-Wilcoxon test.

In some instances, analysis of a particular simulated experiment is also undertaken to give a clearer understanding of both the collective behaviour and the agent behaviour. Such analysis is done through examining the trajectory of the centroid of the team, trajectory of a random agent, team expanse and number of agent breakaways.

Chapter 4

Static Temporal Sampling based Multi-Agent Source Localization

The material in this chapter is an extended version of the author's previously published work [75].

4.1 Background

Recently, a distributed source localization algorithm was proposed [75] which invokes collective behaviour in a small multi-agent system. The social behaviours were based on the passive sensing, as defined in Chapter 2 and the individualistic behaviour assumed a temporal sampling constraint on an agent for sensing the gradient. The primary focus of the author's preliminary work was to highlight the practical issues of implementing conventional social behaviour models which require explicit inter-agent communication. Though it was shown that the proposed source localization algorithm works at par with its explicit communication based counterparts, the study did not validate the robustness of the collective behaviour against different noise sources.

In this chapter, the proposed algorithm is named as Bio-inspired Control Algorithm for Small Teams (Bio-CAST). The algorithm is composed of one individualistic and two social behaviours. The individualistic model is inspired by the biased random-walk of a bacterium, *Escherichia coli*, performing chemotaxis [77] which helps us investigate the role of uncertainty in an agent's

decision making, both at the individualistic and the collective level. This is in contrast to the earlier version proposed in [75] where the uncertainty in agent's decision making was discounted. The performance of the collective behaviour is validated for the arrival time of the last agent (as defined in Section 3.1) which also contrasts with the less conservative arrival scenario of [75]. Extensive optimization of the agent behaviours is carried out on a range of initialization distances, team sizes and neighbourhood radii. The optimized algorithm is estimated by an analytical model. Simulated experiments validate the resulting collective behaviour against agent's sensor and actuator noise, strong multipath interference in gradient sensing due to environment variability, noise in passive neighbour sensing, initialization distance sensitivity and agent loss. Investigation of team's trajectories and expanse reveal that a cooperative team's expanse is well regulated during the simulated experiments and no agents break away from the team. Proof-of-concept real-robot experiment validates the optimized Bio-CAST against realistic noise patterns in sensors and actuators of the robots.

4.2 Bio-CAST

In this section, the component behaviours of Bio-CAST are introduced starting with Target Drive (TD), a self-sufficient individualistic behaviour which helps an agent localize a source with or without the social information. Then the social behaviours are introduced, i.e., Collision Avoidance (CA) and Group Cohesion (GC). This section concludes with the general behavioural structure of Bio-CAST.

4.2.1 Individualistic Behaviour: Target Drive

Some bacteria, being very small, cannot sense the gradient via instantaneous spatial comparisons of their chemoreceptors and instead use temporal sensing [73]. Also, a bacterium swims in a straight path interrupted by abrupt random turns at constant intervals [74, p. 225]. Increasing concentrations would result in decreased frequency of abrupt turns and decreasing concentrations would result in increased frequency. If a bacterium detects increasing concentrations then it swims relatively straight and takes random turns otherwise [77].

On a similar note, we assume that an agent, n , estimates the average acoustic intensity, $I_n(t)$, at position, $\mathbf{x}_n(t)$, every T seconds. The unit heading vector of the agent, dictated by TD is updated at each sample as

$$\mathbf{d}_{\text{TD}_n}(t+T) = \begin{cases} \mathbf{d}_{W_n}(t) & \text{if } \hat{I}_n(t+T) \geq \hat{I}_n(t) \\ R_{\Theta_c(t+T)} \mathbf{d}_{W_n}(t) & \text{otherwise} \end{cases} \quad (4.1)$$

where $\mathbf{d}_{W_n}(t)$ is the unit directional vector of the agent, $\hat{I}_n(t)$ is the estimated mean acoustic intensity, R_{Θ_c} is the counter clockwise rotation matrix for the angle $\Theta_c \sim \mathcal{N}(\theta_c, \sigma_{\theta_c})$ which is a Gaussian random variable with mean θ_c , and standard deviation σ_{θ_c} .

Effectively, if the focal agent, after taking a sample, estimates that it is going in the direction of increasing sound levels, it keeps its direction otherwise it takes a random corrective turn.

4.2.2 Group Cohesion

GC assumes that an agent can detect the majority of its neighbours in its left or right half within some local neighbourhood of radius, r_{GC} , called attraction

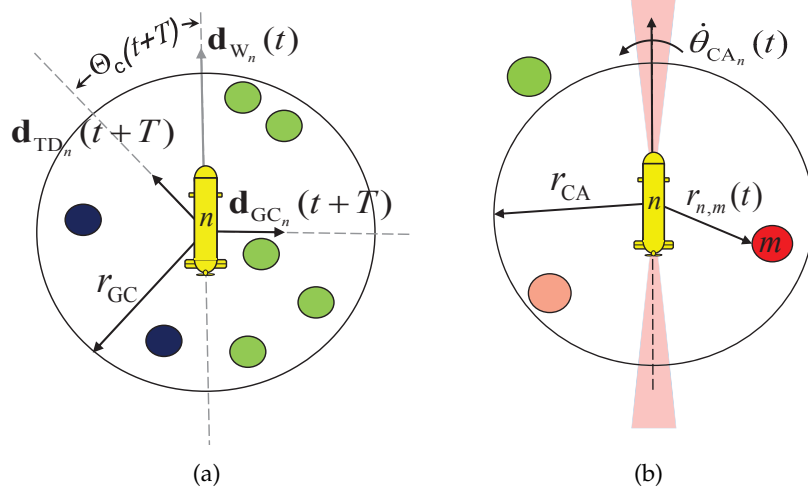


Figure 4.1. (a) The neighbourhood of an AUV with respective unit vectors dictated by TD and GC. (b) An AUV n detects an AUV m in its closest proximity within the repulsion neighbourhood and takes the evasive action by turning towards the opposite half. The uncertainty zone is highlighted with red where an AUV cannot resolve a threat to be either in its left or right half.

radius. As shown in Fig. 4.1(a), GC calculates the unit heading vector of the n^{th} agent as

$$\mathbf{d}_{GC_n}(t+T) = \begin{cases} R_\phi \mathbf{d}_{w_n}(t) & \text{if more neighbours on left} \\ R_\phi^- \mathbf{d}_{w_n}(t) & \text{if more neighbours on right} \\ \mathbf{d}_{w_n}(t) & \text{otherwise} \end{cases} \quad (4.2)$$

where R_ϕ, R_ϕ^- are the counter clockwise and the clockwise rotation matrices for an angle of $\phi = 90^\circ$.

Effectively, GC dictates a left turn to the focal agent if the number of neighbours to its left are more than the number of neighbours on its right and vice versa. In case of the numbers being equal in both the left and the right half, it keeps the agent's heading unchanged.

4.2.3 Collision Avoidance

CA operates at the highest priority. As the sampling time, T , for TD and GC is generally in tens of seconds, CA has a relatively much smaller sampling time, T_{CA} . In case an agent n detects a neighbour within its repulsion zone of radius, $r_{CA} \leq r_{GC}$, it starts an evasive action and ignores any other behaviours such as going towards the goal or towards the neighbours. The focal agent turns away from the nearest neighbour with a turning rate that is proportional to how close the nearest neighbour is. The turning rate as a function of the estimated distance, $\hat{r}_{n,m}(t)$, between the focal agent, n , and the nearest neighbour, m , is given as

$$\dot{\theta}_{CA_n}(t + T_{CA}) = \begin{cases} \text{sgn}(m)\alpha\dot{\theta}_{\max} & \text{if } r_{\min} < \hat{r}_{n,m}(t) \leq r_{CA} \\ \text{sgn}(m)\dot{\theta}_{\max} & \text{if } \hat{r}_{n,m}(t) \leq r_{\min} \end{cases} \quad (4.3)$$

where

$$\text{sgn}(m) = \begin{cases} +1 & \text{if } m \text{ is in right half} \\ -1 & \text{if } m \text{ is in left half} \\ X & \text{otherwise} \end{cases} \quad (4.4)$$

and $\alpha = \left(\frac{r_{CA} - \hat{r}_{n,m}(t)}{r_{CA} - r_{\min}} \right)$, positive turning rates being counter clockwise and vice versa, r_{\min} is the minimum distance (see Section 3.2 for details) where the turning rate is maximum and X is a bernoulli random variable that takes on values ± 1 with probability 0.5. Randomness in (4.4) caters for an agent finding the nearest neighbour within the uncertainty zone, shown in red in Fig. 4.1(b). Then the focal agent, n , assumes heading according to the following direction

vector

$$\mathbf{d}_{CA_n}(t + T_{CA}) = \frac{\Delta \mathbf{d}_{CA_n}(t + T_{CA}) + \mathbf{d}_n(t)}{\|\Delta \mathbf{d}_{CA_n}(t + T_{CA}) + \mathbf{d}_n(t)\|} \quad (4.5)$$

where $\mathbf{d}_n(t) = 1\angle\theta_n(t)$ is the instantaneous unit direction vector of an agent n and $\Delta \mathbf{d}_{CA_n}(t + T_{CA}) = 1\angle\{T_{CA} \cdot \dot{\theta}_{CA_n}(t + T_n)\}$ is the desired change in the instantaneous unit direction vector dictated by CA module.

4.2.4 Resultant Bio-CAST

Now, we can write the desired direction of the focal agent n , commanded by Bio-CAST as

$$\mathbf{d}_{BC_n}(t) = \begin{cases} \mathbf{d}_{CA_n}(t) & \text{if } \hat{r}_{n,m}(t) \leq r_{CA} \\ \mathbf{d}_{W_n}(t) & \text{otherwise} \end{cases} \quad (4.6)$$

where

$$\mathbf{d}_{W_n}(t) = \eta \mathbf{d}_{TD_n}(t) + (1 - \eta) \mathbf{d}_{GC_n}(t) \quad (4.7)$$

and $\eta \in [0.5, 1]$ is the source-bias coefficient where any values of $\eta < 0.5$ result in unsuccessful source localization. Note that higher values of η mean less team cohesion and vice versa. Also note that (4.6) is only the desired heading dictated by Bio-CAST whereas the transition from the n^{th} agent's current angle, θ_n to $\theta_{BC_n} = \angle \mathbf{d}_{BC_n}$ follows the non-holonomic constraints as specified in Section 3.2. The overall block diagram of the Bio-CAST is given in Fig. 4.2.

4.3 Optimization Results

The optimization process assumes the experimental setup and GA settings as stipulated in Section 3.2. For the constant parameters, refer to the settings given in Table 3.1. Behavioural parameters, i.e., the sampling time T , source bias coefficient η , correction-angle θ_c and its associated SD σ_{θ_c} are optimized,

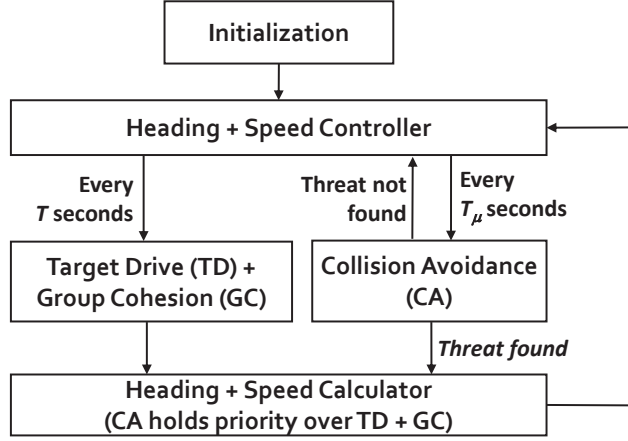


Figure 4.2. Block diagram of BioCAST.

for a range of team sizes, initialization distances and attraction radii as given in Table 3.1. The optimized vector, $\mathbf{w}^* = [T^*, \eta^*, \theta_c^*, \sigma_{\theta_c}^*]$ is defined as a function of the initialization distance, attraction radius and team size as

$$\mathbf{w}^*(r_0, r_{GC}, N) = [T^*(r_0, r_{GC}, N), \eta^*(r_0, r_{GC}, N), \theta_c^*(r_0, r_{GC}, N), \sigma_{\theta_c}^*(r_0, r_{GC}, N)] \quad (4.8)$$

The bounds for the optimization parameters are given in Table 4.1. The range of η has been truncated because less than 50 % of its weight results in a failure to localize the source. In Section 4.3.1, the attraction radius, r_{GC} has been set to infinity which ensures strong connectivity of the team [132] and hence maximum cooperation. In Section 4.3.2, the attraction radius has been limited to finite values and the subsequent effect on the optimization results is compared. The noise level, σ in the agent's received intensity levels has been set to 1 dB.

To compare the relative benefit of using a cooperative strategy against an individualistic one, relative efficiency can be calculated as

$$\rho_{\text{rel}}(r_0, r_{GC}, N) = \frac{\text{Mean arrival time for } \mathbf{w}^*(r_0, 0, N)}{\text{Mean arrival time for } \mathbf{w}^*(r_0, r_{GC}, N)} \quad (4.9)$$

Table 4.1. Explored values of the parameters during the optimization process

Parameter	Bounds
T	$[1, 300]$ (s)
η	$[0.5, 1]$
θ_c	$[0^\circ, 180^\circ]$
σ_{θ_c}	$[0^\circ, 90^\circ]$

where $\mathbf{w}^*(r_0, 0, N)$ is the optimized individualistic vector and $\rho \geq 1$. Let $U = \{(r_0, r_{GC}, N) \in \mathbb{R}^+ \times \mathbb{R}^+ \times \mathbb{Z}^+\}$ be a universal set of parameter values, then we have a cooperative set $\mathcal{C} = \{(r_0, r_{GC}, N) \in U \mid \rho_{\text{rel}}(r_0, r_{GC}, N) > 1\}$ and an individualistic set, $\mathcal{C}' = U \setminus \mathcal{C}$.

4.3.1 Arrival Time Optimization and Initialization Distance

The solid lines in Fig. 4.3 represent $\mathbf{w}^*(r_0, \infty, N)$ and the dashed lines represent constrained optimization for the individualistic case, $\mathbf{w}^*(r_0, 0, N)$ where η is set to 1.00. For all the initialization distances considered, $\mathbf{w}^*(r_0, \infty, N)$ represents a cooperative team as is evident by the relative efficiency curves in Fig. 4.3(a) and $\eta^* < 1$ in Fig. 4.3(b). In general, there is a consistent increase in the relative efficiency in N for initialization distances greater than or equal to 600 m. However, the curves slowly flatten out as N increases. For the initialization of 200 m, peak relative efficiency occurs for $N = 9$ and thereafter there is a slow decline. To explain this, we need to consider increasing N as both a source of cooperation and interference [133]. As N increases, the cooperative team thrives on more number of samples and hence its holistic decision making improves. However, since a cooperative team travels cohesively as shown by η^* in Fig. 4.3(b) (also see discussion in Section 4.4.2 on cooperative team's trajectories and expanse), interference due to CA also increases in N . The interference due to CA is significantly more in a cooperative team than an individualistic team since agents moving together

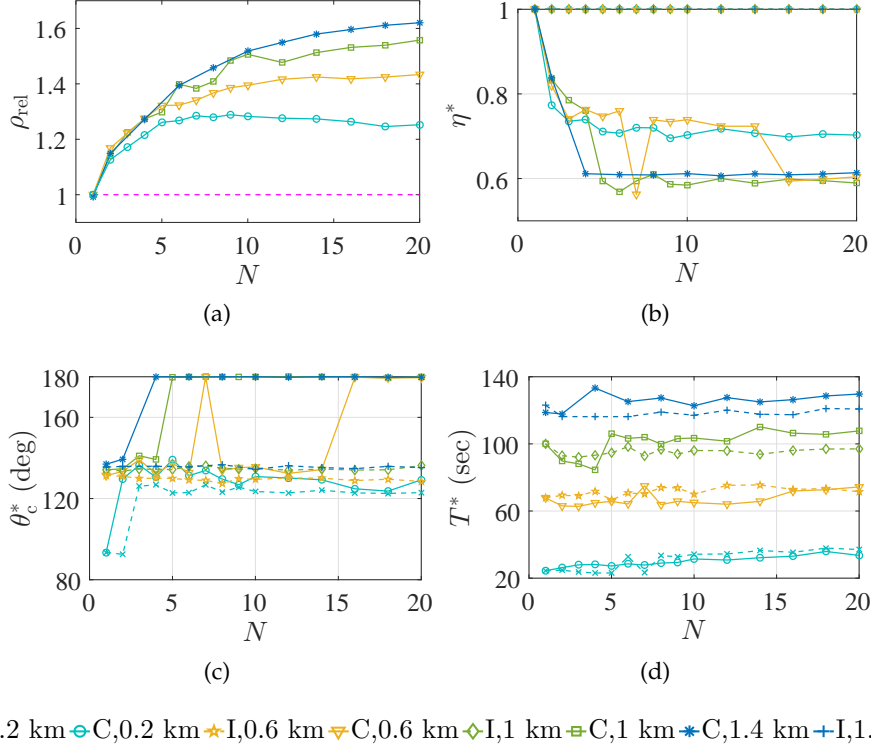


Figure 4.3. Optimization results for varying initialization distances (see legend at the bottom where I denotes an individualistic team and C denotes a cooperative team): (a) Relative efficiency as a function of team size where pink dashed-line represents performance of an optimized individualistic team. (b) Source bias coefficient, η with all the individualistic η are set to 1.00. (c) Correction angle, θ_c . (d) Sampling time, T .

would require more evasive actions on average as compared to agents moving independently. As the initialization distances decrease, the SNR improves and also the agent's gradient estimates. Hence, the relative advantage of a cooperative team and an individualistic team is not much and declines quickly as interference increases with the team size.

The optimized source bias values in Fig. 4.3(b) show an interesting relationship between two optimized cohesion levels, i.e., $\eta^* \approx 0.70$ and $\eta^* \approx 0.60$, and the initialization distances. For a larger initialization distance, i.e., a degraded SNR, the team utilizes more cohesion to make up for agent's poor gradient estimates. It is also interesting to note that the initialization distance of 600 m is nicely placed at the boundary of the two conditions and it switches

between the two cohesion levels without showing any discontinuity in relative efficiency in Fig. 4.3(a).

Also, we have to see the optimized correction angle θ_c^* in the same context. There are two optimized levels, i.e., one in the range of 123° to 134° and the other at 180° in Fig. 4.3(c), which directly relate to the two optimized cohesion levels in Fig. 4.3(b). A team with less cohesion enjoys a smaller correction angle whereas a team with higher cohesion levels enjoys a larger correction angle. This is further substantiated by the behaviour of the individualistic teams where θ_c^* in Fig. 4.3(c) is nearly the same as for the cooperative teams with less cohesion.

Comparing η^* in Fig. 4.3(b) and θ_c^* in Fig. 4.3(c), we can also conclude that very small cooperative teams ($N < 5$) do not use very high cohesion levels and their associated correction-angle behaviours are also identical to the individualistic teams. We can see in Fig. 4.3(b) and Fig. 4.3(c) for all initialization distances that the optimized steady response in N is reached when the team size is in the range of 4 to 6 agents. Same is true for the optimized sampling times in Fig. 4.3(d), especially exaggerated for the initialization distances of 1000 m and 1400 m. The optimized sampling times show nearly identical behaviour for both the cooperative and the individualistic teams as they remain nearly constant in N and increase in r_0 .

The behaviour of the optimized variance, $\sigma_{\theta_c}^*$ drops to very low values, i.e., $\leq 3^\circ$ for $N > 5$ which is comparable to the assumed compass noise of 1° and it does not show any correlation in N as shown in the optimization results for varying initialization distances in Fig. 4.4. For the individualistic case, however, the optimized variance increases with increasing initialization distances and maintains a certain level in N .

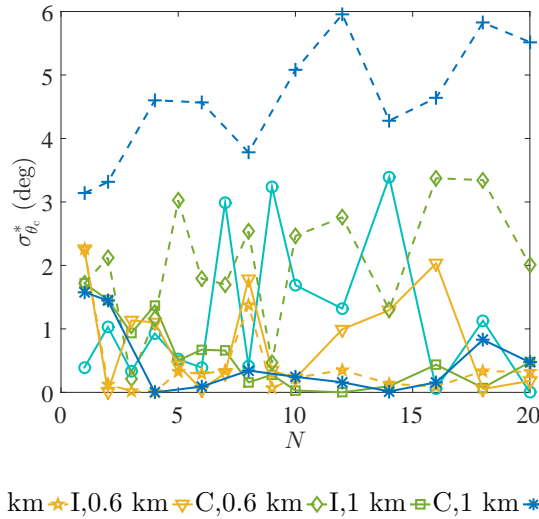


Figure 4.4. Optimized uncertainty in decision making for varying initialization distances (see legend at the bottom).

4.3.2 Arrival Time Optimization and Limited Attraction Neighbourhood

In Fig. 4.5, the optimization results are presented for the initialization distance of 1000 m for limited attraction radii, i.e., in the range of 0 m to 600 m. For a more general inference of the results, interested reader is referred to Fig. B.1 through Fig. B.5 for optimization results of initialization distances in the range of 600 m to 1400 m with a step size of 200 m.

Since the attraction radius was set to infinity for optimization in Fig. 4.3, it is important to see how different limited attraction radii behave. It can be seen in Fig 4.5(a) that an attraction radius of 600 m performs as well as infinity and it also follows nearly the same parameter values in N as shown in Fig 4.5(b), Fig 4.5(c) and 4.5(d). If we consider initialization distances in the range of 800 m to 1400 m in Appendix B.1, an attraction radius that behaves as well as infinity remained in the range of 57% to 62.5% of the initialization distance (see Fig. B.1(a) through Fig. B.4(a)). Also, the relative efficiency increases consistently in initialization distance and the relative increase between an

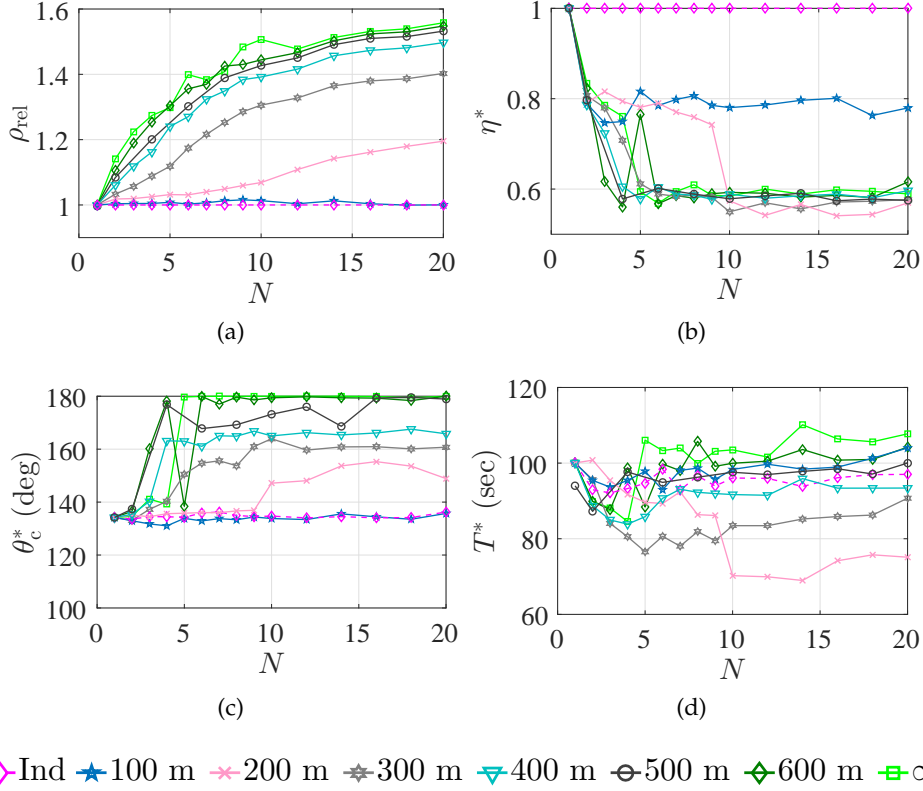


Figure 4.5. Optimization results for initialization distance, r_0 of 1000m and varying attraction neighbourhood radii, r_{GC} (see legend at the bottom): (a) Arrival time performance as a function of team size N . (b) Source bias coefficient, η . (c) Correction angle, θ_c . (d) Sampling time, T .

initialization distance of 600 m and an initialization distance of 1400 m is about 15%.

As we reduce the attraction radius, the relative efficiency starts degrading in Fig 4.5(a) until the attraction radius is about 10% of the initialization distance where the performance is only marginally better than the individualistic team. It is not only the performance that becomes similar but also the optimized correction angles and the optimized sampling times as shown in Fig. 4.5(c) and Fig. 4.5(d) respectively. Such an attraction radius, which results in a cooperative team (since $\eta^* \approx 0.80$ in Fig 4.5(b)) being marginally better than an individualistic team, can be considered as a break-even attraction radius. In fact, attraction radius of 100 m shows identical characteristics in terms

of relative performance and optimized parameters for all the initialization distances considered in the range of 600 m to 1400 m in Appendix B.1.

In Fig 4.5(b), we can see that there are two distinct optimal cohesion windows for the cooperative teams, i.e., around 0.80 and around 0.60. Only the cooperative teams that have optimal cohesion levels in the latter window show significant performance improvement over the individualistic teams. These more cohesive teams also show distinctly different behaviours, i.e., correction angles and sampling times, than the individualistic or less cohesive teams. Hence, it is of interest to identify which conditions on team sizes and attraction radii for a specific initialization distance are required to invoke collective behaviour in a team. In other words, it is of interest to identify a set $\mathcal{C}^* \subset \mathcal{C}$ which results in highly cohesive and significantly better performing cooperative teams than the individualistic ones.

To identify the more cohesive subset, let us consider the example of the attraction radius being 200 m, i.e., 20% of the initialization distance in Fig. 4.5. We can see in Fig. 4.5(b) that a switch from the less cohesive window to a more cohesive window happens at $N = 10$. If we consider initialization distances in the range of 800 m to 1400 m in Appendix B.1 for the same attraction radius of 200 m, we see a particular trend. As the ratio of the attraction radius to the initialization distance decreases, it takes a larger team size to invoke collective behaviour. For example, $N = 16$ for an initialization distance of 1400 m, $N = 14$ for 1200 m and $N = 8$ for 800 m in Fig. B.1(c), Fig. B.2(c) and Fig. B.4(c) respectively. Another trend is that a larger initialization distance requires a lower ratio of the attraction radius to the initialization distance to invoke collective behaviour for a specific team size. For example, let us consider a team size of 6 agents and look for the ratios that invoke collective

behaviour in different initialization distances. In Fig. 4.5(b), we can see that for an initialization distance of 1000 m, a ratio of 0.30 invokes collective behaviour. However, this ratio is reduced to 0.25 for an initialization distance of 1200 m and to 0.21 for an initialization distance of 1400 m in Fig. B.2(c) and Fig. B.1(c) respectively.

Now let us consider the behaviour of the optimized parameters within \mathcal{C}^* . As far as η^* in Fig. 4.5(b) is concerned, it remains nearly constant in N for a specific attraction radius. However, η^* varies slightly as a function of attraction radius in the range of 0.55 to 0.60. The mean η^* decreases from 0.59 to 0.56 as the ratio of the attraction radius to the initialization decreases. Same inference is true for the optimal correction angle in Fig. 4.5(c) and the optimal sampling times in Fig. 4.5(d) where they remain nearly constant in N for a specific attraction radius, however, their mean optimal values decrease as attraction radii decrease. This pattern is generic as it also holds for other initialization distances in Appendix B.1.

The behaviour of the optimized variance, $\sigma_{\theta_c}^*$ shows the same behaviour for limited neighbourhood radii as was discussed in the preceding subsection where the attraction radius was set to infinity. Since $\sigma_{\theta_c}^*$ plays an integral part in the original bacterium model [77] and also in many bio-inspired robotic implementations [67, 71], it was included in TD to validate the role of uncertainty in collective decision making. This addition is in contrast to the earlier version of TD in [75]. Given $\sigma_{\theta_c}^*$ has an effect on agent's heading every T seconds, its optimized behaviour in Fig. B.1(e) through Fig. B.5(e) does not seem significant when compared with the compass error of 1° which is being added every 1 s. This is further substantiated by statistical analysis of arrival time performance for a cooperative team with different initialization distances,

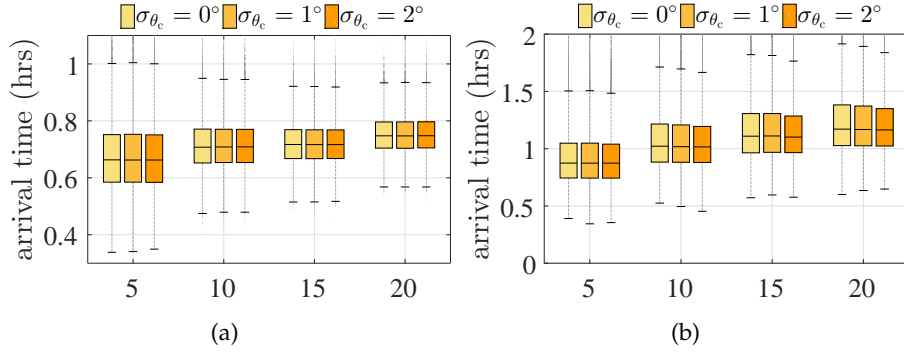


Figure 4.6. Arrival time performance for initialization distance, r_0 of 1000 m and varying uncertainty in correction angle, σ_{θ_c} : (a) Cooperative team with $r_{GC} = 600$ m. (b) Individualistic team.

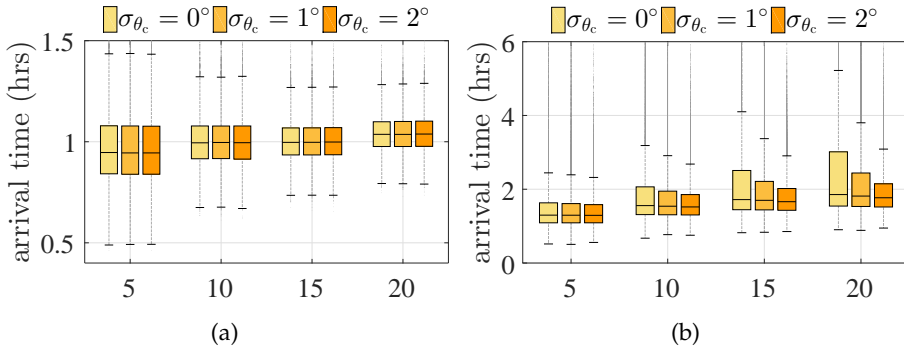


Figure 4.7. The arrival time performance shown for initialization distance, r_0 of 1400 m and varying uncertainty in correction angle, σ_{θ_c} : (a) Cooperative team with $r_{GC} = 600$ m. (b) Individualistic team.

i.e., for 1000 m in Fig. 4.6(a) and 1400 m in Fig. 4.7(a) where controlled variability in σ_{θ_c} shows identical performance.

Hence, there is no evidence from the optimization data or the statistical analysis that uncertainty in collective decision making plays a beneficial role. However, for the individualistic teams, it was shown in the preceding section that as initialization distance increases, the teams seem to benefit from increased uncertainty in decision making. That has been further substantiated in Fig. 4.6(b) and Fig. 4.7(b) for the case of $r_0 = 1000$ m and $r_0 = 1400$ m respectively.

4.3.3 Estimated Optimized Bio-CAST

Based on the discussion in Section 4.3.1 and Section 4.3.2, we can write a general analytical model for the estimated optimized behavioural vector for Bio-CAST. Let us take advantage of almost constant behaviour of the optimized parameters in team size while the attraction radius was set to infinity in Section 4.3.1. The trend of decreasing optimized parameter values as the attraction radius was decreased in Section 4.3.2 is approximated by a general analytical model. Finally, an example is presented for the estimated optimized Bio-CAST for initialization distance of 1000 m as a special case.

4.3.3.1 Estimation for Infinite Attraction Radius

As indicated in Section 4.3.1, the optimized values of the source bias coefficient and the optimized correction angle remain nearly constant in team sizes $N \geq 5$ and also in the initialization distance. Hence we can exploit the specified range of the team size to write a simple estimate of the optimized behaviours in terms of their respective means, $\bar{\eta}^*$ and $\bar{\theta}_c^*$. Also, for a specific initialization distance, the optimized sampling times also remain constant in team size, however, show a significant change as the initialization distance varies. Hence for $N \geq 5$, we can drop the dependence of $\hat{\mathbf{w}}^*$ on N and rewrite (4.8) for attraction radius set to infinity as

$$\hat{\mathbf{w}}^*(r_0, \infty) = [\hat{T}^*(r_0, \infty), \bar{\eta}^*(r_0, \infty), \bar{\theta}_c^*(r_0, \infty), 0^\circ] \quad (4.10)$$

where $\hat{T}^*(r_0, \infty) = ar_0^2 + br_0 + c$, $a = -2.77 \times 10^{-5} \text{ s m}^{-2}$, $b = 0.12 \text{ s m}^{-1}$, $c = 12.55 \text{ s}$, Root Mean Square Error (RMSE) = 2.50 s, is the estimate for the

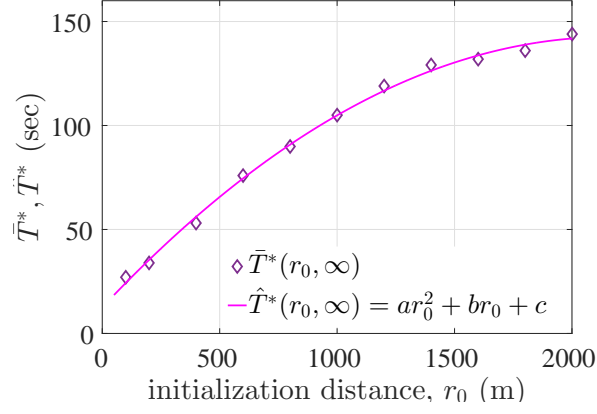


Figure 4.8. Estimating optimized sampling time for infinite attraction radius as a function of initialization distance.

average optimized sampling times, $\bar{T}^*(r_0, \infty)$ calculated for N in the range of 5 to 20 agents for each r_0 in the range of 100 m to 2000 m in Fig. 4.8.

4.3.3.2 Estimation for Limited Attraction Radius

We can write a general form for the estimated optimized behavioural vector considering the optimization trends for limited attraction radii with respect to the infinite attraction radius as given in Section 4.3.2. For $N \geq 5$, the estimated optimized vector can be written as

$$\hat{\mathbf{w}}^*(r_0, r_{GC}) = \begin{cases} \hat{\mathbf{w}}^*(r_0, \infty) \diamond \beta(r_0, r_{GC}) & \text{if } (r_0, r_{GC}, N) \in \mathcal{C}^* \\ \hat{\mathbf{w}}^*(r_0, 0) & \text{otherwise} \end{cases} \quad (4.11)$$

where \diamond is the Hadamard product of two vectors, $\hat{\mathbf{w}}^*(r_0, 0)$ is the optimized individualistic vector, $\beta(r_0, r_{GC}) = [\beta_T(r_0, r_{GC}), \beta_\eta(r_0, r_{GC}), \beta_\theta(r_0, r_{GC}), 1]$ compensates the decrease in the optimized correction angles and the optimized sampling times as r_{GC} is reduced from infinity.

4.3.3.3 Example: Estimation for a Specific Initialization Distance & Limited Attraction Radius

As a special case, let us consider the optimized parameters for an initialization distance of 1000 m when the attraction radius is limited as discussed in Section 4.3.2. First, let us write (4.10) following the discussion in Section 4.3.1 for infinite attraction radius as

$$\hat{\mathbf{w}}^*(1000, \infty) = [105 \text{ s}, 0.59, 180^\circ, 0^\circ] \quad (4.12)$$

Now let us find $\beta(1000, r_{GC})$ in (4.11) which models the variability of the optimal parameter values as a function of the attraction radius. We can estimate $\eta^*(1000, r_{GC})$ as

$$\hat{\eta}^*(1000, r_{GC}) = \bar{\eta}^*(1000, \infty) \cdot \beta_\eta(1000, r_{GC}) \quad (4.13)$$

and since it remained nearly constant both in N and r_{GC} , $\beta_\eta(1000, r_{GC})$ is set to 1.

Also, each $\theta_c^*(1000, r_{GC})$ remained nearly constant in N in Fig. 4.5(c) and hence we can estimate it by its mean, $\bar{\theta}_c^*(1000, r_{GC})$ in Fig. 4.9(a). However, $\theta_c^*(1000, r_{GC})$ varied significantly with r_{GC} and to model that variability, the mean optimized points are plotted against r_{GC} in Fig. 4.9(b) and estimate $\bar{\theta}_c^*(1000, r_{GC})$ as

$$\hat{\theta}_c^*(1000, r_{GC}) = \bar{\theta}_c^*(1000, \infty) \cdot \beta_\theta(1000, r_{GC}) \quad (4.14)$$

where $\beta_\theta(1000, r_{GC}) = a_\theta r_{GC} + b_\theta$, $\hat{\theta}_c^*(1000, \infty) = 180^\circ$, $a_\theta = 3.8 \times 10^{-4} \text{ m}^{-1}$, $b_\theta = 0.77$, $\text{RMSE} = 1.04^\circ$. Similarly, each $T^*(1000, r_{GC})$ in Fig. 4.5(d) is modeled by its mean, $\bar{T}^*(1000, r_{GC})$ in Fig. 4.9(c). Then $\bar{T}^*(1000, r_{GC})$ is plotted against r_{GC} in Fig. 4.9(d) and is estimated as

$$\hat{T}^*(1000, r_{GC}) = \bar{T}^*(1000, \infty) \cdot \beta_T(1000, r_{GC}) \quad (4.15)$$

where $\beta_T(1000, r_{GC}) = a_T r_{GC}^2 + b_T r_{GC} + c_T$, $\bar{T}^*(1000, \infty) = 105 \text{ s}$, $c_T = 0.40$, $a_T = -1.27 \times 10^{-6} \text{ m}^{-2}$, $b_T = 1.7 \times 10^{-3} \text{ m}^{-1}$, $\text{RMSE} = 0.82 \text{ s}$. Equation (4.14) and (4.15) model the decrease in the optimized correction angles and the optimized sampling times as attraction radius is decreased from infinity.

Now, we can write (4.11) for the initialization distance of 1000 m as

$$\hat{\mathbf{w}}^*(1000, r_{GC}) = \begin{cases} \hat{\mathbf{w}}^*(1000, \infty) \diamond \beta(1000, r_{GC}) & \text{if } (1000, r_{GC}, N) \in \mathcal{C}^* \\ \hat{\mathbf{w}}^*(1000, 0) & \text{otherwise} \end{cases} \quad (4.16)$$

where $\hat{\mathbf{w}}^*(1000, 0) = \bar{\mathbf{w}}^*(1000, 0) = [96 \text{ s}, 1.00, 134^\circ, 0^\circ]$ (see estimation in Fig. 4.9(a) and Fig. 4.9(c)).

4.4 Robustness Analysis

In this section, robustness of the collective behaviour resulting from Bio-CAST is validated against various noise sources. For simulated experiments robustness is analyzed via arrival time statistics, team trajectories and team expanse. Team expanse, e , is defined as the average distance of all the agents from the team's centroid, i.e.,

$$e = \frac{1}{N} \sum_i^N \|\mathbf{x}_c(t) - \mathbf{x}_i(t)\| \quad (4.17)$$

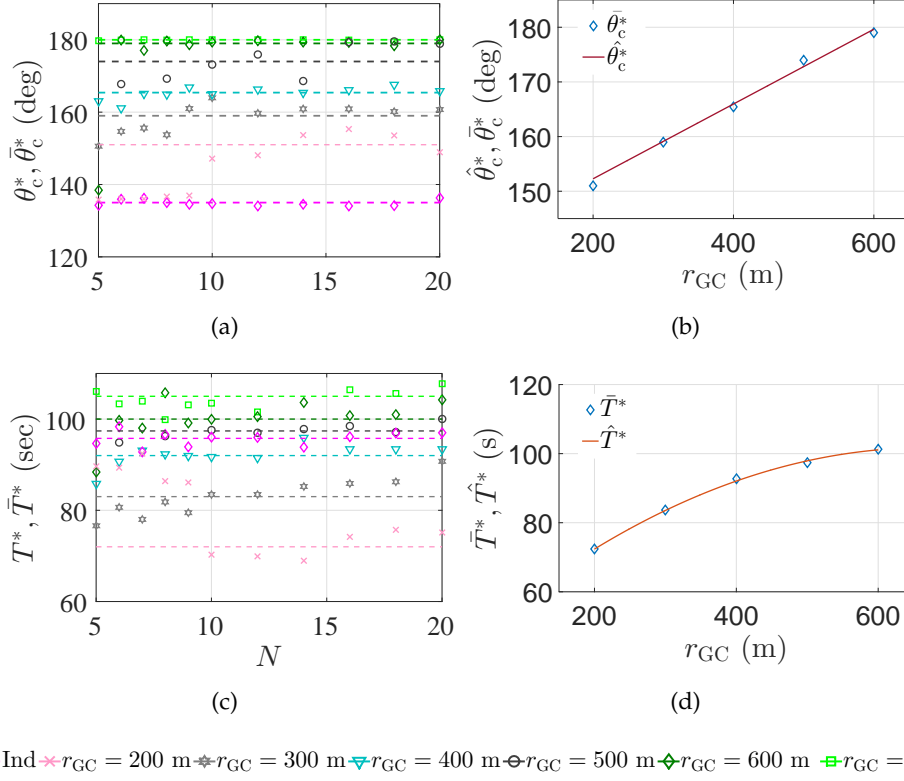


Figure 4.9. Estimating optimized parameters as function of the attraction radius: (a) Estimated optimized correction angle. (b) Estimated optimized sampling time.

where $\mathbf{x}_c(t) = \frac{1}{N} \sum_i^N \mathbf{x}_i(t)$ is the team centroid at time t . Keeping in mind, the problem statement in Section 3.1, it is of interest to see if the expense remains bounded. We assume an initialization distance of 1000 m with teams having different attraction radii. We use the cooperative or individualistic Bio-CAST following (4.16).

4.4.1 Arrival Time Performance

The arrival time performance for $\sigma = 1$ dB and $\sigma = 6$ dB has been shown in Fig. 4.10(a) and Fig. 4.10(b) respectively. As mentioned in the optimization discussion in Section 4.3.2, $r_{GC} = 500$ m performs as good as infinity throughout N and for both cases of σ , not only in the sense of the median but also the variance (uncertainty) of the arrival time distribution. The

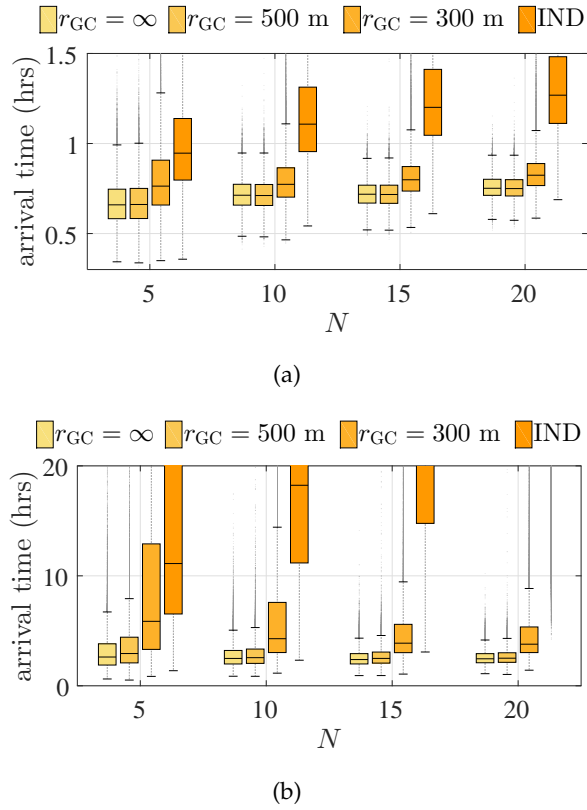


Figure 4.10. Comparative arrival performance for: (a) $\sigma = 1$ dB. (b) $\sigma = 6$ dB.

only exception where $r_{GC} = 500$ m performs slightly worse than the infinity case is $N = 5$ and $\sigma = 6$ dB in Fig. 4.10(b).

It is interesting to note that the uncertainty in arrivals keeps on decreasing in N for the cooperative teams in Fig. 4.10(a) and Fig. 4.10(b). In fact, the median arrival times also improve significantly for $r_{GC} = 300$ m in N for $\sigma = 6$ dB. This is in contrast to the case of the individualistic team where not only its median arrival time significantly degrades in N but also the uncertainty in arrivals.

4.4.2 Trajectories and Expanse

Trajectories of a random agent and team's centroid have been shown in Fig. 4.11 for $N = 20$ with a cooperative team having $r_{GC} = 300$ m or an individualistic team.

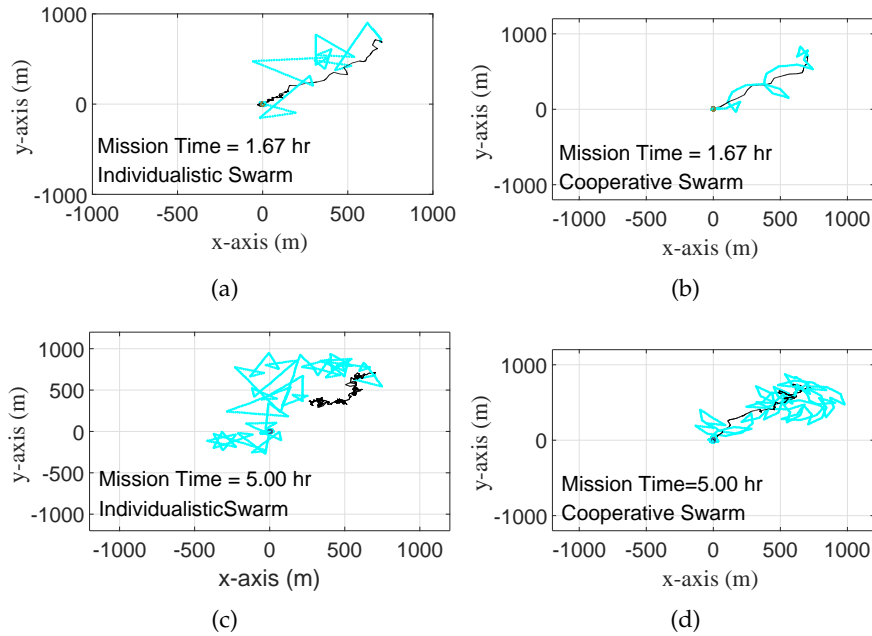


Figure 4.11. Trajectory of a random agent and the centroid of the team in varying noise conditions: (a) Individualistic team for $\sigma = 1$ dB. (b) Cooperative team for $\sigma = 1$ dB. (c) Individualistic team for $\sigma = 6$ dB. (d) Cooperative team for $\sigma = 6$ dB.

For $\sigma = 1$ dB, let us compare the individualistic trajectory of a random agent and team's centroid versus the cooperative case in Fig. 4.11(a) and Fig. 4.11(b) respectively. The individualistic trajectory for a random agent in Fig. 4.11(a) is similar to the one of the swimming bacteria performing chemotaxis [77] whereas the centroid's trajectory is jittery but overall directed towards the source. The cooperative agent's trajectory is similar to a moth's casting behaviour localizing a plume source [134] whereas the centroid travels more smoothly when compared to the individualistic case. Also, the cooperative team remains more cohesive as compared to the individualistic team during the localization process as is evident by the respective expanses in Fig. 4.12(a). The expanse of the cooperative team is regulated at an average value of half of the attraction radius, i.e., 150 m till 0.47 h from where it transitions to a much smaller expanse at an average value of 11.3 m reached at 0.68 h. However, the

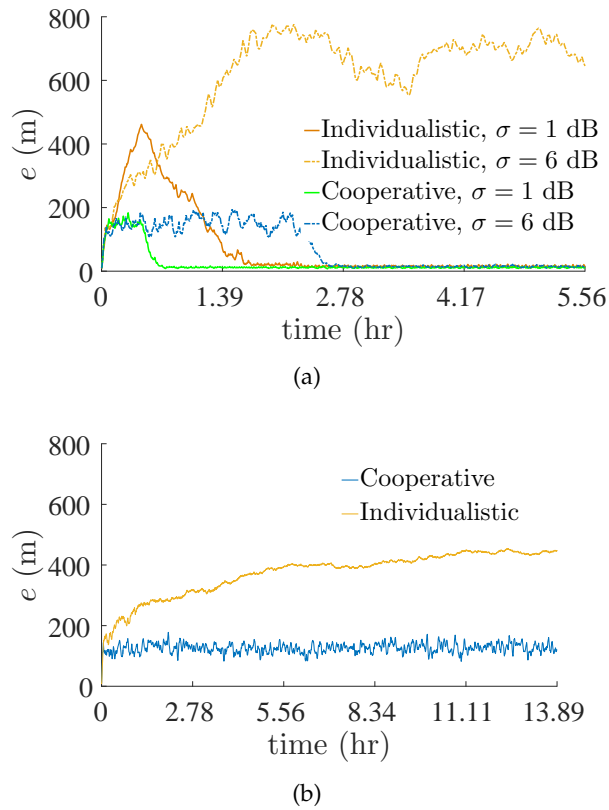


Figure 4.12. (a) Expande of the team in different noise levels. (b) Expande of the team when there is no source signal present.

expande of the individualistic team shows a peak of 460 m at 0.46 h from where it starts transiting to the expande at an average value of 12.3 m reached at 2.40 h. The cooperative team has two steady states whereas the individualistic team has only one. The first steady state of the cooperative team occurs at about 120 s after initialization where the cooperative Bio-CAST regulates the expande of the team during the search process. The transition from the first steady state to a much lower steady state occurs after the first agent converges and continues until all the agents converge. Since the team travels cohesively, the time difference in the first and the last arrival is only 0.21 h. On the other hand, the peak expande in the individualistic case may or may not signify a first arrival since the arrivals are independent of each other.

For the case of $\sigma = 6$ dB, the trajectory of a random agent and the centroid for the individualistic team and the cooperative team are shown in Fig. 4.11(c) and Fig. 4.11(d) respectively. Qualitatively, the motion patterns remain the same as were for $\sigma = 1$ dB. The jitter in the individualistic centroid is well pronounced when compared to the case of $\sigma = 1$ dB in Fig. 4.11(a). The cooperative centroid shows jittery behaviour in the start (lower SNR region) and becomes smoother as it moves closer to the source. The cooperative team remained cohesive and its expanse was regulated at the same average value of half the attraction radius in Fig. 4.12(a) as was the case for $\sigma = 1$ dB. This substantiates the effectiveness of the cooperative Bio-CAST in regulating the team expanse in extremely noisy conditions. The expanse of the individualistic team grew immensely for the case of $\sigma = 6$ dB where it peaks around 775 m.

4.4.3 Absence of Source

It is of interest to see how a cooperative team behaves in case the source signal disappears for some time. The primary concern in such a case is agents breaking away from the team. Figure 6.9(a) and Fig. 6.9(b) show the trajectories of all the agents in such a case during a 12 h interval for the individualistic team and the cooperative team respectively. The individualistic team's expanse gradually increases as shown in Fig. 4.12(b) where offshoots of agents breaking away from the team can be seen in Fig. 6.9(a). The cooperative team is regulated at the same expanse value as was the case in Fig. 4.11(a) when a source signal is present.

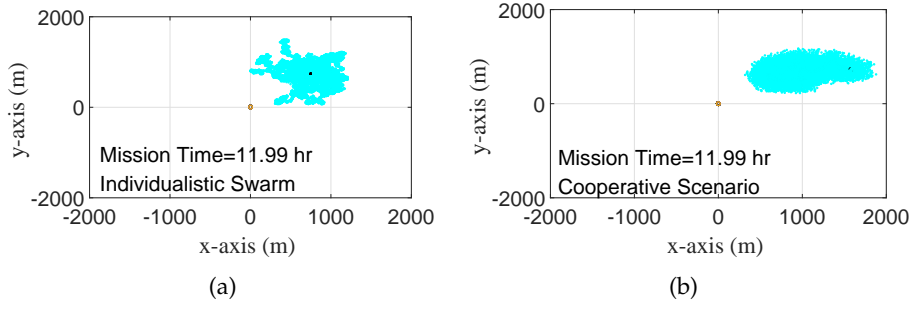
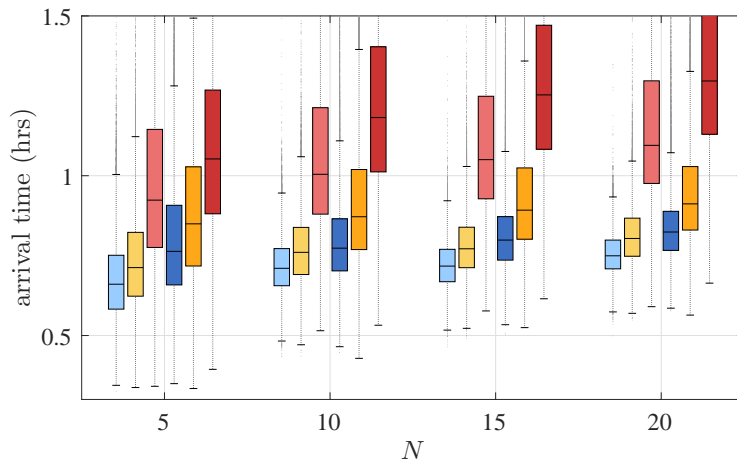


Figure 4.13. Trajectories of all the agents over a time interval of 12 h when there is no source signal present: (a) Individualistic team. (b) Cooperative team.

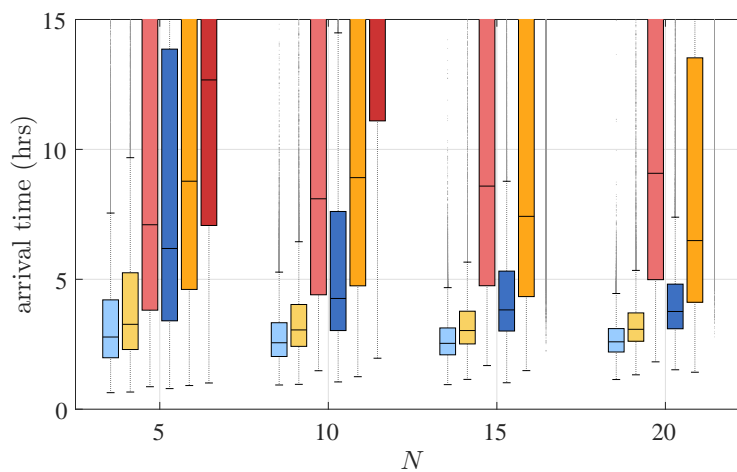
4.4.4 Neighbour-majority Detection Sensitivity

Since the cooperative Bio-CAST relies on agent's ability to detect the neighbour majority in right or left half, it is important to see if Bio-CAST is robust against detection noise. Given the neighbour detection can be implemented via different sensing mechanisms, we do not assume a specific distribution function as the noise model for the two sensors. Instead, we assume that an agent can make the correct decision between two available options with probability, p and the wrong decision with probability, $1 - p$. For example $p = 0.9$ means that an agent detects the correct half (right or left) having the majority of the neighbours 90 % of the instances on average.

The arrival time performance for $\sigma = 1$ dB is shown in Fig. 4.18(a). Attraction radius, $r_{GC} = 500$ m handles the detection noise better than $r_{GC} = 300$ m for all p considered. Also, for both attraction radii, the performance improves with increasing team size for $p = 1.00$ and $p = 0.90$. However for $p = 0.70$, there is a subtle degradation in performance as team size increases. Similarly for $\sigma = 6$ dB in Fig. 4.18(b), for $p = 1.00$ and $p = 0.90$, performance improves with the increasing team size. However, for $p = 0.70$ there is a subtle degradation for $r_{GC} = 500$ m but catastrophic for $r_{GC} = 300$ m.



(a)



(b)

■ 500m, $p = 1$
■ 500m, $p = 0.9$
■ 500m, $p = 0.7$
■ 300m, $p = 1$
■ 300m, $p = 0.9$
■ 300m, $p = 0.7$

Figure 4.14. Comparative arrival time performance for noiseless and noisy passive sensing of the neighbour-majority: (a) $\sigma = 1$ dB. (b) $\sigma = 6$ dB.

We can say that below a certain threshold for p , performance starts degrading instead of becoming better as team size increases. Also, the magnitude of the improvement or the degradation is a function of the attraction radii. A larger attraction radius, i.e., more samples of uncertain estimates, is better than a smaller attraction radius.

4.4.5 Initialization Distance Sensitivity

In real world applications, initialization distance may or may not be a controllable parameter. Hence it is important to see if the optimized parameter values for a specific initialization distance scales well with uncertainty in initialization distance. In Fig. 4.15, for $r_{GC} = 300$ m, we show results for effect on performance for optimized parameter values for an initialization distance of 1000 m along with 40 % increase and decrease. It can be seen that the optimized collective behaviour scales well with change in the initialization distance for both $\sigma = 1$ dB and $\sigma = 6$ dB and the performance becomes better as the team size grows.

4.4.6 Agent Loss

Given the extensive discussion on invariability of the optimized parameter values in team size in Section 4.3, the robustness of the algorithm against agent loss is implicit in the analysis carried out for different team sizes in the preceding subsections. For example, let us take the example of the arrival time performance in Fig. 4.10. As discussed in Section 4.4.1, the performance remained consistent in the range of 10 to 20 agents. However, as the team size reduces to $N = 5$, there is a significant relative degradation in performance. For team sizes $N < 5$, since the optimized parameters' behaviour is different than the estimated optimized model in (4.16) and comparatively more individualistic, the algorithm's performance may substantially degrade if an agent loss happens for a small team, e.g., $N = 5$. To investigate this, let us compare the cooperative team's performance following (4.16) for $N = 5$ against the individualistic team's performance as team size is reduced from 5

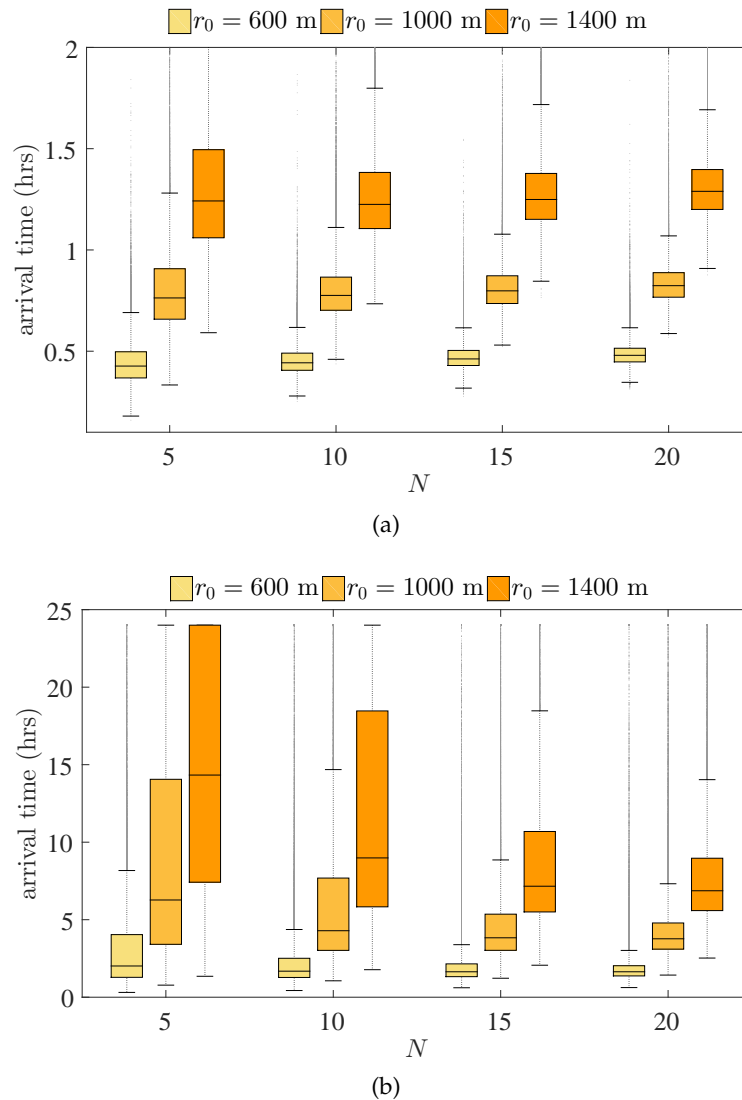


Figure 4.15. Comparative arrival time performance for increasing initialization distances with optimized solution for 1000 m: (a) $\sigma = 1$ dB. (b) $\sigma = 6$ dB.

agents to 1 agent. As expected, there is a gradual performance degradation for the cooperative team until $N = 3$ where its performance is almost identical to the individualistic team in Fig. 4.16. However, the performance degradation is not catastrophic and the cooperative team optimized for $N = 5$ handles the smaller teams gracefully.

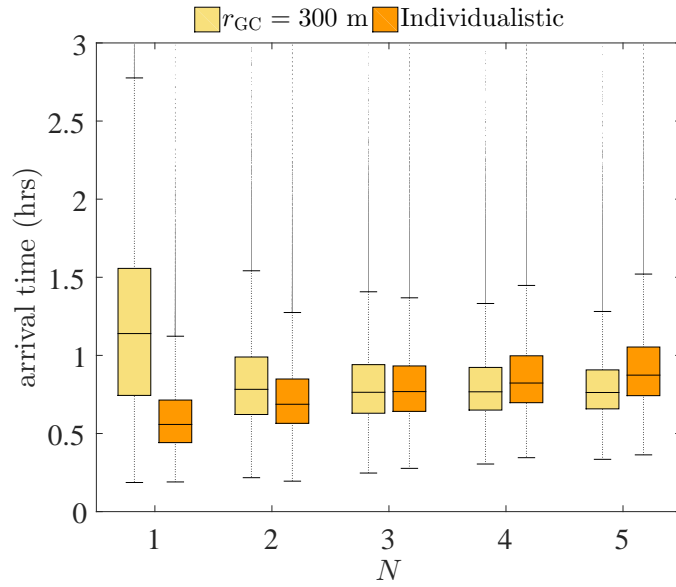


Figure 4.16. The arrival time performance shown for initialization distance, r_0 of 1000 m and $\sigma = 1$ dB for a cooperative team with $r_{GC} = 300$ m and an individualistic team.

4.4.7 Real-robot Analysis

The state of the art in using real-robot experiments in multi-agent or swarm robotics has been effectively discussed in [16, p. 14] along with the classification of such experiments into two types, i.e., *proof-of-concept* experiments and *extensive* experiments. Proof-of-concept real-robot experiment was conducted to validate the robustness of the collective behaviour against realistic noise patterns in sensors and actuators of the robots. Trial involving 4 Swarmbots operating as surface vehicles (Fig. 3.1), was conducted in Pandan Reservoir, Singapore, in light to gentle breeze conditions (Beaufort number 2 to 3). Global Positioning System (GPS) (accuracy of less than or equal to ± 10 m) was used as a virtual sensor to simulate the spatial acoustic intensity, following the source model in Section 3.2.1 and $\sigma = 1$ dB. A WiFi network was used to simulate the passive sensing of an agent's local-neighbourhood. Empirical results in Pandan Reservoir suggest a communication range of less than 50 m between

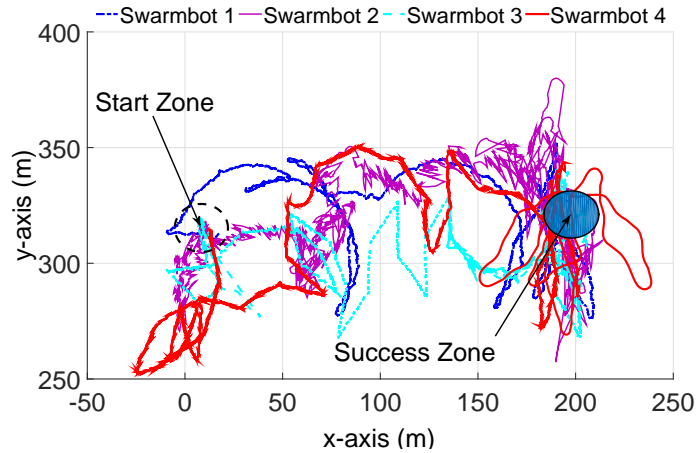


Figure 4.17. Trajectories of 4 Swarmbots initialized 200 m away from the source.

a Swarmbot and the WiFi router. The starting zone, having a radius of 10 m, was centered around ($1^{\circ}19'7.68''\text{N}$, $103^{\circ}44'15.72''\text{E}$) as shown in Fig. 4.17 and was approximately 200 m away from the success zone, having a radius of 10 m, centered around ($1^{\circ}19'6.24''\text{N}$, $103^{\circ}44'21.84''\text{E}$).

The team was initialized 200 m away from the source. The control parameters were first optimized for the given conditions and the optimized parameters, i.e., $T^* = 20$ s, $\eta^* = 0.70$, $\theta_c^* = 134^{\circ}$ and $\sigma_{\theta_c}^* = 0^{\circ}$ were downloaded into Swarmbots. The trajectories for the four Swarmbots are shown in Fig. 4.17. The qualitative similarity in trajectories can be seen when we compare this result with the case of Fig. 4.11(b) and Fig. 4.11(f). The trajectories remained directed towards the source as was the case for the simulations. The last arrival time was 0.186 h (within simulated missions' 25th percentile: 0.16 h and 75th percentile: 0.23 h) and the individual arrival times of each Swarmbot were 0.186, 0.113, 0.153 and 0.1784 h.

4.4.8 Passive Sensing vs. Explicit Communication

Passive sensing based social behaviours using neighbour-majority information lose a lot of information when compared to the lossless explicit communication based social behaviours using precise inter-agent position information (see Section 2.2). We compare the localization performance of passive sensing based Bio-CAST against an optimized explicit communication based counterpart using centroid based social behaviours (see Section 2.2.2). The reason for choosing the centroid based social behaviours over the unit-vector based social behaviours is their marginally superior performance [75].

The comparative arrival time performance for $\sigma = 1$ dB is shown in Fig. 4.18(a). For attraction radius, $r_{GC} = 500$ m, the performance difference between passive sensing and explicit communication is not so significant. However, for $r_{GC} = 300$ m, the explicit communication based counterpart is significantly better for all team sizes considered. Interestingly, for $\sigma = 6$ dB and for attraction radius, $r_{GC} = 500$ m in Fig. 4.18(b), passive sensing works marginally better than explicit communication for $N > 5$. However, for $r_{GC} = 300$ m, the explicit communication based counterpart is significantly better for all team sizes considered as was the case for $\sigma = 1$ dB.

Given the significant information loss due to passive sensing and the cost of implementing explicit communication underwater, the marginal performance degradation in case of the optimized case of $\sigma = 1$ dB is an intuitive and a satisfactory outcome. However, it is interesting to note that when the optimized solution is validated against a higher noise level such as $\sigma = 6$ dB, the passive

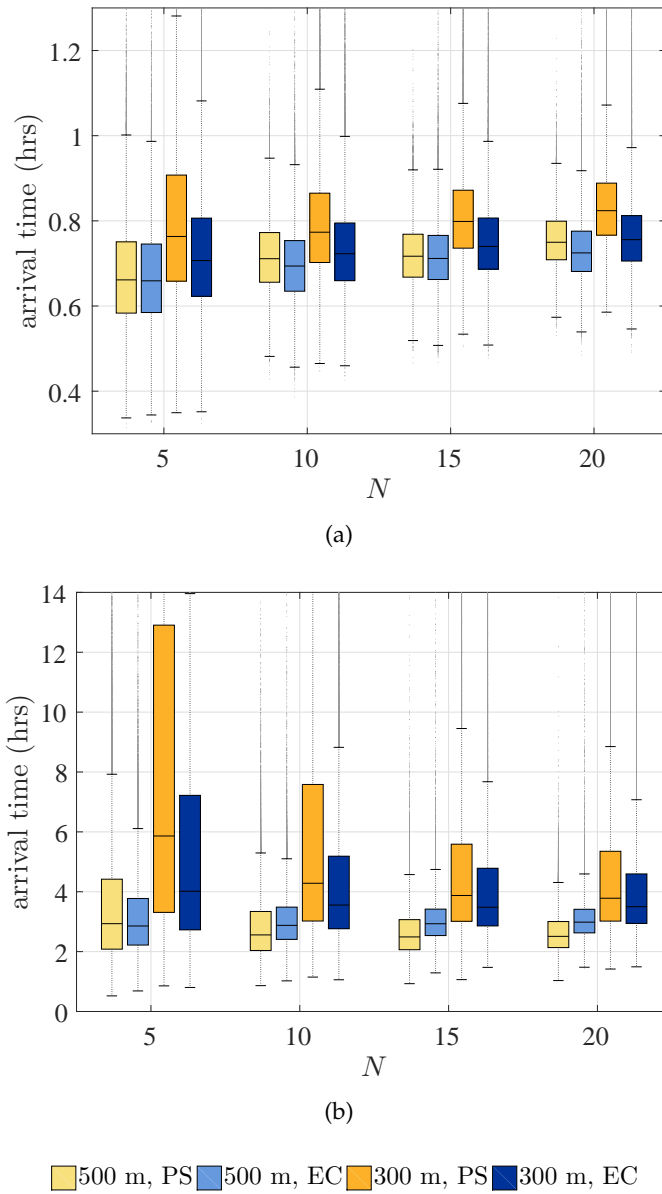


Figure 4.18. Comparative arrival time performance for passive sensing (PS) vs. explicit communication (EC) based social behaviours: (a) $\sigma = 1$ dB. (b) $\sigma = 6$ dB.

sensing strategy shows more robustness than the explicit communication based strategy.

4.5 Conclusion

A distributed source localization algorithm was presented by the name of Bio-inspired Control Algorithm for Small Teams (Bio-CAST). The algorithm

uses passive sensing to invoke collective behaviour in a team where each agent is assumed to have only one sensor for gradient sensing. There are one individualistic and two social behaviours that constitute Bio-CAST. Inspired by the biased random-walk of a bacterium performing chemotaxis, uncertainty was introduced in an agent's decision making in the individualistic model of [75]. The aim was to investigate the role of uncertainty in decision making both at the individualistic and the collective level. Based on the extensive optimization that was carried out on a range of team sizes, initialization distances and attraction radii, no evidence supported that uncertainty in decision making played a beneficial role at the collective level. It was only the individualistic teams that benefitted marginally from uncertainty in decision making for larger initialization distances.

The optimization results also showed that the optimized behaviours of cohesive teams which invoke collective behaviour remain nearly constant in team size. This helped develop a simple model for the optimized Bio-CAST which captures variation in the optimized behaviours as a function of the initialization distance and the attraction radius. Attraction radius, a key parameter for the long-range attraction social behaviour, is critical for invoking collective behaviour in a team. Physical world limits the range of a sensor and hence attraction radius cannot have an arbitrarily large value. The optimization data helped us identify the finite ratio of the attraction radius to the initialization distance that boosts maximum localization performance for the cooperative team. The break-even attraction radius or the minimum ratio of the attraction radius to the initialization distance was also identified where the localization performance of a cooperative team becomes nearly identical to the individualistic team. It was shown that as the attraction radius decreases

from the maximum value to the break-even point, a larger team is required to invoke collective behaviour.

Simulated experiments in a realistic underwater source localization scenario validated the collective behaviour against various ambient conditions, e.g., strong multipath interference in gradient sensing due to environment variability, noise in neighbour-majority detection, loss of agents and loss of the source signal. Statistical analysis of the arrival time in these ambient conditions showed that the cooperative team is more robust as its size and attraction radius increases. The analysis also showed that the uncertainty in arrival time decreases both in team size and attraction radius; an important aspect of swarm engineering where a multi-agent system is expected to complete the desired task reliably and on time [135]. Investigation of team's trajectories and expanse reveal that a cooperative team's cohesion is well regulated during the simulated experiments and no agents break away from the team. Furthermore, proof-of-concept real-robot experiment validates the optimized Bio-CAST against realistic noise patterns in sensors and actuators of the robots.

The localization performance of the passive sensing based Bio-CAST was also compared against an optimized explicit communication based counterpart using centroid based social behaviours. Considering the significant information loss due to passive sensing and the cost of implementing explicit communication underwater, passive sensing strategy results in only a marginal performance degradation as compared to the explicit communication strategy for the optimized case of $\sigma = 1$ dB. However, it is interesting to note that when the optimized solution is validated against a higher noise level such as $\sigma = 6$ dB, the passive sensing strategy is more robust than the explicit communication strategy.

Chapter 5

Adaptive Temporal Sampling based Multi-Agent Source Localization

The material in this chapter is an extended version of the author's previously published work [76].

5.1 Background

In [76], an adaptive temporal sampling strategy was proposed where sampling time is a function of sensed intensity values, referred to as Intensity based Adaptation (IbA) in this thesis. IbA improved the performance of Bio-CAST in [75] which was originally based on Static temporal Sampling (SS). In [76], IbA was assumed to be an arbitrary non-linear function of the sensed intensity values. The performance of Bio-CAST against common noise sources was not validated and only a team size of 10 agents was considered. In this thesis, these gaps are addressed where IbA along with other behaviours of an agent are optimized across a range of team sizes, initialization distances and neighbourhood radii. An optimized shape for the sampling function is identified which emerges from the optimization data. Analytical model is developed as an estimate of the agent's optimized behavioural parameters for the updated IbA. The resulting collective behaviour from the analytical model is validated against varying noise sources in a realistic source localization scenario. It is revealed in the robustness analysis that IbA is sensitive to high

ambient noise such as strong constructive or destructive multipath interference due to environment variability.

To address the noise sensitivity of IbA, Connectivity based Adaptation (CbA) is introduced which varies the optimized adaptive sampling times of IbA based on an agent's estimate of number of its neighbours within a local neighbourhood. Effectively, CbA regulates the expanse of the team by eliminating the number of agents breaking away from the team as a mechanism for robust behaviour. The combined strategy which is denoted as IbA+CbA shows remarkable robustness against strong multipath interference as well as outperforms SS or IbA in all the other test scenarios considered in this chapter. Note that all the comparisons in this thesis consider optimized strategies.

5.2 Optimization Setup

The optimization process assumes the experimental setup and GA settings as stipulated in Section 3.2. For the constant parameters, refer to the settings given in Table 3.1. We optimize the behavioural parameters of the localization algorithm, i.e., source bias coefficient η , mean of the correction-angle θ_c , its associated SD σ_{θ_c} and the static sampling time T or the associated coefficients of the adaptive sampling time strategy ($a_\tau, b_\tau, c_\tau, \beta_\tau$, see Section 5.3) for a range of team sizes, initialization distances and attraction radii as given in Table 3.1. The bounds for the optimization parameters are given in Table 5.1. The range of η has been truncated because less than 50% of its weight results in a failure to localize the source. The noise level, σ , in the agent's received intensity levels has been set to 1 dB.

5.3 Intensity based Adaptation

Intensity based Adaptation (IbA) is the adaptive temporal sampling approach that updates the synchronous Static Sampling (SS) approach given in (4.1) and (4.2) for TD and GC modules as a function of the sensed intensity values. IbA replaces the constant sampling time T with an adaptive sampling time, $\tau_n := t_{i+1} - t_i$ for an n^{th} agent, where i^{th} sample is taken at time, t_i , and $(i + 1)^{\text{th}}$ sample is taken at time, $t_i + \tau_n$. In [76], the adaptive sampling time was chosen as a Negative Sigmoid (NS) function of the received mean intensity as

$$\tau_n = \frac{a_\tau}{1 + \exp\{c_\tau(\hat{I}_n(t_i) - b_\tau)\}} + T_{\min} \quad (5.1)$$

where T_{\min} is the minimum sampling time and $a_\tau + T_{\min}$ is the maximum sampling time, $c_\tau, b_\tau \in \mathbb{R}^+$ are parameters which respectively determine the rate-of-transition and the mean value of \hat{I}_n around which the transition starts and ends. Let us refer to (5.1) as IbA-NS.

Intuition behind using an adaptive temporal sampling approach is based on the relationship between the initialization distance and size of the success zone. The radius of the success zone, r_s , is generally very small as compared to r_0 . Starting hundreds of meters away from the source, an agent thrives on larger T to improve its Decision Accuracy (DA), i.e., the probability of detecting the correct gradient in presence of noise. However as large a T would be, it will be as difficult to enter inside a success zone with a small radius. This can be seen in Fig. 5.1(a) where the optimized sampling times of SS get saturated after the initialization distance is increased beyond a certain limit whereas IbA-NS is not affected by the relationship of the initialization distance and the size of the success zone. It also means that the static approach will suffer from significantly

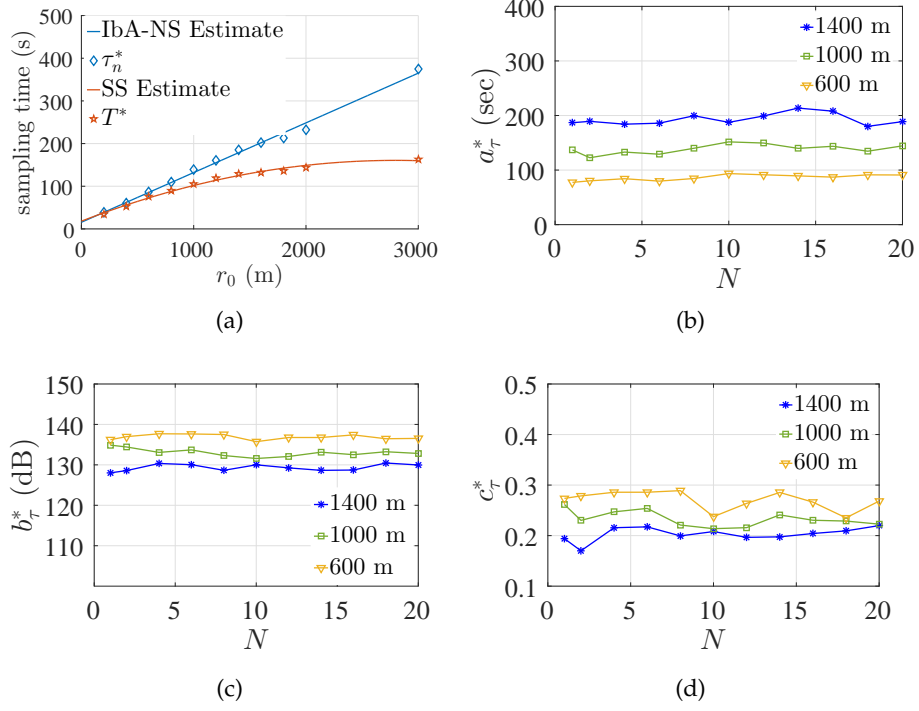


Figure 5.1. (a) Comparison between the maximum optimized sampling times for an adaptive temporal sampling strategy (IbA) versus a static temporal sampling strategy (SS). (b), (c), (d) : Optimization data for the parameters of IbA-NS as defined in (5.1) for varying initialization distances.

deteriorated DA as initialization distances increase further than the saturation point. The choice of a negative-sigmoid function in [76] was only arbitrary, however, in this chapter, the optimization data is used to find the optimized shape which comes out to be an exponential function.

5.3.1 Optimized Shape for IbA

Let us define the optimized behavioural vector as $\mathbf{w}^* = [\tau_n^*, \eta^*, \theta_c^*, \sigma_{\theta_c}^*]$ where we investigate $\mathbf{w}^*(r_0, r_{GC}, N)$, i.e., the optimized behaviours as a function of the initialization distance, attraction radius and team size respectively. The explored values of the parameters during the optimization process are given in Table 5.1.

First, let us set the attraction radius to infinity to ensure team connectivity and find $\tau_n^*(r_0, \infty, N)$ in (5.1) for varying initialization distances and team sizes. It is shown in Fig. 5.1(b) through Fig. 5.1(d) that the optimized parameters are nearly constant in team size, however vary significantly in initialization distance. Given the constant behaviour in N , we can plot in Fig. 5.2(a) the average response, $\bar{\tau}_n^*(r_0, \infty) = \sum_N \tau_n^*(r_0, \infty, N)$ for each initialization distance. The blue hexagrams in Fig. 5.2(a) depict the optimized sampling times for the intensity values at these initialization distances. The fall-offs of all the negative sigmoid curves are nearly identical. The shape of these fall-offs is also similar to the shape of the fall-off of the blue hexagrams suggesting an optimal shape which can be estimated by an exponential function as

$$f_{\text{exp}}(\hat{I}_n) = a'_\tau \exp(b'_\tau \hat{I}_n) \quad (5.2)$$

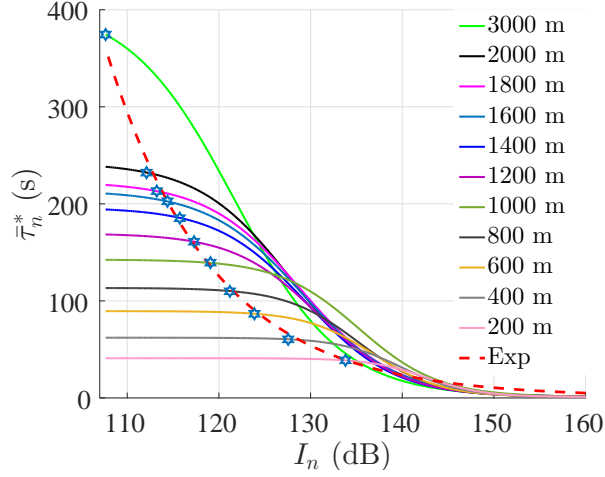
which is shown as red dashed line in Fig. 5.2(a) and Fig. 5.2(b) where $a'_\tau, b'_\tau \in \mathbb{R}^+$ (see Table 5.2 for parameter values). Let us modify (5.1) as

$$\tau_n = \beta_\tau [a'_\tau \exp(b'_\tau \hat{I}_n(t_i))] + T_{\min} \quad (5.3)$$

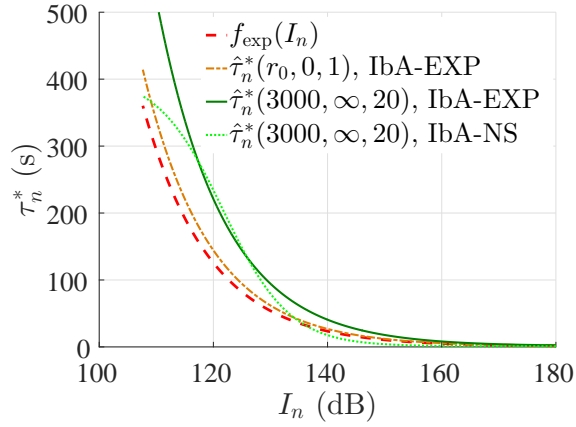
and redefine the optimized behavioural vector as $\mathbf{w}^* = [\beta_\tau^*, \eta^*, \theta_c^*, \sigma_{\theta_c}^*]$ where (5.3) can be used to calculate τ_n and investigate the optimized adaptive sampling coefficient, $\beta_\tau^* \in \mathbb{R}^+$, as a function of initialization distance, attraction radius and team size. For comparative purposes, let us refer to (5.3) as IbA-EXP.

5.3.2 IbA-EXP Optimization for Infinite Attraction Radius

The relative performances of IbA-EXP versus IbA-NS along with the respective optimized behaviours are compared in Fig. 5.3. Relative efficiency



(a)



(b)

Figure 5.2. (a) Estimating the optimized shape from the optimization data of IbA-NS. (b) Comparison of optimized IbA-EXP and IbA-NS.

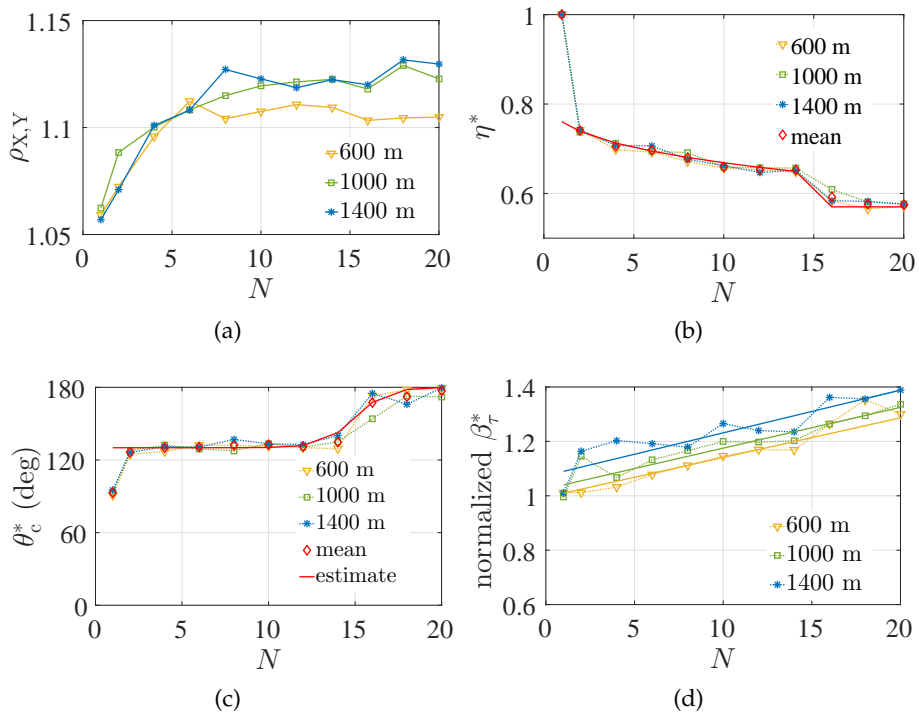
is defined as

$$\rho_{X,Y} = \frac{\text{Mean arrival time for } \mathbf{w}_Y^*}{\text{Mean arrival time for } \mathbf{w}_X^*} \quad (5.4)$$

where \mathbf{w}_X^* is the optimized behavioural vector for strategy X, $\rho > 1$ if strategy X is more efficient than the strategy Y and vice versa. In Fig. 5.3(a), the relative efficiencies are shown where X is IbA-EXP and Y is IbA-NS. The relative efficiency of IbA-EXP increases over IbA-NS in team size as well as initialization distance.

Table 5.1. Explored values of the parameters during the optimization process

Param.	Description	Bounds
η	source bias coefficient	[0.5, 1]
θ_c	Mean of the correction angle	[0°, 180°]
σ_{θ_c}	SD of the correction angle	[0°, 90°]
T	Static Sampling Time	[1, 600] (s)
a_τ	Coefficient of Negative-Sigmoid Function	[1, 600] (s)
b_τ	Coefficient of Negative-Sigmoid Function	[0, 180] (dB)
c_τ	Coefficient of Negative-Sigmoid Function	[0, 5]
β_τ	Coefficient of Exponential Function	[0, 2]

**Figure 5.3.** IbA-EXP Optimization for infinite attraction radius and varying initialization distances: (a) Relative efficiency of IbA-EXP vs. IbA-NS. (b) Source bias coefficient. (c) Mean correction angle. (d) Adaptive sampling coefficient.

The behaviour of the optimized parameters, i.e., η^* and θ_c^* , as a function of team size and initialization distance for IbA-EXP are shown in Fig. 5.3(b) and

Table 5.2. Parameter and Root Mean Square Error (RMSE) values for respective equations

Eq.	Parameter Values	RMSE
(5.2)	$a'_\tau = 3.625 \times 10^6, b'_\tau = -0.086$	7.55 s
(5.5)	$a_\eta = -0.09736, b_\eta = 0.2889, c_\eta = 0.858, N_s(\infty) = 16$	0.007
(5.6)	$\theta_{c_{\max}} = 180^\circ, \theta_{c_{\min}} = 130^\circ, c_\theta = 1.10, N_s(\infty) = 16$	3.48°
(5.7)	$\hat{\beta}_\tau^*(r_0, 0, 1) = 1.15, a_\beta = 8.959 \times 10^{-9}, b_\beta = 2.23, c_\beta = 0.98, a'_\beta = 0.0146, b'_\beta = 1$	0.002
(5.8)	$a(r_{GC}) = 4.524 \times 10^5 r_{GC}^{-2.384} + 0.9078, b(r_{GC}) = 83.44 r_{GC}^{-0.9028} - 0.2331$	0.022
(5.12)	$\hat{\beta}_\tau^*(r_0, 0, 1) = 1.15, \hat{\beta}_{\tau_{\max}}^* = 1.53$	0.042

Fig. 5.3(c) respectively where they show identical behaviour in team size for different initialization distances. Optimal source bias values decrease in N , i.e., the team cohesion increases in team size. Also, there is a switching to higher cohesion values at about $N = 16$ which correlates with the switching in the optimized mean correction angles from 130° to 180° . This switching behaviour and the underlying correlation between the optimized source bias values and the mean correction angles is consistent with the SS approach in [75]. The optimized behaviour of the source bias and the mean correction angle can be estimated as

$$\hat{\eta}^*(r_0, r_{GC}, N) = \begin{cases} 1.00, & \text{for } N = 1 \\ a_\eta N^{b_\eta} + c_\eta, & \text{for } 2 \leq N < N_s(r_{GC}) \\ 0.57, & \text{for } N \geq N_s(r_{GC}) \end{cases} \quad (5.5)$$

$$\hat{\theta}_c^*(r_0, r_{GC}, N) = \begin{cases} 90^\circ, & \text{for } N = 1 \\ \frac{\theta_{c_{\max}} - \theta_{c_{\min}}}{1 + f(N)} + \theta_{c_{\min}}, & \text{for } 2 \leq N \leq 20 \end{cases} \quad (5.6)$$

where function, $f(N) = \exp[-c_\theta\{N - N_s(r_{GC})\}]$, and the estimates have been shown as solid red lines in Fig. 5.3(b) and Fig. 5.3(c) with red diamonds as a reference for the average response over considered initialization distances (see Table 5.2 for parameter values). The attraction radius, r_{GC} is not substituted with ∞ in (5.5) and (5.6) because these equations hold in general for limited attraction radius as well, as shown in the following subsection.

The adaptive sampling coefficient, β_τ^* , varies both in team size and initialization distance and can be estimated by the product of two separable functions as follows

$$\hat{\beta}_\tau^*(r_0, \infty, N) = \begin{cases} \hat{\beta}_\tau^*(r_0, 0, 1), & \text{for } N = 1 \\ \hat{\beta}_\tau^*(r_0, 0, 1)h(r_0)g(N), & \text{for } 2 \leq N \leq 20 \end{cases} \quad (5.7)$$

where $h(r_0) = a_\beta r_0^{b_\beta} + c_\beta$ and $g(N) = a'_\beta N + b'_\beta$ (see Table 5.2 for parameter values). The optimization data with the respective estimates for the normalized adaptive sampling coefficient, i.e., $\hat{\beta}_\tau^*(r_0, \infty, N)/\hat{\beta}_\tau^*(r_0, 0, 1)$, is given in Fig. 5.3(d). Note that the optimized response for a single individual, $\hat{\beta}_\tau^*(r_0, 0, 1)$, remains invariant in initialization distance. Hence, it is the interaction between the agents that increases the optimized maximum sampling times both in r_0 and N . It is known that the cooperation in a team grows either linearly, sub-linearly or super-linearly in team size [133] and that may be related to the the linear increase of sampling times in team

size. However, since we are assuming an infinite attraction radius and hence a guaranteed team connectivity, this behaviour changes significantly for limited attraction radius as discussed in the following subsection.

For reference, the optimized IbA-EXP and optimized IbA-NS for $\hat{\tau}_n^*(3000, \infty, 20)$ are shown in Fig. 5.2(b) where it can be seen that the fall-off for both the curves is very similar, however, since the exponential function does not flatten-off at higher values like the negative sigmoid, the maximum optimized sampling times for IbA-EXP are much larger than for the case of IbA-NS; resulting in IbA-EXP being a more efficient strategy.

5.3.3 Optimization Results for Limited Attraction Radius

Let us express the attraction radii as ratios of the initialization distance and show the optimization results in Fig. 5.4. Though estimates are developed for the optimized behaviours considering an initialization distance of 1000 m, it is shown at the end of this subsection that these estimations hold in general.

The relative efficiencies where X is IbA-EXP and Y is the optimized individualistic IbA-EXP (η set to 1.00 during optimization) for varying attraction radii are plotted in Fig. 5.4(a). The relative efficiency increases both in team size and $r_{GC} \geq 0.3r_0$. As the attraction radius falls below 30% of the initialization distance, there are only marginal returns compared to using an individualistic team. We can correlate this with the optimized behaviours of source bias values in Fig. 5.4(b). For $r_{GC} \geq 0.3r_0$, the optimized cohesion values are decreasing in N , i.e., higher team cohesion as team size increases and the trend is nearly identical to the case of attraction radius set to infinity. However, the team cohesion decreases with team size if we consider $r_{GC} \leq 0.2r_0$, i.e., more individualism is preferred in such cases.

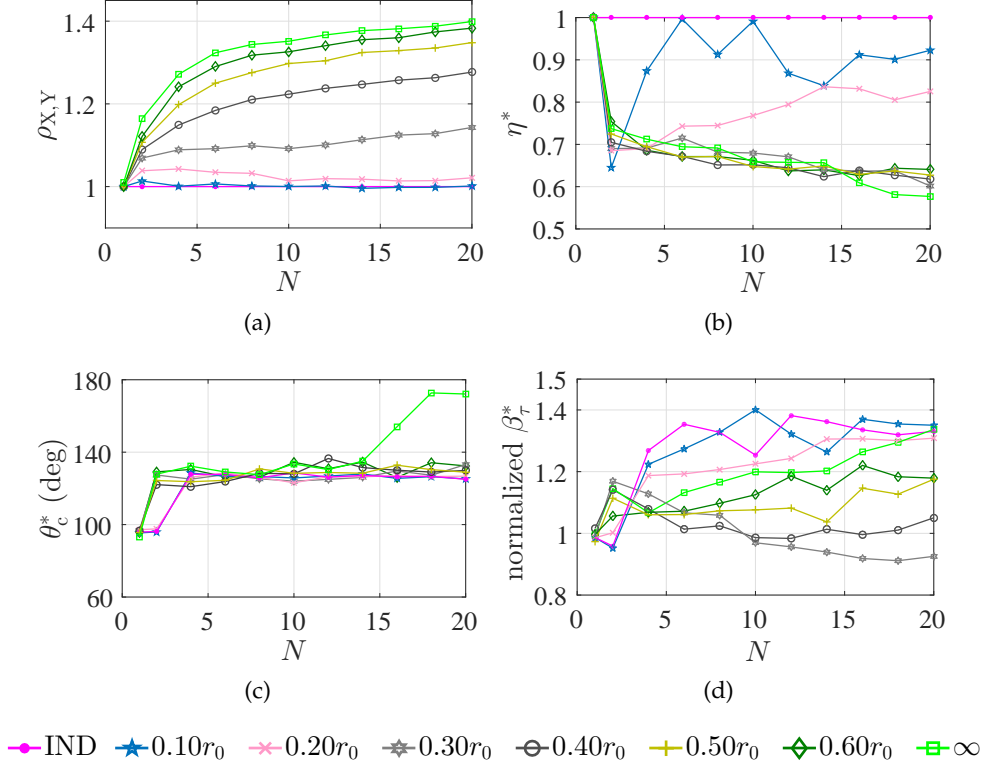


Figure 5.4. IbA-EXP Optimization for limited attraction radius as a function of initialization distance, $r_0 = 1000$ m (see legend at the bottom of the figure for values of the considered attraction radii, IND means an individualistic team, i.e., $\eta = 1, r_{GC} = 0$): (a) Relative efficiency of IbA-EXP vs. IbA-NS. (b) Source bias coefficient. (c) Mean correction angle. (d) Adaptive sampling coefficient.

The only difference between the optimized source bias values for the limited attraction radius in the range of 30% to 60% of the initialization distance and the infinite attraction radius is the switching team size where $N_s(\infty)$ is 15 agents. This correlates with the optimized mean correction angle values in Fig. 5.4(c). However, for the considered range of attraction radius, $N_s(r_{GC})$ is greater than the maximum team size considered in this chapter. For example for $r_{GC} = 0.6$, N_s is 24 agents and it keeps on increasing as we decrease the attraction radius. We can estimate the optimized source bias coefficient and the mean correction angle for limited attraction radius using (5.5) and (5.6) respectively.

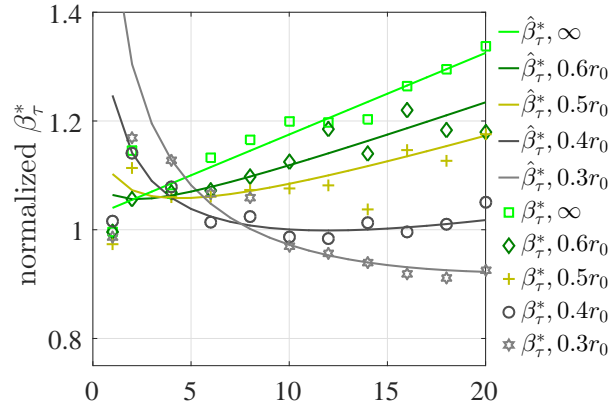
The adaptive sampling coefficient, β_τ^* , varies both in team size and attraction radius. It is interesting to note that as the attraction radius decreases from infinity, the optimized sampling times decrease until r_{GC} is $0.3r_0$ and then there is an abrupt increase where the optimized sampling times approach the individualistic case. It is also worth noting that even with the infinite attraction radius, the cooperative teams thrive on smaller sampling times than the individualistic teams. As large a sampling time would be, an agent would risk breaking away from the team and hence as the attraction radius decreases, the associated risk increases. This explains why teams with decreasing attraction radii have smaller sampling times to help keep the team cohesive. We can estimate this behaviour for attraction radius, $r_{GC} > 0.3r_0$, as

$$\hat{\beta}_\tau^*(r_0, r_{GC}, N) = \begin{cases} \hat{\beta}_\tau^*(r_0, \infty, N), & \text{for } N = 1 \\ f(r_{GC})\hat{\beta}_\tau^*(r_0, \infty, N), & \text{for } 2 \leq N \leq 20 \end{cases} \quad (5.8)$$

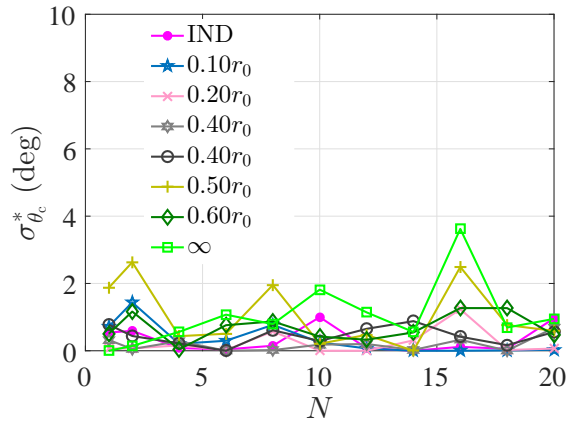
where the function, $f(r_{GC}) = a(r_{GC})N^{-b(r_{GC})}$ (see Table 5.2 for parameter values) and the estimation curves are shown in Fig. 5.5(a).

So far we have assumed an initialization distance of 1000 m as a special case for estimating the optimized behaviours. However, it was shown in the preceding subsection that all the behavioural parameters are insensitive to initialization distance other than the adaptive sampling coefficient, β_τ (see Fig. 5.3(d)). Hence to make sure that the worked out estimations are valid for other initialization distances, let us apply (5.8) to initialization distances of 600 m and 1400 m in Fig. 5.6(a) and Fig. 5.6(b) to show its generality.

The behaviour of the optimized variance, $\sigma_{\theta_c}^*$ is shown in Fig. 5.5(b) for an initialization distance of 1000 m. It shows the same behaviour from infinite



(a)



(b)

Figure 5.5. (a) Estimation of optimized adaptive sampling coefficient. (b) Behaviour of optimized SD of correction angle.

to zero attraction radius, i.e., there is no correlation with the team size or the attraction radius. Optimization results for initialization distances of 600 m and 1400 m show similar results. The average values across N is less than 2° for all instances of attraction radius or initialization distance which is comparable to the heading sensor noise. Given $\sigma_{\theta_c}^*$ has an effect on agent's heading every τ_n seconds, its optimized behaviour does not seem significant when compared with the compass error of 1° which is being added every 1 s. Hence we can

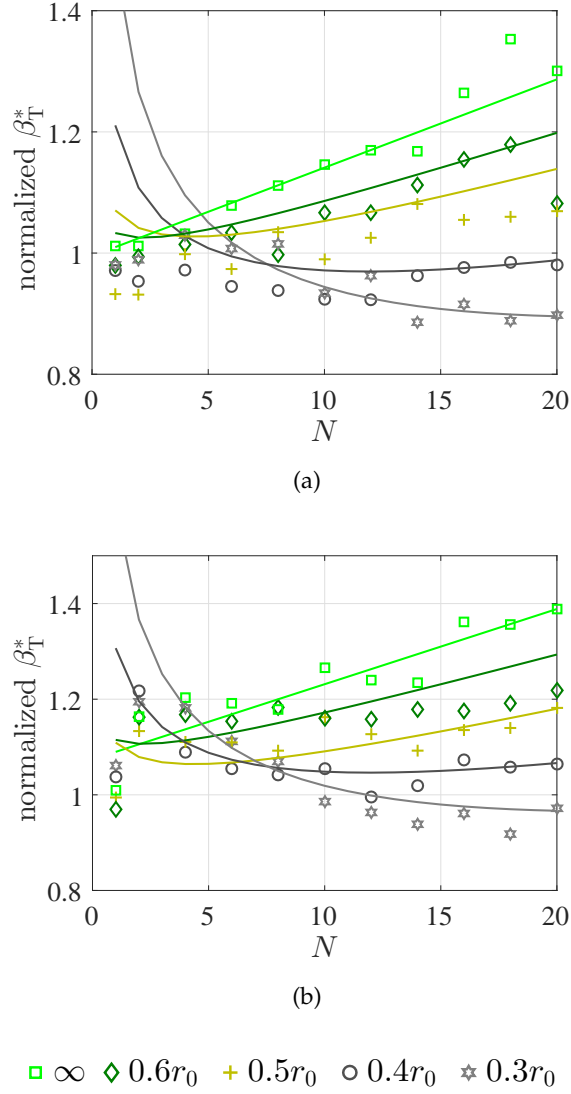


Figure 5.6. Estimation (shown in solid lines) for optimized values (see legend below) of normalized adaptive sampling coefficient: (a) For initialization distance of 600 m and $r_0 \geq 0.3r_0$. (b) For initialization distance of 1400 m and $r_0 \geq 0.3r_0$.

estimate the optimized response as

$$\hat{\sigma}_{\theta_c}^*(r_0, r_{GC}, N) = 0 \quad (5.9)$$

For a range of initialization distances, attraction radii and team sizes, the estimated optimized behaviours were formulated for the cooperative teams ($r_{GC} > 0.3r_0$) in this subsection. The source bias coefficient, $\hat{\eta}^*$, mean correction

angle, $\hat{\theta}_c^*$, adaptive sampling coefficient, $\hat{\beta}_\tau^*$, and the SD correction angle, $\hat{\delta}_{\theta_c}^*$, are defined by (5.5), (5.6), (5.8) and (5.9) respectively.

5.3.4 Estimated Optimized Behaviour for Individualistic Teams

Since the attraction radii less than $0.30r_0$ do not give significant advantage over the individualistic case, we can estimate them as an individualistic case. Following the discussion on the optimized data in the preceding subsections, we can write the following estimated optimized behaviours for the individualistic teams or for $r_0 < 0.3r_0$ as follows (see Table 5.2 for parameter values)

$$\hat{\eta}^*(r_0, 0, N) = 1.00 \quad (5.10)$$

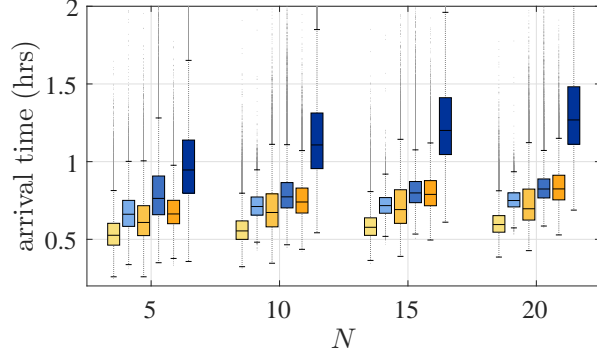
$$\hat{\theta}_c^*(r_0, 0, N) = \begin{cases} 90^\circ, & \text{for } 1 \leq N \leq 2 \\ 130^\circ, & \text{for } 2 < N \leq 20 \end{cases} \quad (5.11)$$

$$\hat{\beta}_\tau^*(r_0, 0, N) = \begin{cases} \hat{\beta}_\tau^*(r_0, 0, 1), & \text{for } N = 1 \\ \hat{\beta}_{\tau_{\max}}^*, & \text{for } 2 \leq N \leq 20 \end{cases} \quad (5.12)$$

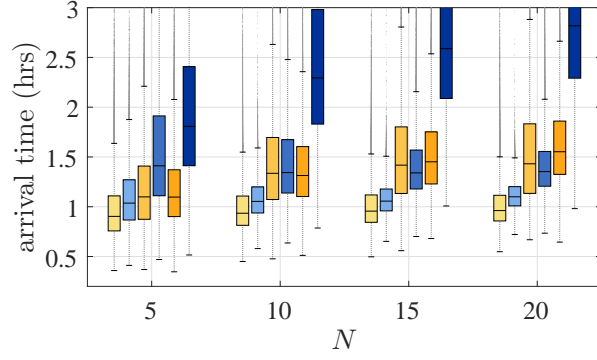
$$\hat{\delta}_{\theta_c}^*(r_0, 0, N) = 0 \quad (5.13)$$

5.3.5 Robustness Analysis

The performance of the collective behaviour resulting from the estimated optimized algorithm is validated for the cooperative and individualistic teams against $\sigma = 1$ dB and $\sigma = 2$ dB in Fig. 5.7(a) and Fig. 5.7(b) respectively. The cooperative teams have an attraction radius of $r_{GC} = 0.3r_0$ and $r_{GC} = 0.6r_0$ and the initialization distance has been set to 1000 m. The arrival time performance is shown using box-plots following the details given in Section 3.2.3.



(a)

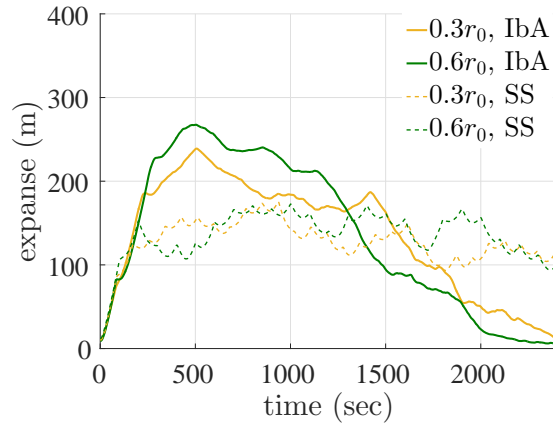


(b)

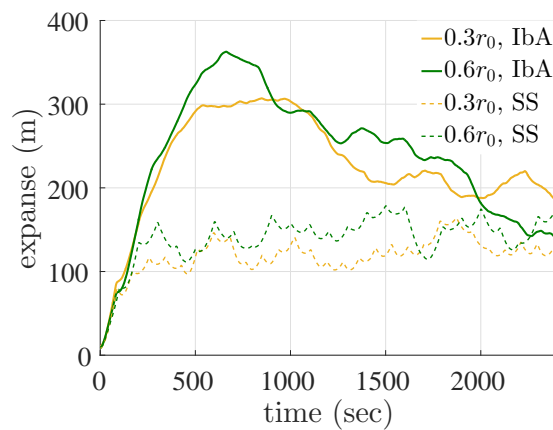
■ IbA, $0.6r_0$
■ SS, $0.6r_0$
■ IbA, $0.3r_0$
■ SS, $0.6r_0$
■ IbA, IND
 ■ SS, IND

Figure 5.7. Arrival time performance for IbA vs. SS arrival time performance for limited attraction radii, $r_{GC} = 0.3r_0$ and $r_{GC} = 0.6r_0$ and noise levels: (a) $\sigma = 1$ dB. (b) $\sigma = 2$ dB.

For $\sigma = 1$ dB, the case for which the optimization of the algorithm was carried out, IbA outperforms SS in all the scenarios in terms of median arrival times. However, when we double the noise, IbA still outperforms SS for larger neighbourhood of $r_{GC} = 0.6r_0$ and for the individualistic team but the median arrival times become nearly similar for $r_{GC} = 0.3r_0$. Considering the temporal sampling strategies, it comes as no surprise that IbA is more susceptible to environment noise than SS. More environment noise will contribute to much larger or smaller sampling times than the optimized ones where the larger sampling times may result in agents breaking away from the team. To see this, the team expanse (see Section 4.4 and (4.17) for definition) is plotted in



(a)



(b)

Figure 5.8. Team expande: (a) For $\sigma = 1$ dB. (b) For $\sigma = 2$ dB.

Fig. 5.8(a) and Fig. 5.8(b) for $\sigma = 1$ dB and $\sigma = 2$ dB respectively. We can see that the team expande for SS is well regulated for both the attraction radii and the noise scenarios. However, IbA is very sensitive to ambient noise for both the attraction radii resulting in a much larger team expande for $\sigma = 2$ dB as compared to $\sigma = 1$ dB.

5.4 Connectivity based Adaptation

For improving the performance of the cooperative teams in noisy environments, Connectivity based Adaptation (CbA) is introduced in this

section. CbA updates IbA based on an agent's estimation of the number of its neighbours within the attraction radius. The adaptive sampling time τ_n of IbA is replaced by the CbA regulated sampling time as

$$\tau'_n = \begin{cases} \tau_n \left(\frac{1}{1 + \exp\{-\hat{N}_{GC_n}(t) - N_c\}} \right) & \text{if } \hat{N}_{GC_n}(t) > 0 \\ \tau_n & \text{otherwise} \end{cases} \quad (5.14)$$

where $\hat{N}_{GC_n}(t)$ is the estimated number of neighbours of agent n within r_{GC} at time t , N_c is the critical number of neighbours, the sigmoid function is CbA which updates the IbA's adaptive sampling time, τ_n , following the definition as given earlier in Section 5.3 where the next sample for TD and GC modules, $i + 1$, is taken at time, $t = t_i + \tau'_n$.

Effectively, CbA decreases the originally calculated sampling time by IbA in case an agent's number of neighbours fall around the critical number of agents. This is to increase the decision-making frequency to improve the connectivity of the team, i.e., to reduce or ideally eliminate the number of agents breaking away from the team. As large the sampling time, the better an agent's DA and hence the more an agent travels before making another decision. However, there is no check in the meanwhile which would stop an agent from potentially breaking away from the team. If we consider the current heading of an agent, $\mathbf{d}_{W_n}(t)$, such that it is travelling in the direction of a potential breakaway, increasing the frequency of updating (4.7) as the number of neighbours drop biases the agent towards the team. To guarantee this behaviour, we can set $\theta_c = 0$ while (5.14) takes effect. However, in this chapter, the optimized behaviour is kept unchanged and it is shown that CbA eliminates the number of breakaways for

varying degrees of noise levels and hence addressing the sensitivity issues of IbA towards the ambient noise.

5.4.1 Optimization Results

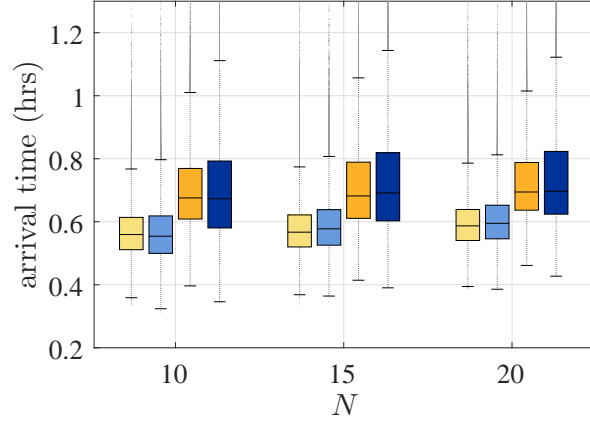
The critical team size, N_c , is optimized following the estimated optimized Bio-CAST for IbA as discussed in Section 5.3. The optimization is carried out for varying team sizes, ambient noise levels and a limited attraction radius of $r_{GC} = 0.3r_0$. No evidence was found for CbA being useful for team sizes, $N \leq 6$ agents. However, for $N = 8$, N_c^* was in a range of 4.6 to 5.1 and for $N \geq 10$ agents it varied within a range of 6.5 to 7.5 without any correlation with team size. We can estimate $\hat{N}_c^* = 7$ for $N \geq 10$ agents for the following analysis.

5.4.2 Robustness Analysis

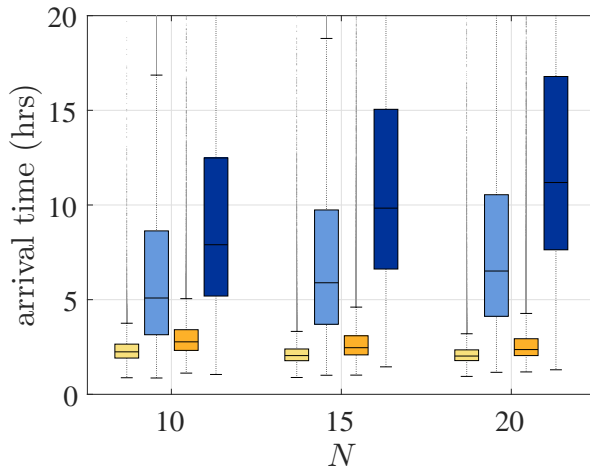
First, let us see what effect CbA has on IbA for $\sigma = 1$ dB, the noise level for which IbA was originally optimized. Limited attraction radius in the range of 30% to 60% of initialization distance is considered. Let us denote (5.14) as IbA+CbA and compare it with IbA in Fig. 5.9(a). It can be seen that IbA+CbA maintains the same median arrival times as of IbA but also marginally reduces the variance of the arrival time distribution.

As for $\sigma = 6$ dB which corresponds to strong constructive and destructive interference due to environment variability, IbA's performance is much degraded due to its sensitivity to noise. However, CbA adds remarkable robustness to the multi-agent system as shown in Fig. 5.9(b).

It has been highlighted earlier in Section 5.3.5 that SS is a more robust strategy than IbA for high ambient noise levels. Hence, let us compare performance of IbA+CbA against SS in Fig. 5.10(a) and Fig. 5.10(b) for $\sigma = 2$ dB



(a)



(b)

■ IbA+CbA, $0.6r_0$
■ IbA, $0.6r_0$
■ IbA+CbA, $0.3r_0$
■ IbA, $0.3r_0$

Figure 5.9. CbA compensated IbA (IbA+CbA) vs. IbA arrival time performance for limited attraction radii, $r_{GC} = 0.3r_0$ and $r_{GC} = 0.6r_0$ and noise levels: (a) $\sigma = 1$ dB. (b) $\sigma = 6$ dB.

and $\sigma = 6$ dB respectively. IbA+CbA outperforms SS for both the noise levels and attraction radii. Importantly, IbA+CbA shows performance at par with SS for half the attraction radius if we compare the case of $r_{GC} = 0.3r_0$ for IbA+CbA versus $r_{GC} = 0.6r_0$ in Fig. 5.10(a) and Fig. 5.10(b). Also, the median arrival times and the variance of the arrival time distribution improves for IbA+CbA as team size increases in Fig. 5.10(a) and Fig. 5.10(b).

5.4.2.1 Team Expand

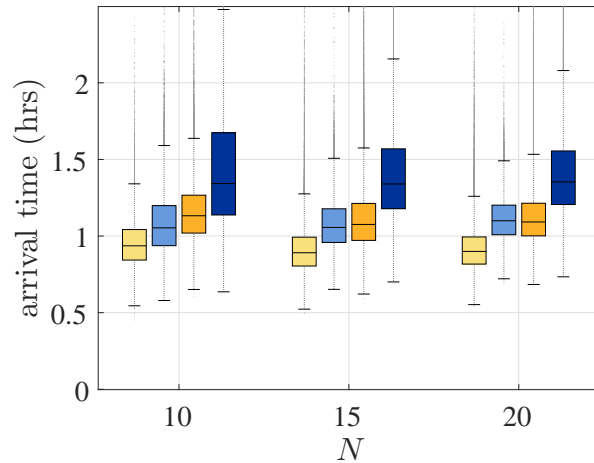
It was shown in Fig. 5.8(a) and Fig. 5.8(b) that as noise increases, the expand of the team also increases substantially due to increasing sampling times. However, with CbA updating IbA, it is no more the case as shown in Fig. 5.11(a) and Fig. 5.11(b) for noise levels $\sigma = 2$ dB and $\sigma = 6$ dB respectively. We can see that the expand is well regulated at nearly the same levels for each attraction radius even when the noise is increased three times. Also, the mean expand levels maintained by the multi-agent system increase with increase in the attraction radius. In other words, CbA maximizes the benefit of IbA's adaptive temporal sampling for a given attraction radius while ensuring a cohesive team.

5.4.2.2 Agent breakaways

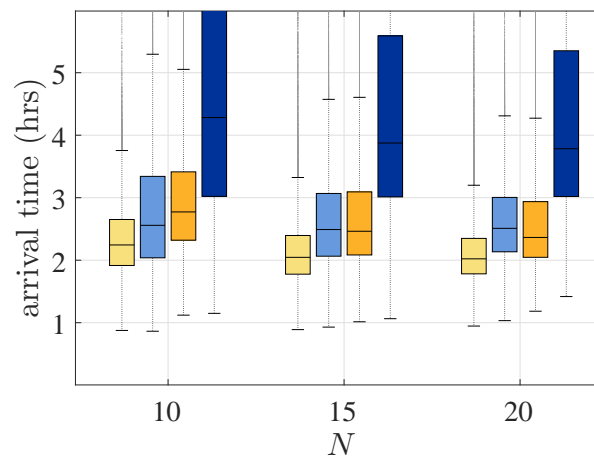
Finally, Fig. 5.12(a) and Fig. 5.12(b) show the number of breakaway agents for $\sigma = 2$ dB and $\sigma = 6$ dB respectively for a team size of 20 agents with $r_{GC} = 0.3r_0$. We can see that IbA+CbA eliminates the number of breakaway agents in both the scenarios whereas IbA suffers from increasing number of agents breaking away from the team as the noise increases.

5.4.2.3 Initialization Distance Sensitivity

As far as the problem statement discussed in this paper is concerned, the initialization distance can be controlled within a tight uncertainty range. However, it is desired that the optimized solution for a specific distance scales well for a wide range of distances. We conduct sensitivity analysis for an optimized solution for $r_0 = 1000$ m and $r_{GC} = 0.3r_0$ for a change of ± 400 m in Fig. 5.13(a) and Fig. 5.13(b) for $\sigma = 1$ dB and $\sigma = 6$ dB respectively. We can



(a)



(b)

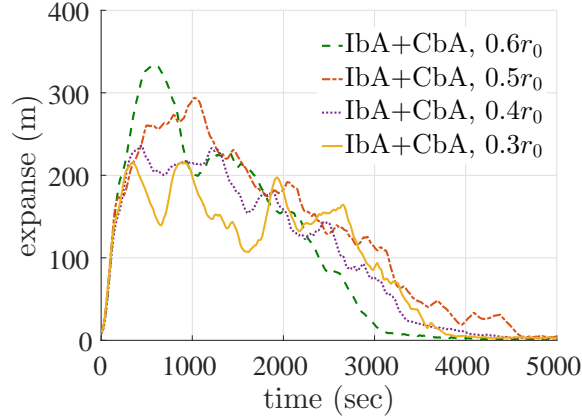
■ IbA+CbA, $0.6r_0$
 ■ SS, $0.6r_0$
 ■ IbA+CbA, $0.3r_0$
 ■ SS, $0.3r_0$

Figure 5.10. CbA compensated IbA (IbA+CbA) vs. SS arrival time performance for limited attraction radii, $r_{GC} = 0.3r_0$ and $r_{GC} = 0.6r_0$ and noise levels: (a) $\sigma = 2$ dB. (b) $\sigma = 6$ dB.

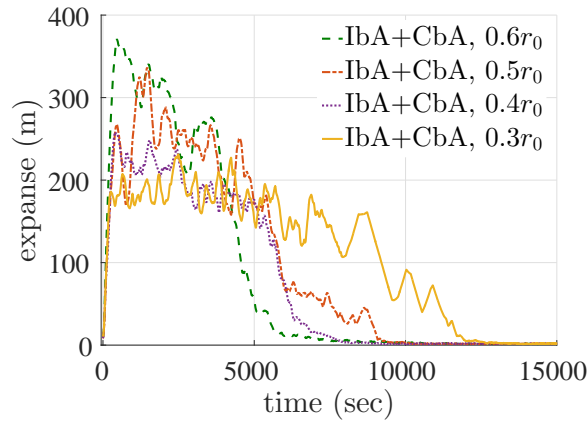
see that the optimized solution for both the IbA and IbA+CbA scales well with the change in distance.

5.4.2.4 Neighbour-majority Detection Sensitivity

Since the localization algorithm relies on agent's ability to detect the neighbour majority in right or left half, it is important to see if IbA+CbA approach is robust against detection noise. Given the neighbour detection



(a)

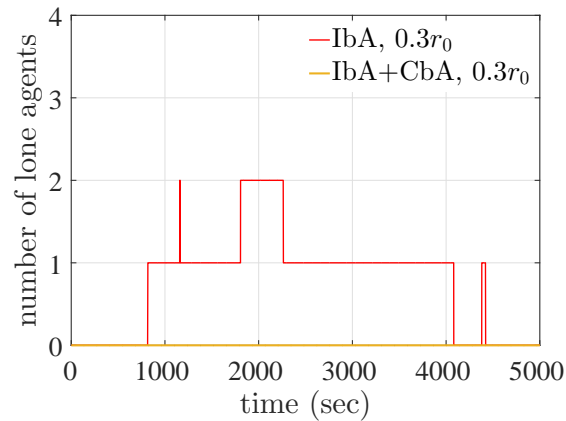


(b)

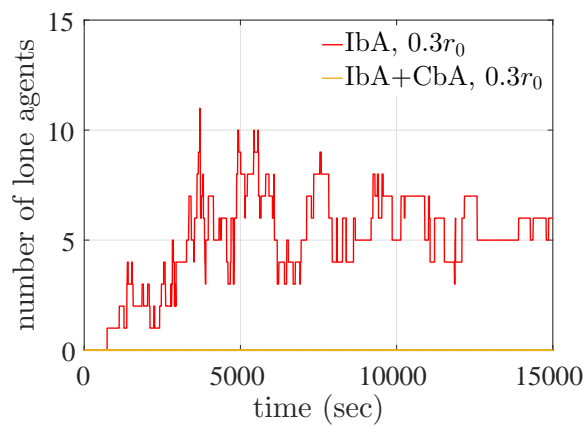
Figure 5.11. Expanse for CbA compensated IbA (IbA+CbA) during a localization mission for $N = 20$, varying attraction radii, $r_{GC} = 0.3r_0$ and $r_{GC} = 0.6r_0$ and noise levels: (a) $\sigma = 2$ dB. (b) $\sigma = 6$ dB.

can be implemented via different sensing mechanisms, we do not assume a specific distribution function as the noise model for the two sensors. Instead, we assume that an agent can make the correct decision between two available options with probability, p and the wrong decision with probability, $1 - p$. For example $p = 0.9$ means that an agent detects the correct half (right or left) having the majority of the neighbours 90 % of the instances on average.

The arrival time performance for $\sigma = 1$ dB and $\sigma = 6$ dB is shown in Fig. 5.14(a) and Fig. 5.14(b) respectively. Attraction radius, $r_{GC} = 0.6r_0$ handles the detection noise better than $r_{GC} = 0.3r_0$ for all p considered which means



(a)



(b)

Figure 5.12. Number of agents breaking away from a team during a localization mission for $N = 20$, $r_{GC} = 0.3r_0$ and noise levels: (a) $\sigma = 2$ dB. (b) $\sigma = 6$ dB.

that a larger attraction radius, i.e., more samples of uncertain estimates, is better than a smaller attraction radius. In fact, $r_{GC} = 0.6r_0$ for $p = 0.80$ performs better than $r_{GC} = 0.3r_0$ for $p = 0.90$. Overall, there was no catastrophic degradation in performance of the collective behaviour as detection accuracy was degraded for both cases of ambient noise. The only significant degradation in terms of arrival time variance is for the case of $p = 0.80$ and $r_{GC} = 0.3r_0$ for both $\sigma = 1$ dB and $\sigma = 6$ dB.

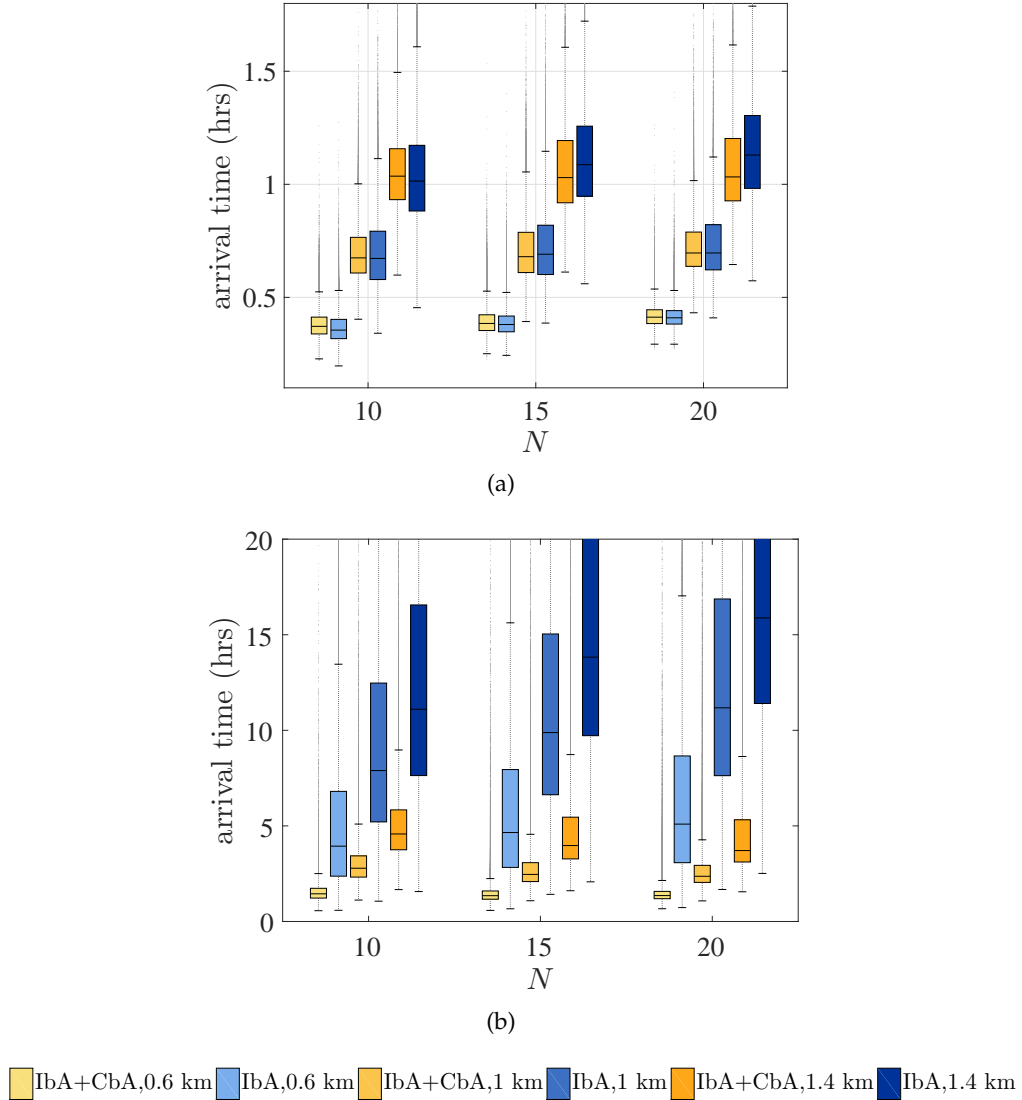
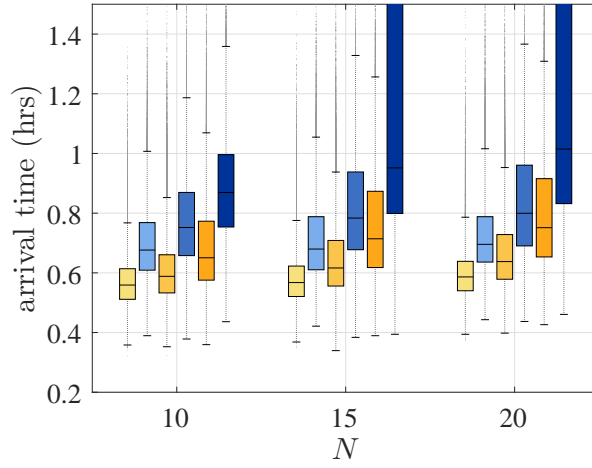


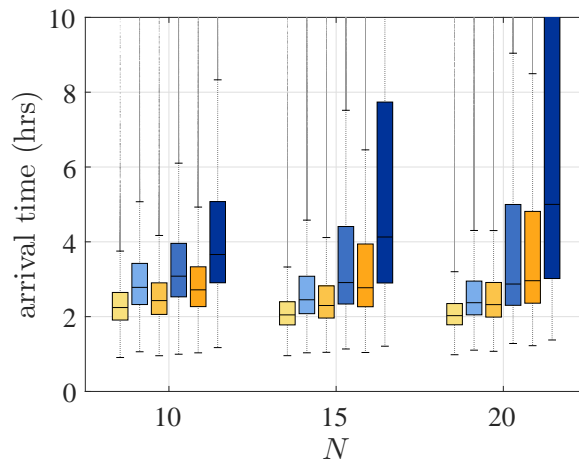
Figure 5.13. Initialization distance sensitivity analysis for optimized solution for $r_0 = 1000$ m and $r_{GC} = 0.3r_0$ and noise levels: (a) $\sigma = 1$ dB. (b) $\sigma = 6$ dB.

5.4.3 Passive Sensing vs. Explicit Communication

Now let us investigate the effect of the information loss in case of the passive sensing strategy on the localization performance when compared to the lossless explicit communication based counterpart. We compare the localization performance of passive sensing based IbA+CbA against an optimized explicit communication based counterpart using centroid based social behaviours (see Section 2.2.2).



(a)

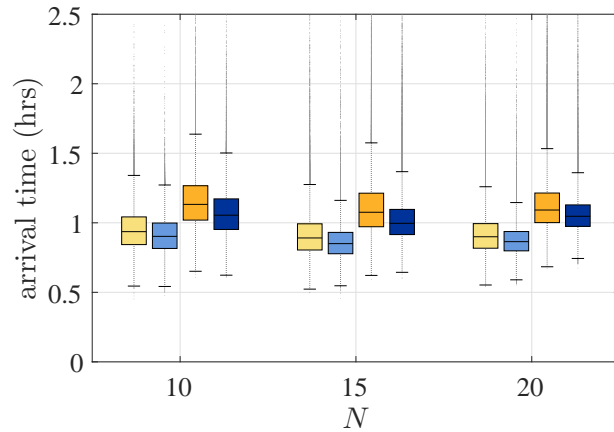


(b)

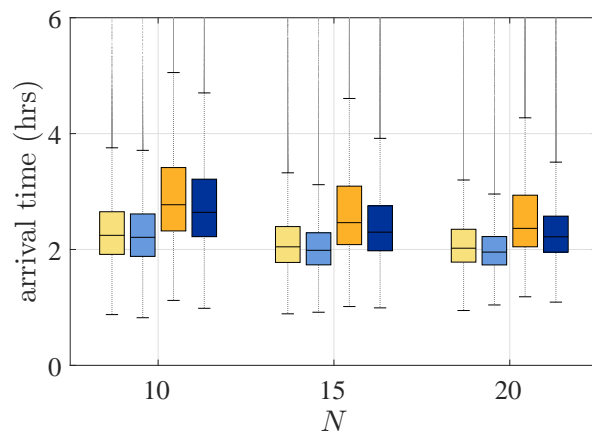
■ $0.6r_0, p = 1$
■ $0.3r_0, p = 1$
■ $0.6r_0, p = 0.9$
■ $0.3r_0, p = 0.9$
■ $0.6r_0, p = 0.8$
■ $0.3r_0, p = 0.8$

Figure 5.14. Neighbour majority detection sensitivity analysis for IbA+CbA with varying attraction radii as a function of r_0 and detection probability p where $r_0 = 1000$ m and noise levels: (a) $\sigma = 1$ dB. (b) $\sigma = 6$ dB.

The comparative arrival time performance for $\sigma = 2$ dB and $\sigma = 6$ dB is shown in Fig. 5.15(a) and Fig. 5.15(b) respectively. For both the attraction radii considered, i.e., $r_{GC} = \{0.3r_0, 0.6r_0\}$, the explicit communication based strategy is only marginally better than the passive sensing based implementation. Given the significant loss of information in the proposed passive sensing strategy and the cost of implementing an explicit communication network, the marginal performance difference is both an intuitive and a satisfactory result.



(a)



(b)

■ $0.6r_0$, PS
 ■ $0.6r_0$, EC
 ■ $0.3r_0$, PS
 ■ $0.3r_0$, EC

Figure 5.15. Passive Sensing (PS) versus Explicit Communication (EC) implementation of IbA+CbA, $r_0 = 1000$ m and noise levels: (a) $\sigma = 2$ dB. (b) $\sigma = 6$ dB.

5.5 Conclusion

A robust adaptive temporal sampling approach was presented for a distributed multi-agent source localization algorithm. The algorithm is composed of simple individualistic and social behaviours. The individualistic behaviour is a biased random walk inspired from a bacterium performing chemotaxis. It assumes a single sensor per agent and hence requires it to conduct temporal sampling for gradient sensing. The social behaviours are

based on the long-range attraction and the short-range repulsion behaviours. Cooperation between agents is based on passive sensing and the algorithm has the potential to invoke collective behaviour in a small multi-agent system.

The proposed adaptive temporal sampling approach has two components, i.e., IbA and CbA. IbA varies the sampling times based on agent's sensed source-intensity levels while CbA varies the sampling times based on agent's sensed number of neighbours within a local neighbourhood. It was shown that IbA enhances the performance of a multi-agent system in terms of its mean and median arrival times as compared to a static sampling strategy. However, it was also shown that IbA is sensitive to the ambient noise and the multi-agent system's performance degrades as the ambient noise increases. Based on IbA, Bio-CAST was optimized using an evolutionary algorithm for varying initialization distances, attraction radii and team sizes. An analytical model was developed as an estimate for the optimized behaviours. The resulting collective behaviour was validated against an agent's sensor and actuator noise along with strong multipath interference in gradient sensing due to environment variability.

It was shown that the performance degradation in IbA due to ambient noise is a result of increasing number of agents breaking away from the team as the noise increased, i.e., not a well-regulated team expansion. CbA was introduced which reduces IbA's sampling times as a function of an agent's number of neighbours within the attraction radius. Being a very simple strategy, CbA shows remarkable improvement in robustness of the collective behaviour. It was shown that CbA-regulated IbA results in significantly improved performance for varying noise levels in terms of mean, median and variance of the arrival time distribution when compared to the static sampling

approach or the unregulated IbA. It was also shown that CbA results in a well regulated team expense where number of agent breakaways were eliminated in the simulated source localization missions.

Chapter 6

Adaptive Behaviours in Multi-Agent Source Localization

6.1 Background

In this chapter, the role of adaptive group cohesion in a multi-agent source localization problem is investigated. A distributed source localization algorithm is presented which does not require a self-sufficient individualistic behaviour to localize a source. Source localization is achieved as an emergent property through agent's local interactions with its neighbours and the environment. Given absence of a self-sufficient individualistic behaviour, CbA is crucial in controlling agent loss. Even a single agent breakaway would mean an increasing team expanse in time. A two phase optimization strategy is introduced which is simpler than the previous optimization strategies of Chapter 4 and Chapter 5. In the first phase, IbA and the adaptive cohesion behaviour are optimized for infinite attraction radius and in the second phase CbA is optimized to minimize agent breakaways for limited neighbourhoods. The optimized behaviours are estimated with an analytical model and the resulting collective behaviour is validated against strong multi-path interference and other common noise sources. The statistical analysis of the arrival time distributions shows robustness of the collective behaviour in high ambient noise. The proposed strategy has been compared against an emergent speed variation based localization scheme as well as Bio-CAST with CbA compensated IbA.

6.2 Adaptive Cohesion based Localization Algorithm

The proposed algorithm, Adaptive Cohesion based Localization Algorithm (ACLA), only draws the GC and CA modules from Bio-CAST (see Chapter 4) and discounts the TD module. Hence, there is no self-sufficient individualistic model to help a lone agent localize the source. The constituent behaviours of ACLA are as follows:

6.2.1 Group Cohesion (GC)

GC in ACLA is the same as for Bio-CAST as defined in Section 4.2.2 and hence the unit direction vector, $\mathbf{d}_{GC_n}(t)$, is calculated following (4.2). To summarize, GC dictates a left 90° turn to the focal agent if the number of neighbours to its left are more than the number of neighbours on its right and vice versa. In case of the numbers being equal in both the left and the right half, it keeps the agent's heading unchanged.

6.2.2 Collision Avoidance (CA)

CA in ACLA is the same as for Bio-CAST as defined in Section 4.2.3 and hence the unit direction vector, $\mathbf{d}_{CA_n}(t)$, is calculated following (4.5). Effectively, if an agent detects a neighbour within its repulsion zone, it starts an evasive action and ignores any other behaviours such as going towards the goal or towards the neighbours. The focal agent turns away from the nearest neighbour with a turning rate that is proportional to how close the nearest neighbour is.

6.2.3 Adaptive Cohesion

The adaptive cohesion behaviour defines ACLA where an agent varies its group cohesion based on the sensed source-intensity values. Let us write the

desired direction of the focal agent n , commanded by ACLA as

$$\mathbf{d}_{AC_n}(t) = \begin{cases} \mathbf{d}_{CA_n}(t) & \text{if } \hat{r}_{n,m}(t) \leq r_{CA} \\ \mathbf{d}_{W_n}(t) & \text{otherwise} \end{cases} \quad (6.1)$$

where

$$\mathbf{d}_{W_n}(t) = \eta(t)\mathbf{d}_{W_n}(t - \tau_n) + (1 - \eta(t))\mathbf{d}_{GC_n}(t), \quad (6.2)$$

$$\eta(t) = \alpha_I \Delta \hat{I}_n(t) + \frac{1}{2}, \quad (6.3)$$

such that $0 \leq \eta \leq 1$, $\alpha_I \in \mathbb{R}^+$ is the adaptive cohesion coefficient and $\Delta \hat{I}_n(t) = \hat{I}_n(t) - \hat{I}_n(t - \tau_n)$. Equation (6.3) varies the source bias coefficient around the nominal value of 0.5 where values, $\eta > 0.5$ bias an agent more towards its previously calculated heading and values, $\eta < 0.5$ bias an agent more towards the majority of the neighbours. If an agent estimates that it is heading in the direction of decreasing intensity levels, it biases itself more towards its neighbours. On the contrary if an agent estimates it is heading in the direction of increasing intensity levels, it keeps its heading and biases itself less towards its neighbours. In (6.2), individualistic behaviour can be seen as an agent simply keeping its previous heading and hence is not a self-sufficient behaviour to localize the source. Once an agent loses contact with any other agents, it will continue to travel in a straight path. Also note that (6.1) is only the desired heading dictated by ACLA whereas the transition from the n^{th} agent's current angle, θ_n to $\theta_{AC_n} = \angle \mathbf{d}_{AC_n}$ follows the non-holonomic constraints as specified in Section 3.2.

6.2.4 Temporal Sampling

For ACLA, we use IbA (see Section 5.3.3) as the adaptive temporal sampling approach given its superior performance over the static sampling approach of Chapter 4.

Given the reasons in the preceding subsection pertaining to the individualistic model being not self-sufficient, it is imperative to have CbA regulated IbA (see Section 5.4). For CbA regulation, (5.14) is used.

6.3 Optimization Results

The optimization process assumes the experimental setup and GA settings as stipulated in Section 3.2. The optimization process for ACLA is composed of two phases. First we optimize the algorithm's two key parameters for infinite attraction radius, i.e., adaptive cohesion coefficient, α_I and the adaptive sampling coefficient, β_τ . In the second phase, we optimize the critical number of agents, N_c , for limited attraction radii and show that we can achieve performance at par with the infinite attraction radius beyond a certain finite attraction radius. This optimization scheme is simpler and more intuitive than the earlier schemes in Chapter 4 and Chapter 5 which optimized the whole set of behavioural parameters for each limited attraction radius. The explored values of the parameters during the optimization process are given in Table 6.1. For the constant parameters, refer to the settings given in Table 3.1.

6.3.1 Optimization for Infinite Attraction Radius

For the infinite attraction radius and varying initialization distances in the range of 600 m to 1400 m, the results for the optimized α_I and β_τ are

Table 6.1. Explored values of the parameters during the optimization process

Param.	Description	Bounds
α_I	Adaptive cohesion coefficient	[0, 2]
β_τ	Adaptive sampling coefficient	[0, 2]
N_c	Critical number of neighbours	[0, 20]

shown in Fig. 6.1(a) and Fig. 6.1(b) respectively. It can be seen that the values of α_I^* are nearly identical for the considered initialization distances in Fig. 6.1(a). The average behaviour of α_I^* over the initialization distances, $\bar{\alpha}_I(N) = \frac{1}{3} \sum_{r_0} \alpha_I^*(r_0, N)$, is shown as a red-dashed line in Fig. 6.1(a) which we approximate as

$$\hat{\alpha}_I^*(N) = a_\alpha N^{b_\alpha} + c_\alpha \quad (6.4)$$

as shown in Fig. 6.2(a) and the values of the parameters are given in Table 6.2.

The values of β_τ^* vary significantly in initialization distance consistent with the case in Chapter 5. We choose to approximate β_τ^* by its average response over the team sizes in the range of 2 to 20 agents, $\bar{\beta}_\tau(r_0) = 0.1 \sum_N \beta_\tau^*(r_0, N)$, shown as dashed lines in Fig. 6.1(b), as

$$\hat{\beta}_\tau^*(r_0) = a_\beta r_0^{b_\beta} + c_\beta \quad (6.5)$$

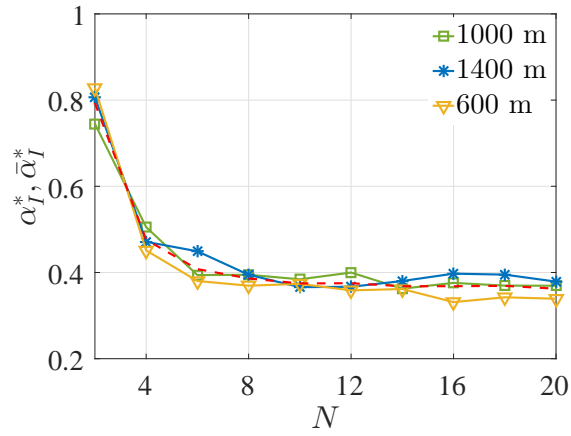
as shown in Fig. 6.2(b) and the values of the parameters are given in Table 6.2.

6.3.2 Optimization for Limited Attraction Radius

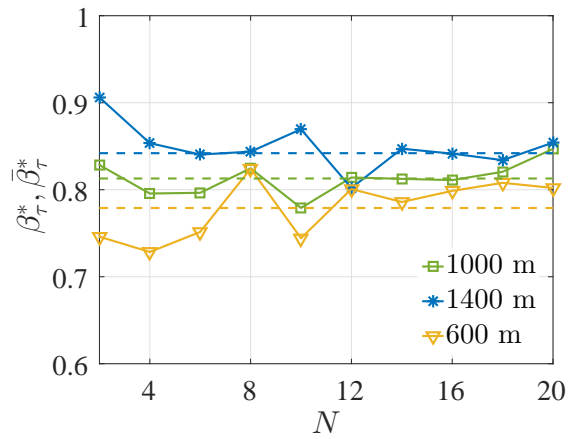
Now, let us optimize the critical number of agents, N_c , for limited attraction radii. Objective is to see if we can achieve performance for a certain limited attraction radius at par with the infinite attraction radius just by controlling

Table 6.2. Parameter and Root Mean Square Error (RMSE) values for respective equations

Eq.	Parameter Values	RMSE
(6.4)	$a_\alpha = 1.661, b_\alpha = -1.935, c_\alpha = 0.3588$	0.003
(6.5)	$a_\beta = 2.247 \times 10^{-5}, b_\beta = 1.175, c_\beta = 0.7379$	2.66×10^{-5}
(6.6)	$a_N = 0.716$	0.5957



(a)



(b)

Figure 6.1. Optimization results for infinite attraction radius and varying initialization distances and team sizes (a) Optimized α_I where the red dashed-line shows the average response over the considered initialization distances. (b) Optimized β_τ where the dashed lines for each initialization distance are the average response over the team sizes in the range of 2 to 20 agents.

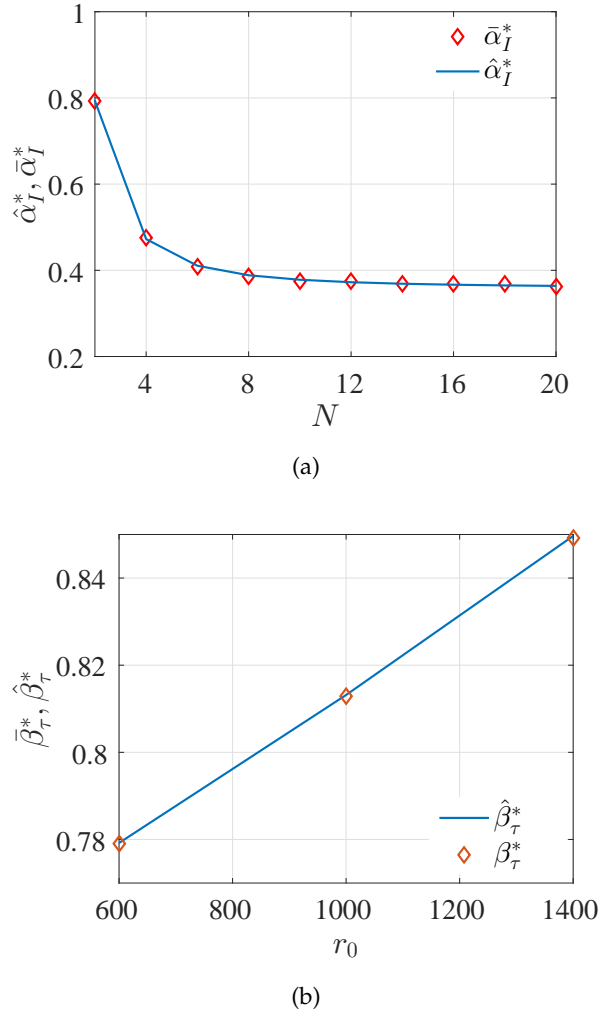


Figure 6.2. For infinite attraction radius, estimates for: (a) $\bar{\alpha}_I^*$. (b) $\bar{\beta}_\tau^*$.

the sampling times through CbA. This would mean that we do not need to optimize the other two parameters, i.e., the adaptive cohesion coefficient and the adaptive sampling coefficient, separately for each limited attraction radius as was the case in the optimization process of Chapter 4 and Chapter 5.

The optimized critical number of agents as a function of team size is shown in Fig. 6.3(a) along with the optimized mean arrival times in Fig. 6.3(b) for limited attraction radii in the range of 10% to 60% of the initialization distance. It can be seen that for limited attraction radii, more than or equal to 30% of the

attraction radius, the arrival performance is almost identical with the infinite attraction radius for team sizes of $N = 8$ and above.

As far as the optimization data for the critical number of agents is concerned in Fig. 6.3(a), it increases almost linearly in N for team sizes less than or equal to 16 agents for all the attraction radii. However, as the attraction radii increase, e.g., $r_{GC} = 0.6r_0$, the N_c^* becomes saturated beyond a certain team size. Also, note that larger the number of N_c , the more conservative the CbA regulation as shown in Fig. 6.4. For attraction radii greater than or equal to $r_{GC} = 0.3r_0$ where the performance is almost identical, we can see that the most conservative curve is for $r_{GC} = 0.3r_0$ and hence we may assume that as a general estimate for all the attraction radii given the choice does not significantly degrade the performance of other attraction radii.

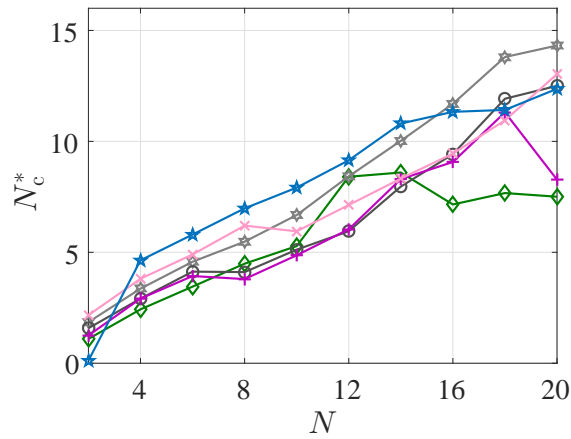
The estimate for the optimized critical number of neighbours can be written simply as a linear function in N as follows

$$\hat{N}_c^*(N) = a_N N \quad (6.6)$$

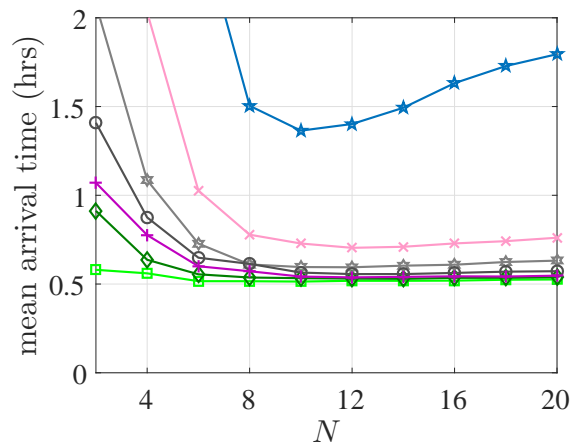
and is shown as a solid line in Fig. 6.5(a) and the value of the parameter is given in Table 6.2. The associated mean arrival times have been shown in Fig. 6.5(b) where we can see that the choice of \hat{N}_c^* has worked well for all the limited attraction radii except $r_{GC} = 0.1r_0$ if we compare the results of Fig. 6.5(b) with the results of Fig. 6.3(b).

6.4 Robustness Analysis

In this section, the robustness of the resulting collective behaviour from the estimated models of the optimized ACLA is validated against noise levels of



(a)



(b)

★ $0.1r_0$
 ✕ $0.2r_0$
 ★ $0.3r_0$
 ⊖ $0.4r_0$
 + $0.5r_0$
 ◇ $0.6r_0$
 □ ∞

Figure 6.3. Optimization for limited attraction radius (see legend at the bottom): (a) Optimized critical number of agents. (b) Mean arrival times.

$\sigma = 1$ dB and $\sigma = 6$ dB. Also, the performance of the collective behaviour is validated against initialization distance sensitivity, loss of source signal and neighbour detection noise. The arrival time performance is either shown by using box-plots following the details given in Section 3.2.3 or by analyzing the team expanse of a single localization mission. An agent breakaway is directly related to the team expanse. In ACLA, if an agent breaks away from the team,

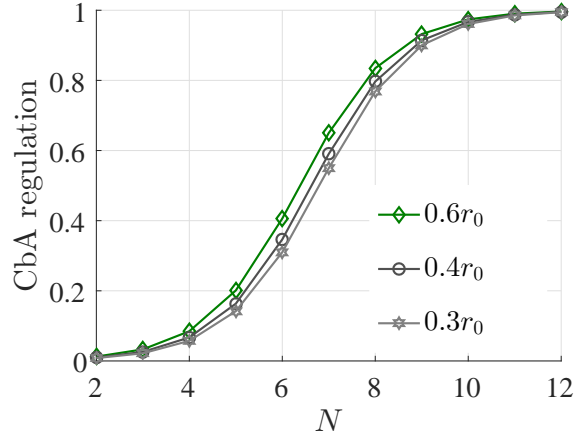


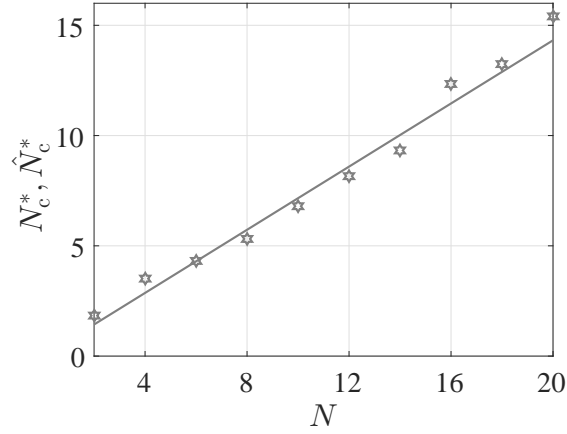
Figure 6.4. Optimized CbA regulation for a team size of 10 agents and various limited attraction radii in the range of $0.3r_0$ to $0.6r_0$.

it will travel in a straight line and hence the the team expanse will continue to increase without bound.

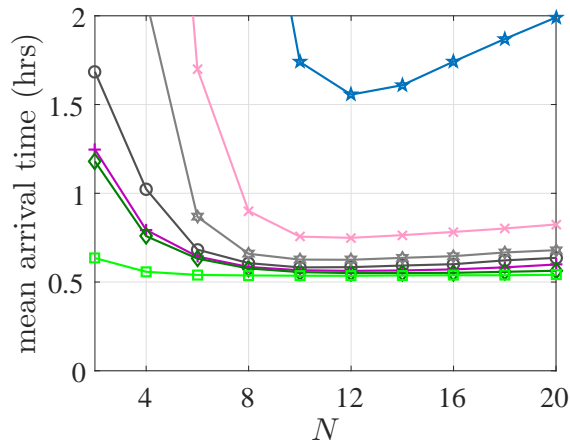
6.4.1 Multipath Interference

The box-plots for ACLA's arrival time performance are shown in Fig. 6.6(a) and Fig. 6.6(b) for noise levels of 1 dB and 6 dB respectively. It can be seen that for both the plots, the variance as well as the median of the arrival time distributions improves as N is increased. Also the difference between the arrival time distribution of infinite attraction radius and $r_{GC} = 0.6r_0$ reduces as the team size increases and for $N > 12$, arrival time distributions are almost identical for both the noise levels of 1 dB and 6 dB.

The number of failed missions in a total number of 5×10^4 missions is equivalent to the number of events in which one or more agent breakaways occurred. The plots for failure rate are given in Fig. 6.7(a) for different attraction radii. It can be seen that for N_c^* , the failure rate has been less than 0.5% for $r_{GC} \geq 0.6r_0$ for the entire range of team sizes and for $r_{GC} = 0.3r_0$, for $N > 6$ agents. However, for N_c^* , it is also seen that the failure rate starts increasing



(a)

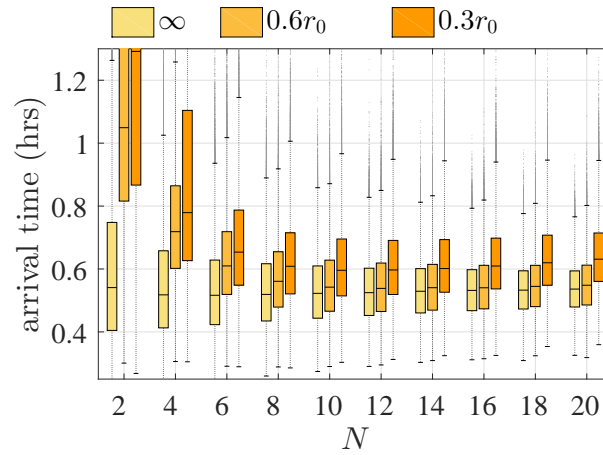


(b)

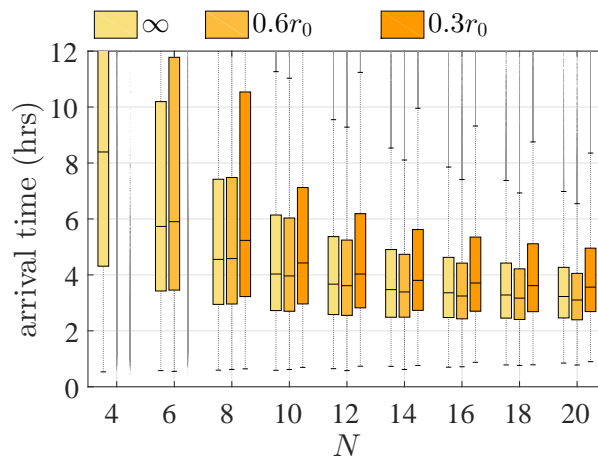
★ $0.1r_0$ ✕ $0.2r_0$ ★ $0.3r_0$ ⊖ $0.4r_0$ + $0.5r_0$ ◆ $0.6r_0$ ■ ∞

Figure 6.5. (a) Estimate for critical number of agents in limited attraction radii where solid line is the estimate for the data points. (b) Mean arrival times for the estimated model (see legend at the bottom for different attraction radii in the range of $0.1r_0$ to $0.6r_0$).

as the number of agents increase. There are two points that need to be noted. First, the optimization process has a single objective function, i.e., the mean arrival time. Second, more conservative CbA regulation, i.e., $N_c > N_c^*$, may result in a lower failure rate but at the same time affect the mean arrival time performance. To substantiate this, we increase the critical number of agents such that $N_c = 1.2N_c^*$ and show in Fig. 6.7(a) that the failure rate goes to zero for $r_{GC} = 0.3r_0$ as N increases beyond 10 agents. However, it is shown in Fig. 6.7(b)



(a)



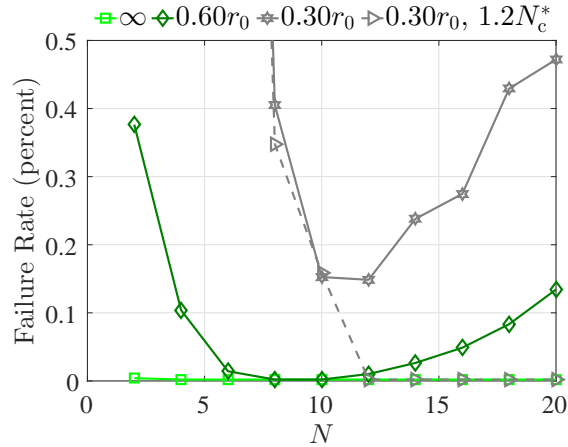
(b)

Figure 6.6. Arrival time performance for varying attraction radii (see legend) and varying levels of ambient noise for the analytical model estimated for the optimized ACLA: (a) $\sigma = 1$ dB. (b) $\sigma = 6$ dB.

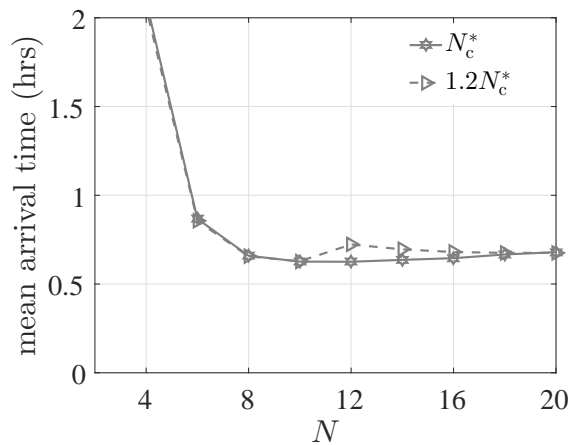
that a more conservative strategy has a slightly degraded mean arrival time. The phenomenon highlights the need of a carefully thought multi-objective optimization setup which penalises the fitness of an individual in case there are any failures.

6.4.2 Initialization Distance Sensitivity

As far as the problem statement discussed in this paper is concerned, the initialization distance can be controlled within a tight uncertainty range.



(a)



(b)

Figure 6.7. (a) Failure rate for varying attraction radii with optimal CbA and a more conservative CbA, i.e., 1.2 times the optimal N_c^* . (b) Mean arrival time comparison for $r_{GC} = 0.3r_0$ with optimal N_c^* against $r_{GC} = 0.3r_0$ with $1.2N_c^*$.

However, it is desired that the optimized solution for a specific distance scales well for a wide range of distances. We conduct sensitivity analysis for an optimized solution for $r_0 = 1000$ m and $r_{GC} = 0.6r_0$ for a change of ± 400 m in Fig. 6.8(a) and Fig. 6.8(b) for $\sigma = 1$ dB and $\sigma = 6$ dB respectively. We can see that the optimized solution scales well with the change in distance for all the team sizes.

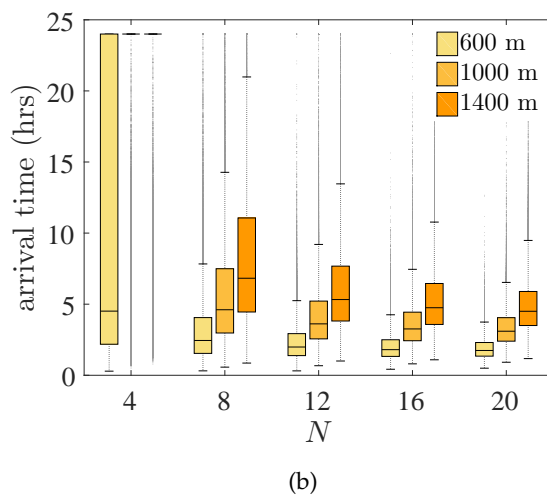
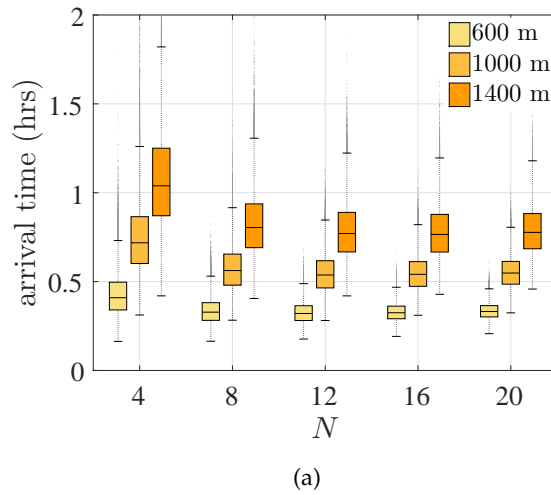


Figure 6.8. Initialization distance sensitivity analysis for optimized solution for $r_0 = 1000$ m and $r_{GC} = 0.6r_0$ and noise levels: (a) $\sigma = 1$ dB. (b) $\sigma = 6$ dB.

6.4.3 Loss of Source Signal

It is of interest to see how a cooperative team behaves in case the source signal disappears for some time. The primary concern in such a case is agents breaking away from the team. We conduct the analysis for a single localization mission for $\sigma = 1$ dB and $\sigma = 6$ dB. Figure 6.9 shows that the team expense for the case of loss of source signal during a 2.8 h interval remains well regulated at approximately 300 m for $N = 20$ agents, $r_0 = 1000$ m and $r_{GC} = 0.6r_0$. We also

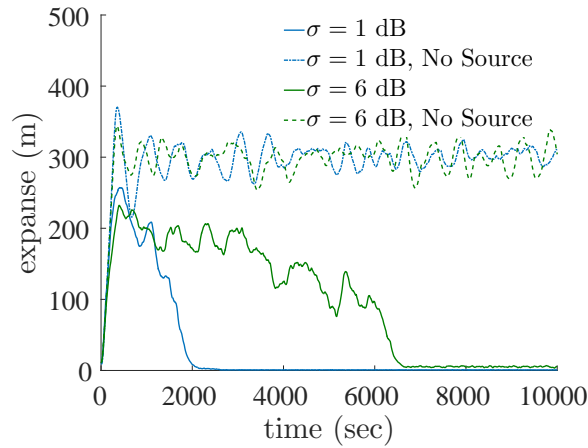


Figure 6.9. Comparative team expande for source signal vs. loss of source signal for $r_0 = 1000$ m and $r_{GC} = 0.6r_0$.

explicitly checked for the number of agent breakaways during the mission and found no agent breakaways for all the four scenarios considered.

6.4.4 Neighbour Detection Noise

Since the proposed algorithm depends on the passive neighbourhood sensing, we conduct comparative analysis for performance degradation in case of different noise levels. Since we have two sensors, one on the right and one on the left, we corrupt the number of neighbours estimation on both sides by an additive Gaussian noise with zero mean and variance, $\sigma_{N_{GC}} = \{1, 2\}$. The output of the estimated neighbours is then truncated to the nearest integer value.

The arrival time performance for $\sigma = 1$ dB and $\sigma = 6$ dB is shown in Fig. 6.10(a) and Fig. 6.10(b) respectively for $r_0 = 1000$ m and $r_{GC} = 0.6r_0$. It can be seen that the relative degradation in performance with respect to a noiseless neighbourhood detection decreases as the team size increases.

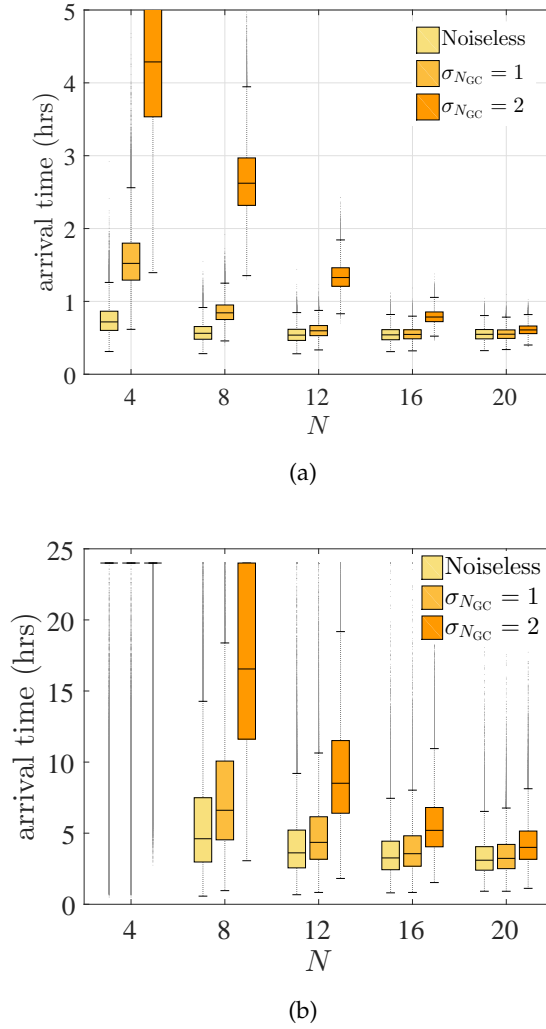


Figure 6.10. Neighbour detection noise analysis for optimized solution for $r_0 = 1000$ m and $r_{GC} = 0.6r_0$ and noise levels: (a) $\sigma = 1$ dB. (b) $\sigma = 6$ dB.

6.4.5 Passive Sensing vs. Explicit Communication

It is also important to compare the performance of passive sensing based ACLA against an explicit communication based counterpart. The explicit communication based counterpart is the centroid-based agent interaction model as discussed in Section 2.2.2 and is assumed to be based on perfect inter-agent communication.

The comparative arrival time performance for $\sigma = 1$ dB and $\sigma = 6$ dB is shown in Fig. 6.11(a) and Fig. 6.11(b) respectively. For $\sigma = 1$ dB in Fig. 6.11(a),

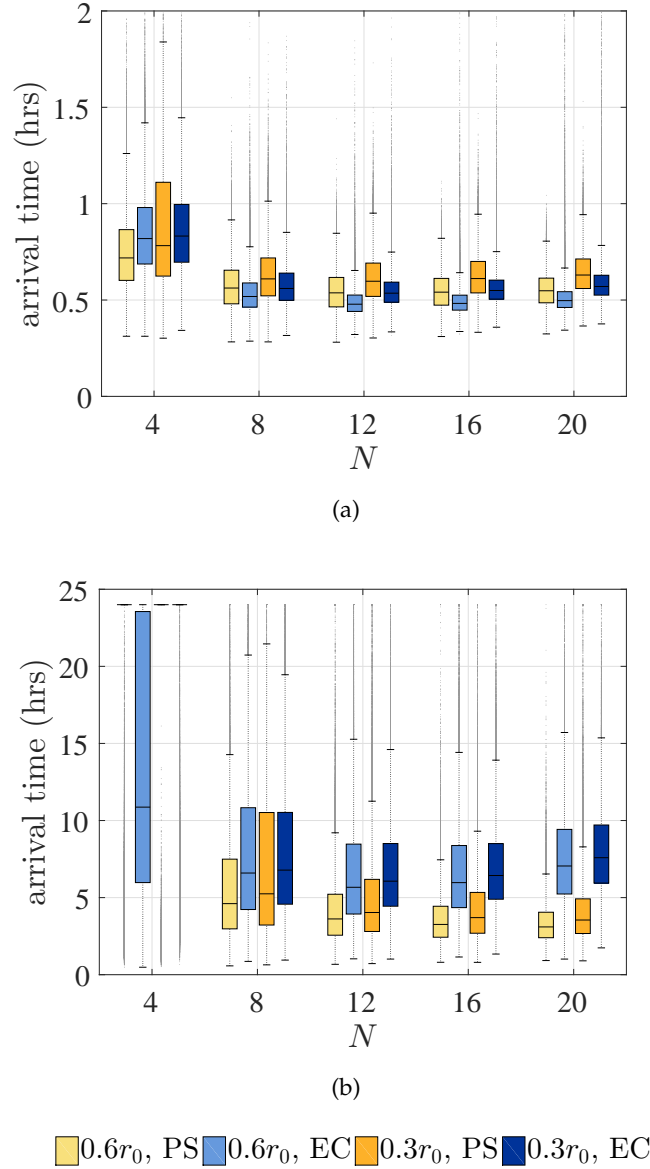


Figure 6.11. Passive Sensing (PS) versus Explicit Communication (EC) implementation of ACLA with varying attraction radii as a function of initialization distance, $r_0 = 1000$ m and noise levels: (a) $\sigma = 1$ dB. (b) $\sigma = 6$ dB.

for both the attraction radii considered, i.e., $r_{GC} = \{0.3r_0, 0.6r_0\}$, the explicit communication based strategy is generally marginally better than the passive sensing based implementation. The only exception is $N = 4$ and $r_{GC} = 0.6r_0$ where passive sensing outperforms the explicit communication.

The results for increased noise level, i.e., $\sigma = 6$ dB in Fig. 6.11(b) are somewhat similar to what we saw for the static temporal sampling based

Bio-CAST in Section 4.4.8. For both the attraction radii and $N > 4$, the passive sensing based strategy outperforms the explicit communication based strategy.

6.5 Comparative Analysis

In this section, let us compare the performance of ACLA against two different source localization strategies in literature. First we investigate the performance of a similar strategy that achieves source localization as an emergent property of agent interactions, i.e., without a self-sufficient individualistic model. Then we compare ACLA against Bio-CAST (as proposed in Chapter 5) which builds on a self-sufficient individualistic model.

6.5.1 Emergent Source Localization Through Speed Variation

One recent and a very interesting study on a school-of-fish shows that source localization can be achieved in a cooperative group without a self-sufficient individualistic behaviour. In this case, the individualistic behaviour is simply an agent varying its speed as a function of instantaneous intensity measurements [56]. The authors proposed the variation in an n^{th} agent's speed as

$$s_n(t) = s_{\min} + I(s_{\max} - s_{\min}) \quad (6.7)$$

where s_{\min} and s_{\max} are the minimum and the maximum speeds respectively and I is the sensed intensity. A light field was projected from a height of 240 cm on a small constrained search space of $213 \times 122 \text{ cm}^2$ and a depth of 8 cm. The directional vectors were calculated using the repulsion, attraction and neighbour alignment behaviours as given in (2.3), (2.4) and (2.5) respectively.

However, the application of the emergent model on the acoustic source localization problem, as discussed in Chapter 3, did not result in source localization for any initialization distance considered in this chapter, i.e., $r_0 \geq 600$ m, within a maximum time window of 8 hrs. A more generic version of speed variation function was used as follows

$$s_n(t) = s_{\min} + \frac{s_{\max} - s_{\min}}{1 + \exp\{a_s(I(t) - b_s)\}} \quad (6.8)$$

where the slope, a_s and the center point, b_s of the curve's transition from s_{\max} to s_{\min} were optimized via GA. The results remain the same whether the explicit communication based sensing model (with or without neighbour alignment) or passive sensing model is used (see Chapter 2 for respective definitions).

The mechanism of the emergent source localization of [56] is such that the team travels towards the source as a collective when there is a significant speed gradient across the mass of the team, i.e., agents closer to the source are significantly slower than the agents further away. Since we initialize the team in a tight cluster, hundreds of meters away from the source and given the source follows the inverse square law (see Fig. 3.2), there is not a significant instantaneous intensity gradient across the team expanse that can result in a sufficient speed difference.

6.5.2 Speed Variation with a Self-sufficient Individualistic Behaviour

Once we add a self-sufficient source localization behaviour such as TD based on a bacterium's random walk (see Chapter 4 for definition), the reported optimal parameters were such that effective $s_n^*(t)$ was always equal to the maximum speed, s_{\max} , for the entire localization experiment, e.g, $b_s^* > I_{\max}$

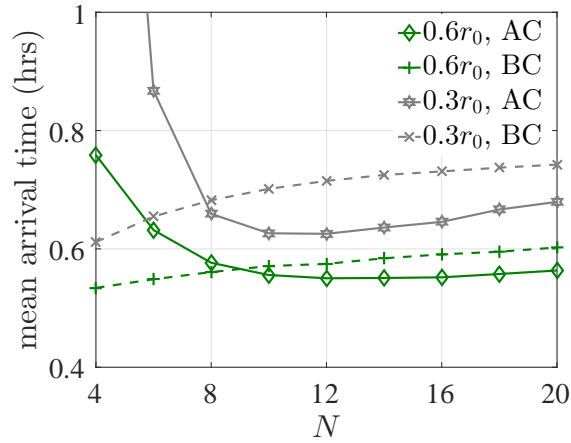
for arbitrary $a_s^* > 1$, where $I_{\max} = 180$ dB at 1 m away from the source (see Section 3.2.1).

In summary, for the considered problem statement and the associated experimental setup, we did not find any evidence of speed variation being helpful in localizing the source with or without a self-sufficient individualistic model.

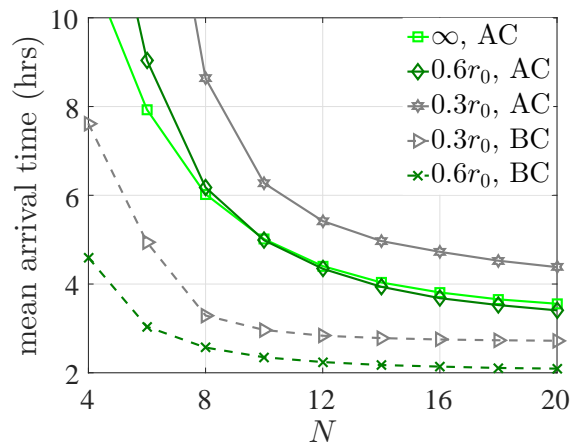
6.5.3 Bio-CAST

Let us compare the performance of ACLA against Bio-CAST which has a self-sufficient individualistic behaviour. The optimized Bio-CAST used here for comparison is based on CbA regulated IbA sampling strategy as defined in Chapter 5. In Fig. 6.12(a), the mean arrival times are shown for a noise level of 1 dB where ACLA is referred to as AC and Bio-CAST as BC in the legend. For both the cases of limited attraction radii, ACLA performs better than Bio-CAST for team sizes greater than 8 agents. However, if we increase the noise to 6 dB for the algorithms optimized for a noise level of 1 dB, we see that Bio-CAST is more robust to the ambient noise than ACLA. We can also see that ACLA is still in the process of improving its performance as N increases within the considered range of 1 to 20 agents while Bio-CAST is able to achieve its maximum performance at about a team size of 16 agents.

The comparative analysis shows that fusing ACLA and Bio-CAST in a more generic optimization setup may result in a more robust and a better performing localization algorithm. The fusion would assume an adaptive turning strategy (correction angle of TD in case of Bio-CAST) which is a function of team size. For smaller team sizes, an agent would assume a more bacterium-like response to the changing intensity levels whereas it may let go off the individualistic



(a)



(b)

Figure 6.12. (a) Mean arrival time comparison for ACLA (AC in legend) versus Bio-CAST (BC in legend) for varying attraction radii and noise levels: (a) $\sigma = 1$ dB. (b) $\sigma = 6$ dB.

behaviour completely in a larger team size. It will also be interesting to investigate how these behaviours evolve once optimized explicitly for a higher ambient noise scenario.

6.6 Conclusion

In this chapter, a source localization algorithm based on adaptive group cohesion was presented. The proposed algorithm, called ACLA, achieves source localization as an emergent property through agent interactions. An

agent does not have a self-sufficient individualistic behaviour and hence is incapable of localizing the source on its own.

For optimizing the behaviours of ACLA, a two phase optimization strategy was introduced which is simpler than the previous optimization strategies of Chapter 4 and Chapter 5. In the first phase, IbA and the adaptive cohesion were optimized for infinite attraction radius and in the second phase CbA was optimized to minimize agent breakaways for limited attraction radii. It was shown that by only having an optimized CbA, the performance of finite attraction radii above a certain threshold can be made identical to the performance of an infinite attraction radius.

The optimized behaviours were then approximated with analytical models which were validated against sensor and actuator noise, strong multipath interference due to environment variability, sensitivities in initialization distance, neighbour detection noise and loss of source signal. The statistical analysis of the arrival time distributions shows robustness of the collective behaviour for all the considered scenarios. The localization failure rate was also studied which shows that by selecting a slightly more conservative CbA, a more robust collective behaviour can be achieved with a zero failure rate.

The localization performance of the passive sensing based ACLA was also compared against an optimized explicit communication based counterpart using centroid based social behaviours. Considering the significant information loss due to passive sensing and the cost of implementing explicit communication underwater, passive sensing strategy results in only a marginal performance degradation as compared to the explicit communication strategy for the optimized case of $\sigma = 1$ dB. However, it is interesting to note that when the optimized solution is validated against a higher noise level such

as $\sigma = 6$ dB, the passive sensing strategy is more robust than the explicit communication strategy.

ACLA was further compared against two different source localization algorithms, one without a self-sufficient individualistic behaviour and one with a self-sufficient individualistic behaviour. The former strategy is an emergent localization strategy based on agent's speed variation as a function of sensed instantaneous intensity values. It was shown that the optimization process failed to report any successful localizations for the experimental setup considered in this thesis. A modified version of a speed variation behaviour which has a self-sufficient individualistic behaviour was also optimized where an agent keeping a constant maximum speed throughout the localization process results in the best solution.

On comparing ACLA with Bio-CAST having a CbA regulated IbA sampling strategy, it was shown that for low ambient noise levels ACLA performs significantly better than Bio-CAST. However, for strong multipath interference, Bio-CAST is more robust than ACLA and performs significantly better. A fusion of the two algorithms which would result in an adaptive turning behaviour as a function of team size was also proposed as future work. The fusion approach may lead to a better performing and a more robust source localization algorithm.

Chapter 7

Conclusion & Future Research

7.1 Conclusion

The thesis focussed on development of three collective behaviours that do not require explicit inter-agent communication for cooperative multi-agent source localization. Each collective behaviour results from a source localization algorithm, i.e., a set of agent's social and individualistic behaviours. In each case, an individualistic behaviour may or may not be self-sufficient for the source localization problem. The social behaviours, i.e., the long-range attraction and the short-range repulsion, assume implicit inter-agent communication without using the memory of the environment, simply referred to as passive sensing. The social behaviours conforming to the passive sensing constraints helped us develop collective behaviours that are realizable in practice and also show remarkable robustness and scalability. The individualistic behaviours assume a single sensor per agent to sense the gradient, i.e., an agent resorts to temporal sampling. In real world source localization problems where gradients are weak and corrupted with high levels of ambient noise, temporal sampling constraint keeps the designed collective behaviours realistic.

A real world underwater source localization problem was used for designing each of the source localization algorithms. An extensive optimization process encompassing a range of team sizes, initialization distances and

attraction radii was used to optimize the social and individualistic behaviours. The optimized behaviours as a function of team size, initialization distance and attraction radius were approximated with analytical models. These analytical models represent a hybrid of behaviour-based design and automatic design [16] where a general behavioural structure was already set in place prior to the optimization process.

The first collective behaviour was based on a source localization algorithm called Bio-CAST with a static temporal sampling approach. Bio-CAST is composed of a self-sufficient individualistic behaviour, inspired by the temporal sampling of a bacterium to sense the gradient, in addition to the two social behaviours of long-range attraction and short-range repulsion. The second collective behaviour was based on Bio-CAST with an adaptive temporal sampling approach. The adaptive temporal sampling approach was composed of two components, i.e., IbA and CbA. IbA varies the sampling times as a function of the sensed intensity values and hence becomes vulnerable to significant performance degradation in environments with very high noise levels. It was shown that IbA-only approach works significantly better than a static temporal sampling approach for low ambient noise levels, however, it loses its advantage over the static temporal sampling approach if the noise is further increased. CbA regulates IbA based on the sensed number of neighbours within the attraction radius of an agent. It was shown that CbA regulation results in remarkable improvement of IbA in high ambient noise scenarios. It was also substantiated that the performance degradation in an IbA-only strategy is linked with the number of agent breakaways from the team and a poorly regulated team expanse. CbA resolves the issue by eliminating the number of agent breakaways and keeping a well regulated team expanse.

The final collective behaviour was based on a source localization algorithm that does not require a self-sufficient individualistic behaviour for source localization. The proposed algorithm, called ACLA, achieves source localization as an emergent property through agent's social behaviours. ACLA assumed an adaptive temporal sampling approach similar to the case of Bio-CAST where CbA regulated IbA is used. The optimization procedure used for ACLA is divided into two phases. In the first phase, IbA and the adaptive cohesion were optimized for infinite attraction radius and in the second phase CbA was optimized to minimize agent breakaways for limited attraction radii. The optimization approach for ACLA is simpler than the earlier optimization procedures for Bio-CAST where optimizations with infinite attraction radius or with limited attraction radius involved all the behavioural parameters. It was shown that by only having an optimized CbA, the performance for finite attraction radii above a certain threshold can be made identical to the performance for an infinite attraction radius. The statistical analysis of the arrival time distributions shows robustness of the collective behaviour in high ambient noise. The localization failure rate was also studied which shows that by selecting a slightly more conservative CbA, a more robust collective behaviour can be achieved with a zero failure rate.

7.2 Future Research

Given the current state of the art in swarm robotics, there are no known examples of robotic swarms solving a real-world problem [16]. It is hoped that the proposed source localization algorithms can bridge that gap. Currently, at Acoustic Research Lab (ARL), we are developing a team of robotic swans for monitoring water quality in natural or artificial water bodies [136]. We believe

that the proposed strategies, having the ability to invoke a robust and a scalable collective behaviour, can result in a persistent search and track multi-agent system.

The extensive optimization of agent's behavioural parameters over a range of team sizes, initialization distances and attraction radii has resulted in valuable insights pertaining to the relationship between them. It will be interesting to see how optimized behavioural parameters vary as a function of the ambient noise level which for now was held constant at a level of 1 dB. Also, both for Bio-CAST with adaptive temporal sampling and ACLA, the relationships between the team size and some of the behavioural parameters were expressed as power laws. This is similar to the case of many swarm robotics implementations where efficiency of task completion due to cooperation also behaves similarly with the team size [133]. It will be interesting to investigate this phenomenon further to see if there exists an underlying relationship between the optimized behavioural parameters, resultant localization efficiency and the team size.

So far, the effect of adding informed individuals [23, 137] has not been investigated for the proposed source localization strategies. It will be interesting to investigate the minimum number of informed agents that can maximize the localization efficiency. Also, it will be interesting to see if there is any change in the optimized agent behaviours in response to the addition of informed individuals.

Finally, there is a need for investigating adaptive behaviours further. For example, while comparing ACLA with Bio-CAST, a fusion of the two algorithms was proposed as the future work which requires an adaptive

turning behaviour as a function of team size. The fusion approach may lead to a better performing and a more robust source localization algorithm.

Appendix A

Implementation Details

A.1 Sound Propagation Model

Let us adopt a simple incoherent model for sound propagation taking into account the transmission losses due to geometric spreading and absorption in a medium [138]. The received level, RL , in dB re 1 μPa , of an acoustic source with sound level, SL , at a distance, R (meters), away from the source is given by

$$RL = SL - TL_g - TL_a \quad (\text{A.1})$$

where $TL_g = 10\alpha_g \log_{10}R$, $\alpha_g \in [1, 2]$ is the transmission loss due to geometric spreading and $TL_a = \alpha_a R$, $\alpha_a \in \mathbb{R}^+$ is the transmission loss due to absorption in the medium (seawater) and hence (A.1) can be written as

$$RL = SL - 10\alpha_g \log_{10}R - \alpha_a R \quad (\text{A.2})$$

Appropriate value of the coefficient α_g sets the geometric spreading to either as cylindrical ($\alpha = 1$) or spherical ($\alpha = 2$) where cylindrical being more appropriate for shallow waters and spherical for deep waters. The absorption coefficient in seawater, α_a (dB m^{-1}), can be estimated by a modified version of Thorp's model [125] as given in [138] for frequencies less than 40 kHz. The absorption coefficient is given as a function of acoustic frequency, f (kHz), as

$$\alpha_a = 1.094 \times 10^{-3} \left(3 \times 10^{-3} + \frac{0.1f^2}{1+f^2} + \frac{40f^2}{4100+f^2} + 2.75 \times 10^{-4}f^2 \right) \quad (\text{A.3})$$

Now, let us assume that $P_{n_{\text{RL}}}(t)$ is the root mean square pressure for RL sensed by the n^{th} agent at time t , then considering the ambient noise level characterized by NL in dB re 1 μPa , the total received pressure $P_n(t)$ can be written as

$$P_n(t) = \sqrt{P_{n_{\text{RL}}}^2(t) + P_{n_{\text{NL}}}^2(t)} \quad (\text{A.4})$$

where $P_{n_{\text{NL}}}(t)$ is the root mean square ambient noise for NL sensed by the n^{th} agent at time t . For simulation purposes, we can estimate received intensity $I_n(t)$ (dB) as

$$\hat{I}_n(t) \sim \mathcal{N}(I_n(t), \sigma) \quad (\text{A.5})$$

where $I_n(t) = 20 \log P_n(t)$ and the value of measurement uncertainty, σ , can be selected according to the assumed noise levels (see discussion in Section 3.2.1).

A.2 Evolutionary Optimization

Let us formulate a numerical optimization problem as

$$\text{Minimize } \varphi(\mathbf{w}), \quad \mathbf{w} = [\omega_1, \dots, \omega_q] \in \mathbb{R}^q \quad (\text{A.6})$$

where $\varphi : \mathbb{R}^q \rightarrow \mathbb{R}$ and $\varphi(\mathbf{w})$ is the objective function, i.e., the mean arrival time of a team of N agents over K number of trials and $\omega_i, i \in \{1, \dots, q\}$ is the control parameter and has bounds $l_i \leq \omega_i \leq u_i$. For a high-dimensional, nonseparable and nonlinear problem without any guarantees of convexity, a GA is an appropriate choice as an optimization strategy [139]– [127]. A GA

also scales well if one wants to investigate multi-objective optimization for Bio-CAST [141].

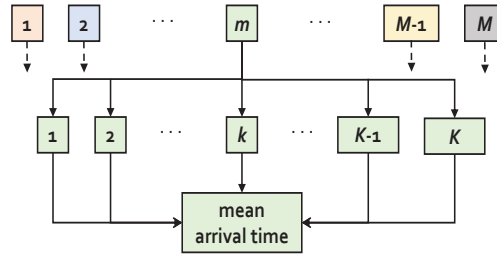
The GA is initialized randomly with a population, $\mathcal{P}^{(0)} = \{\mathbf{w}_1^{(0)}, \dots, \mathbf{w}_M^{(0)}\}$, of $M \in \mathbb{Z}^+$ individuals as shown in Fig. A.1(a). Fitness, $\varphi(\mathbf{w}_i^{(0)})$, $i \in \{1, \dots, M\}$, of each individual is evaluated by running Bio-CAST, K times to achieve a certain level of statistical consistency as discussed in Section A.3. Fig. A.1(b) shows the flow diagram for the GA, where after fitness evaluation of the initial population, $\mathcal{P}^{(0)}$, a parent population, $\mathcal{P}^{(p)} = \{\mathbf{w}_1^{(p)}, \dots, \mathbf{w}_M^{(p)}\}$, is generated based on a Deterministic Binary Tournament [142].

A sample of two parents is randomly drawn from the parent population, $\mathcal{P}^{(p)}$, with replacement to generate two corresponding offsprings until we have the offspring population, $\mathcal{P}^{(o)} = \{\mathbf{w}_1^{(o)}, \dots, \mathbf{w}_M^{(o)}\}$. The offsprings are generated using extended intermediate recombination [143].

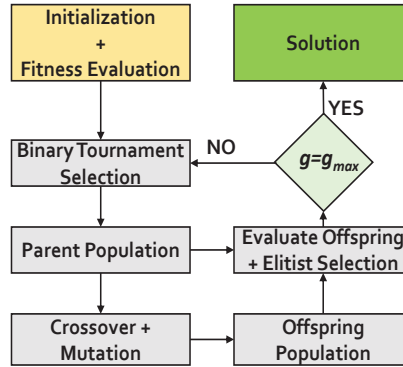
The offspring population, $\mathcal{P}^{(o)} = \{\mathbf{w}_1^{(o)}, \dots, \mathbf{w}_M^{(o)}\}$, then undergoes Normally distributed mutation [144] to generate mutated offspring population, $\mathcal{P}'^{(o)} = \{\mathbf{w}_1'^{(o)}, \dots, \mathbf{w}_M'^{(o)}\}$, with mutation probability, $p_m(\lambda)$, which varies as a function of generation number, $\lambda \in \mathbb{Z}^+$. Mutation probability is kept constant at some maximum value, $p_{m_{\max}}$, for some λ_s initial generations after which it decays exponentially with rate, τ , until the final generation, λ_{\max} .

Afterwards, the fitness, $\varphi(\mathbf{w}_i'^{(o)})$, $i \in \{1, \dots, M\}$ is evaluated and then $\mathcal{P}'^{(o)}$ and $\mathcal{P}^{(p)}$ undergo Elitist selection to generate the final population $\mathcal{P}^{(f)}$ [145]. The final population, $\mathcal{P}^{(f)}$, which is essentially $\mathcal{P}'^{(o)}$ after the elitist selection, is either fed to the Binary Tournament Selection block if $\lambda < \lambda_{\max}$ or else reported as the final optimized solution.

It is to be noted that the effectiveness of the GA was tested empirically and the GA parameters such as $p_{m_{\max}} = 0.4$, $\lambda_s = 150$, $\tau = 0.1$, and $\lambda_{\max} = 400$



(a)



(b)

Figure A.1. (a) A single individual of the GA population runs Bio-CAST multiple times to calculate the mean arrival time. (b) The flow diagram of the GA.

were chosen to ensure repeatability of reporting the same fitness with the same optimized control parameters over multiple optimization runs.

A.3 Consistency Analysis for Number of Simulation Runs

As the performance metrics are set as mean arrival times, it is best to have an informed choice of how many simulation runs (referred to as K in Appendix 3.2.2) would result in a statistically consistent performance metric for the entire population of the optimization algorithm. To perform the consistency analysis, let us compare Q distributions, each of which is a distribution of K runs of the Bio-CAST simulation with identical parameters, where K needs to be large enough so that all the Q distributions are nearly identical. However, K

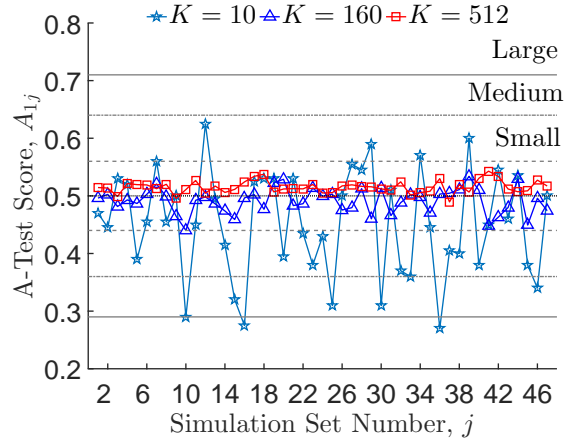
cannot be set arbitrarily large as increasing K , increases the computation load of the GA.

To select an appropriate K , the Vargha-Delaney's A-measurement test [130] is used which is a generalization of the CL method [146], originally developed to measure the difference between two populations in terms of the probability that a score sampled at random from one of the populations is greater than a score sampled at random from the other population. The A-measurement can be directly applied to any discrete or continuous variable that is at least ordinally scaled. It can be used to check for generalized stochastic equality, specifically called Pairwise Stochastic Equality which will serve as a basis for establishing statistical consistence for a particular K . The Pairwise Stochastic Equality states that any two populations (distributions) i and j are statistically equal when

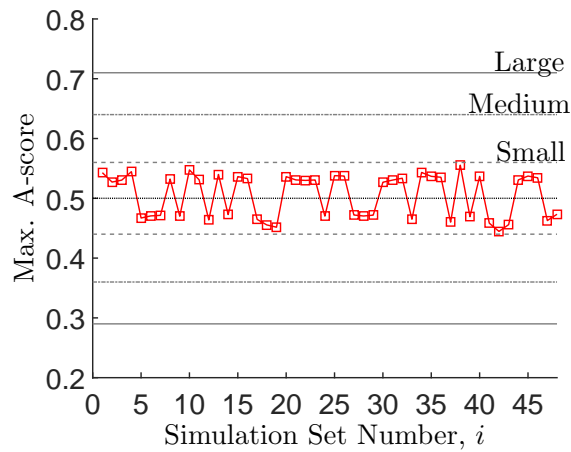
$$A_{ij} = 0.5, \quad \text{for all } (i, j) \text{ pairs} \quad (\text{A.7})$$

Similar to [147], let us compare the first distribution out of $Q = 48$ distributions with all the remaining 47 distributions and plot the response in Fig. A.2. The regions shown in the Fig. A.2 are according to the guidelines for interpreting A_{ij} in [130], where small effect within the range of 0.44 to 0.56 means that the two populations are nearly similar whereas scores above 0.71 or below 0.29 would mean significantly different distributions. It is clear from the figure that a larger K keeps the scores within the small-effect range and hence K is selected such that

$$\arg \max_{1 \leq j \leq 48} |A_{ij} - 0.5| \leq 0.06, \quad \forall i \in \{1, \dots, 48\}, i \neq j \quad (\text{A.8})$$



(a)



(b)

Figure A.2. (a) Vargha-Delaney's A-test for pair-wise stochastic equality of first simulation set with other 47 sets. (b) Maximum A-test for pair-wise stochastic equality for $K = 512$.

A_{ij} in (A.8) are effectively the A-scores that show maximum deviation from the ideal score of 0.5 for any i^{th} set with respect to all the other j sets. These scores are shown as the maximum A-scores in Fig. A.2 for each distribution set. For the optimization process in the thesis, let us choose $K = 1024$, twice the number of runs for which all the maximum A-scores are within the small-effect region.

Appendix B

Supplementary Figures

B.1 Optimization Data for Varying Initialization Distances

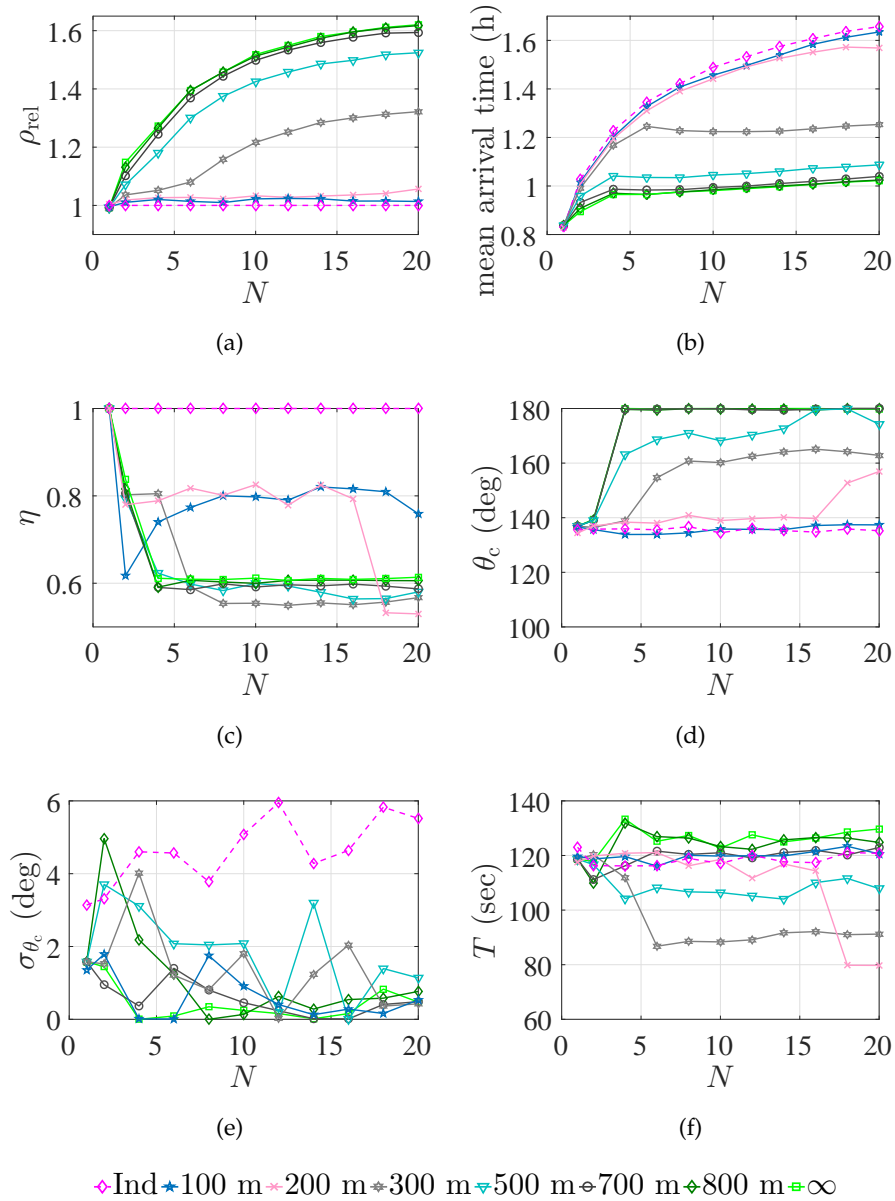


Figure B.1. Optimization results for initialization distance, r_0 of 1400 m and varying attraction neighbourhood radii, r_{GC} (see legend at the bottom): (a) Relative efficiency. (b) Arrival time performance as a function of team size N . (c) Source bias coefficient, η . (d) Correction angle, θ_c . (e) Angle variance, σ_{θ_c} . (f) Sampling time, T .

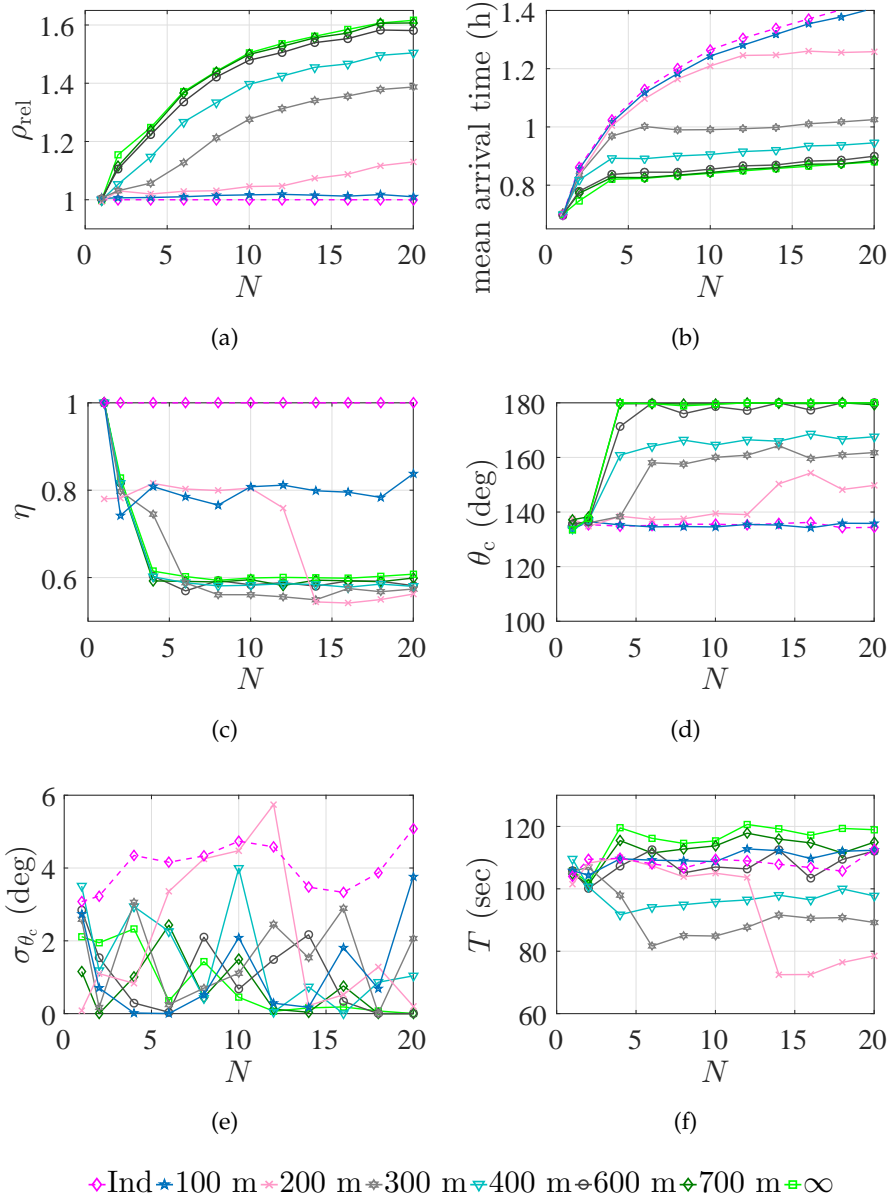


Figure B.2. Optimization results for initialization distance, r_0 of 1200 m and varying attraction neighbourhood radii, r_{GC} (see legend at the bottom): (a) Relative efficiency. (b) Arrival time performance as a function of team size N . (c) Source bias coefficient, η . (d) Correction angle, θ_c . (e) Angle variance, σ_{θ_c} . (f) Sampling time, T .

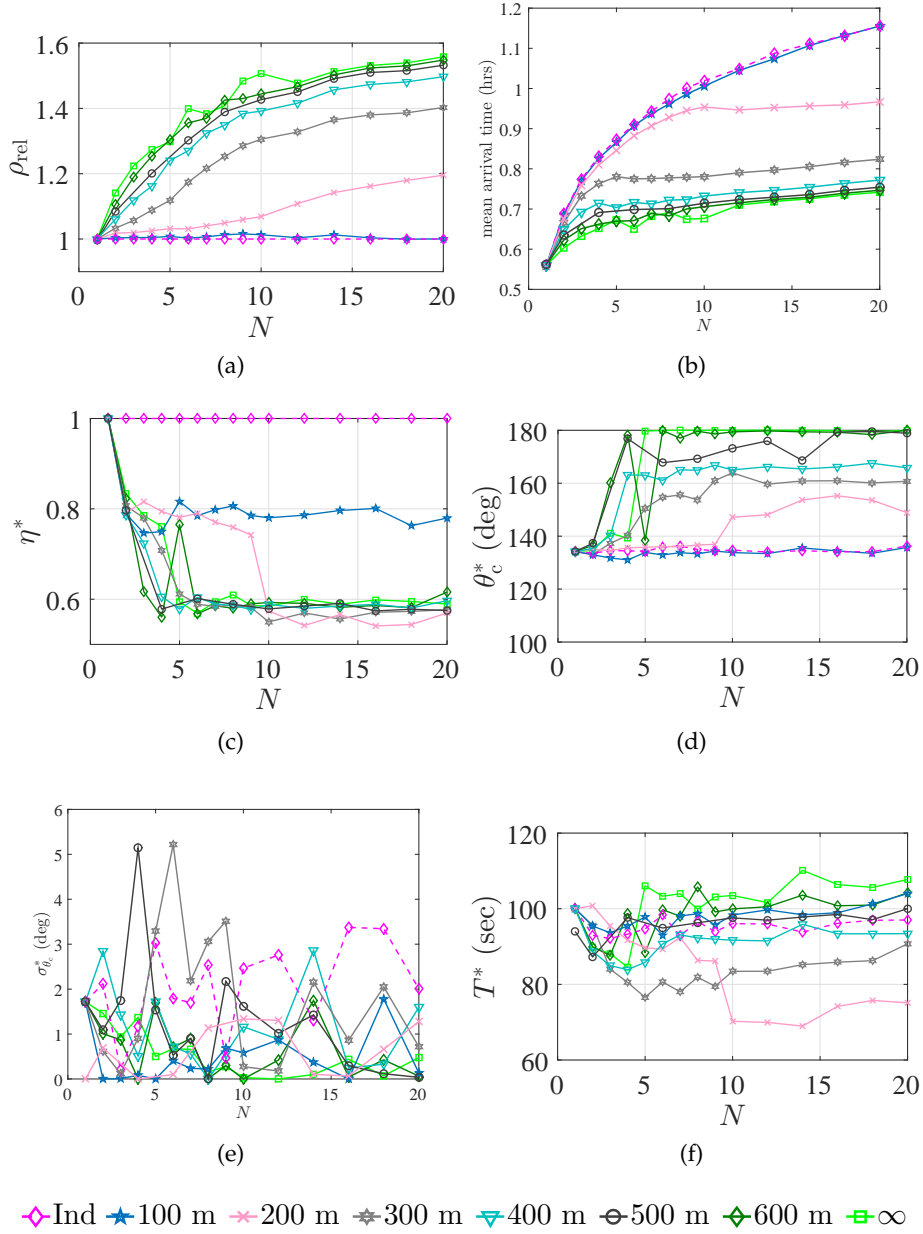


Figure B.3. Optimization results for initialization distance, r_0 of 1000m and varying attraction neighbourhood radii, r_{GC} (see legend at the bottom): (a) Relative efficiency. (b) Arrival time performance as a function of team size N . (c) Source bias coefficient, η . (d) Correction angle, θ_c . (e) Angle variance, σ_{θ_c} . (f) Sampling time, T .

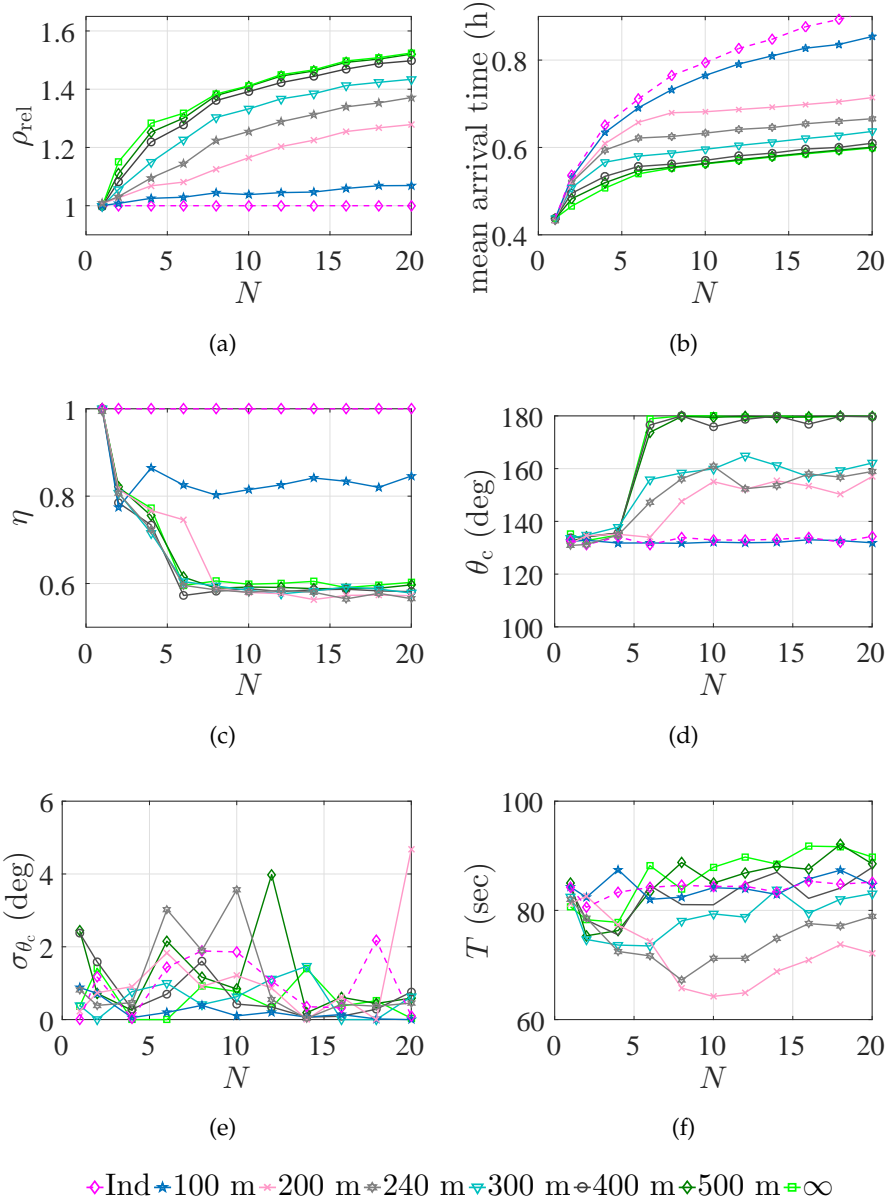


Figure B.4. Optimization results for initialization distance, r_0 of 800 m and varying attraction neighbourhood radii, r_{GC} (see legend at the bottom): (a) Relative efficiency. (b) Arrival time performance as a function of team size N . (c) Source bias coefficient, η . (d) Correction angle, θ_c . (e) Angle variance, σ_{θ_c} . (f) Sampling time, T .

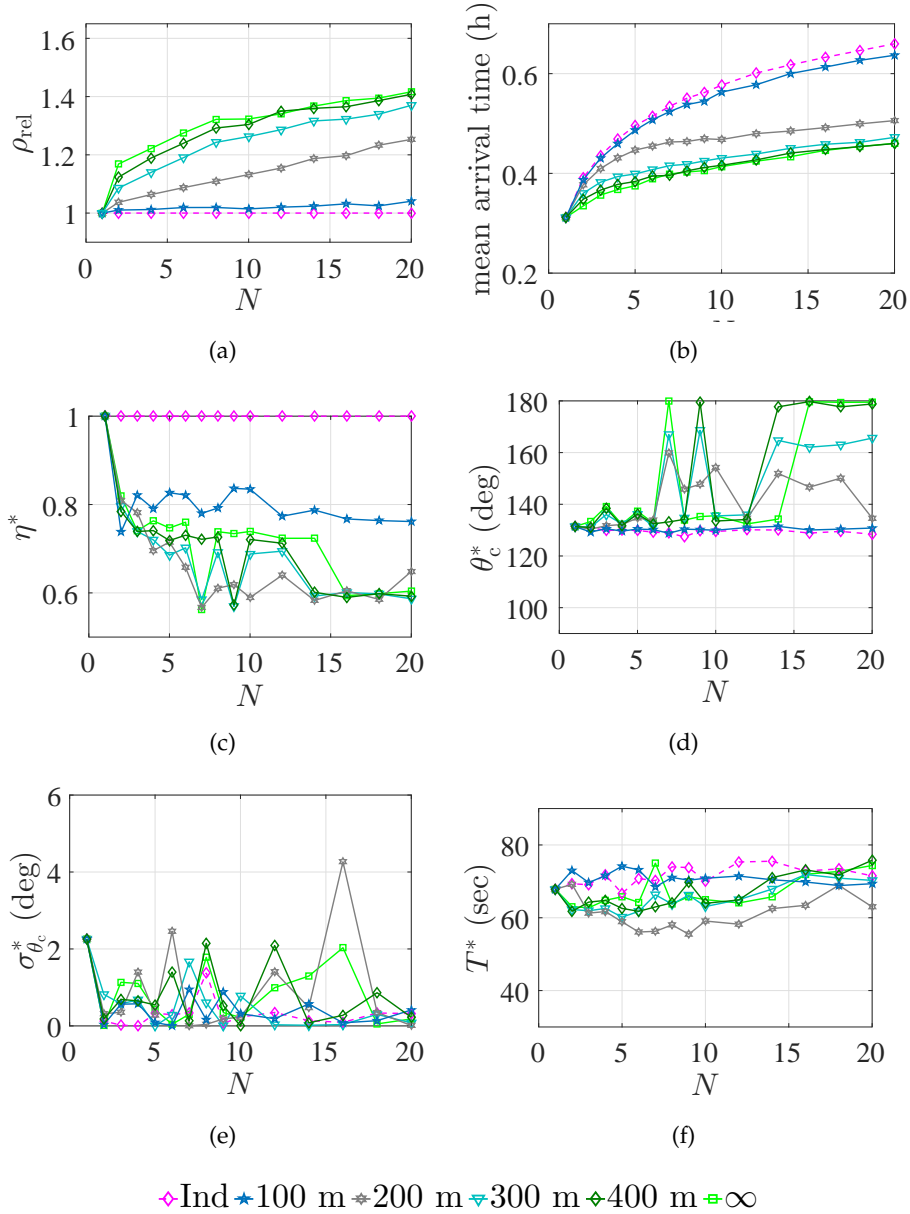


Figure B.5. Optimization results for initialization distance, r_0 of 600 m and varying attraction neighbourhood radii, r_{GC} (see legend at the bottom): (a) Relative efficiency. (b) Arrival time performance as a function of team size N . (c) Source bias coefficient, η . (d) Correction angle, θ_c . (e) Angle variance, σ_{θ_c} . (f) Sampling time, T .

Bibliography

- [1] C. Bernon, M.-P. Gleizes, S. Peyruqueou, and G. Picard, "Adelfe: A methodology for adaptive multi-agent systems engineering," in *Engineering Societies in the Agents World III*. Springer, 2003, pp. 156–169.
- [2] H. V. D. Parunak, "'go to the ant': Engineering principles from natural multi-agent systems," *Annals of Operations Research*, vol. 75, pp. 69–101, 1997.
- [3] S. D. McArthur, E. M. Davidson, V. M. Catterson, A. L. Dimeas, N. D. Hatziaargyriou, F. Ponci, and T. Funabashi, "Multi-agent systems for power engineering applications – part i: Concepts, approaches, and technical challenges," *Power Systems, IEEE Transactions on*, vol. 22, no. 4, pp. 1743–1752, 2007.
- [4] D. C. Parker, S. M. Manson, M. A. Janssen, M. J. Hoffmann, and P. Deadman, "Multi-agent systems for the simulation of land-use and land-cover change: a review," *Annals of the association of American Geographers*, vol. 93, no. 2, pp. 314–337, 2003.
- [5] W. Shen and D. H. Norrie, "Agent-based systems for intelligent manufacturing: a state-of-the-art survey," *Knowledge and information systems*, vol. 1, no. 2, pp. 129–156, 1999.
- [6] Y. Cao, W. Yu, W. Ren, and G. Chen, "An overview of recent progress in the study of distributed multi-agent coordination," *Industrial Informatics, IEEE Transactions on*, vol. 9, no. 1, pp. 427–438, 2013.
- [7] D. Perez, I. Maza, F. Caballero, D. Scarlatti, E. Casado, and A. Ollero, "A ground control station for a multi-uav surveillance system," *Journal of Intelligent & Robotic Systems*, vol. 69, no. 1-4, pp. 119–130, 2013.
- [8] T. Matsuda, T. Maki, T. Sakamaki, and T. Ura, "Performance analysis on a navigation method of multiple auvs for wide area survey," *Marine Technology Society Journal*, vol. 46, no. 2, pp. 45–55, 2012.
- [9] Z. Wang and D. Gu, "Cooperative target tracking control of multiple robots," *Industrial Electronics, IEEE Transactions on*, vol. 59, no. 8, pp. 3232–3240, 2012.
- [10] R. Prins and M. Kandemir, "Time-constrained optimization of multi-auv cooperative mine detection," in *OCEANS 2008*, sept. 2008, pp. 1–13.
- [11] E. Fiorelli, N. E. Leonard, P. Bhatta, D. A. Paley, R. Bachmayer, and D. M. Fratantoni, "Multi-auv control and adaptive sampling in monterey bay," *Oceanic Engineering, IEEE Journal of*, vol. 31, no. 4, pp. 935–948, oct. 2006.
- [12] NOAA. (2013, Aug.) Ocean. [Online]. Available: <http://www.noaa.gov/ocean.html>
- [13] D. Normile, "Lost at sea," *Science*, vol. 344, no. 6187, pp. 963–965, 2014.
- [14] A. M. Michalak, E. J. Anderson, D. Beletsky, S. Boland, N. S. Bosch, T. B. Bridgeman, J. D. Chaffin, K. Cho, R. Confesor, I. Daloglu *et al.*, "Record-setting algal bloom in lake erie caused by agricultural and meteorological trends consistent with expected future conditions," *Proceedings of the National Academy of Sciences*, vol. 110, no. 16, pp. 6448–6452, 2013.

- [15] R. Camilli, C. M. Reddy, D. R. Yoerger, B. A. Van Mooy, M. V. Jakuba, J. C. Kinsey, C. P. McIntyre, S. P. Sylva, and J. V. Maloney, "Tracking hydrocarbon plume transport and biodegradation at deepwater horizon," *Science*, vol. 330, no. 6001, pp. 201–204, 2010.
- [16] M. Brambilla, E. Ferrante, M. Birattari, and M. Dorigo, "Swarm robotics: a review from the swarm engineering perspective," *Swarm Intelligence*, vol. 7, no. 1, pp. 1–41, 2013.
- [17] P. Leitão, J. Barbosa, and D. Trentesaux, "Bio-inspired multi-agent systems for reconfigurable manufacturing systems," *Engineering Applications of Artificial Intelligence*, vol. 25, no. 5, pp. 934–944, 2012.
- [18] A. Halász, M. Hsieh, S. Berman, and V. Kumar, "Dynamic redistribution of a swarm of robots among multiple sites," in *Intelligent Robots and Systems, 2007. IROS 2007. IEEE/RSJ International Conference on*. IEEE, 2007, pp. 2320–2325.
- [19] T. Fong, I. Nourbakhsh, and K. Dautenhahn, "A survey of socially interactive robots," *Robotics and autonomous systems*, vol. 42, no. 3, pp. 143–166, 2003.
- [20] D. Sumpter, *Collective animal behavior*. Princeton University Press, 2010.
- [21] D. Grünbaum, S. Viscido, and J. Parrish, "Extracting interactive control algorithms from group dynamics of schooling fish," *Cooperative Control*, pp. 447–450, 2005.
- [22] E. Şahin, "Swarm robotics: From sources of inspiration to domains of application," in *Swarm robotics*. Springer, 2005, pp. 10–20.
- [23] E. Ferrante, A. E. Turgut, C. Huepe, A. Stranieri, C. Pinciroli, and M. Dorigo, "Self-organized flocking with a mobile robot swarm: a novel motion control method," *Adaptive Behavior*, p. 1059712312462248, 2012.
- [24] E. Ferrante, M. Brambilla, M. Birattari, and M. Dorigo, "Socially-mediated negotiation for obstacle avoidance in collective transport," in *Distributed Autonomous Robotic Systems*. Springer, 2013, pp. 571–583.
- [25] A. Gutiérrez, A. Campo, F. Monasterio-Huelin, L. Magdalena, and M. Dorigo, "Collective decision-making based on social odometry," *Neural Computing and Applications*, vol. 19, no. 6, pp. 807–823, 2010.
- [26] T. Balch and R. C. Arkin, "Communication in reactive multiagent robotic systems," *Autonomous Robots*, vol. 1, no. 1, pp. 27–52, 1994.
- [27] R. C. Arkin, "Cooperation without communication: Multiagent schema-based robot navigation," *Journal of Robotic Systems*, vol. 9, no. 3, pp. 351–364, 1992.
- [28] J.-H. Cui, J. Kong, M. Gerla, and S. Zhou, "The challenges of building mobile underwater wireless networks for aquatic applications," *Network, IEEE*, vol. 20, no. 3, pp. 12 – 18, may-june 2006.
- [29] M. Chitre, S. Shahabudeen, and M. Stojanovic, "Underwater acoustic communications and networking: Recent advances and future challenges," *Oceanic Engineering, IEEE Journal of*, pp. 103 –116, spring 2008.
- [30] M. Stojanovic and J. Preisig, "Underwater acoustic communication channels: Propagation models and statistical characterization," *Communications Magazine, IEEE*, vol. 47, no. 1, pp. 84 –89, january 2009.

- [31] M. Stojanovic, "Underwater wireless communications: Current achievements and research challenges," *IEEE Oceanic Engineering Society Newsletter*, 2006.
- [32] S. Redfield, "Cooperation between underwater vehicles," in *Marine Robot Autonomy*, M. L. Seto, Ed. Springer New York, 2013, pp. 257–286. [Online]. Available: http://dx.doi.org/10.1007/978-1-4614-5659-9_6
- [33] L. Steels, "Cooperation between distributed agents through self-organisation," in *Intelligent Robots and Systems '90. Towards a New Frontier of Applications', Proceedings. IROS '90. IEEE International Workshop on*, Jul 1990, pp. 8–14 suppl.
- [34] R. A. Brooks, P. Maes, M. J. Mataric, and G. More, "Lunar base construction robots," in *Intelligent Robots and Systems '90. Towards a New Frontier of Applications', Proceedings. IROS '90. IEEE International Workshop on*. IEEE, 1990, pp. 389–392.
- [35] M. J. Mataric, "Minimizing complexity in controlling a mobile robot population," in *Robotics and Automation, 1992. Proceedings., 1992 IEEE International Conference on*. IEEE, 1992, pp. 830–835.
- [36] R. C. Arkin, T. Balch, and E. Nitz, "Communication of behavioral state in multi-agent retrieval tasks," in *Robotics and Automation, 1993. Proceedings., 1993 IEEE International Conference on*. IEEE, 1993, pp. 588–594.
- [37] P.-P. Grassé, "La reconstruction du nid et les coordinations interindividuelles chez *bellicositermes natalensis* et *termites* sp. la théorie de la stigmergie: Essai d'interprétation du comportement des termites constructeurs," *Insectes sociaux*, vol. 6, no. 1, pp. 41–80, 1959.
- [38] Y. U. Cao, A. S. Fukunaga, and A. Kahng, "Cooperative mobile robotics: Antecedents and directions," *Autonomous robots*, vol. 4, no. 1, pp. 7–27, 1997.
- [39] R. Beckers, O. Holland, and J.-L. Deneubourg, "From local actions to global tasks: Stigmergy and collective robotics," in *Artificial life IV*, vol. 181, 1994, p. 189.
- [40] L. Panait and S. Luke, "A pheromone-based utility model for collaborative foraging," in *Proceedings of the Third International Joint Conference on Autonomous Agents and Multiagent Systems-Volume 1*. IEEE Computer Society, 2004, pp. 36–43.
- [41] K. Sugawara, T. Kazama, and T. Watanabe, "Foraging behavior of interacting robots with virtual pheromone," in *Intelligent Robots and Systems, 2004.(IROS 2004). Proceedings. 2004 IEEE/RSJ International Conference on*, vol. 3. IEEE, 2004, pp. 3074–3079.
- [42] V. Braitenberg, *Vehicles: Experiments in synthetic psychology*. MIT press, 1986.
- [43] F. W. Grasso, T. R. Consi, D. C. Mountain, and J. Atema, "Biomimetic robot lobster performs chemo-orientation in turbulence using a pair of spatially separated sensors: Progress and challenges," *Robotics and Autonomous Systems*, vol. 30, no. 1, pp. 115 – 131, 2000. [Online]. Available: <http://www.sciencedirect.com/science/article/pii/S0921889099000688>
- [44] H. Ishida, Y. Wada, and H. Matsukura, "Chemical sensing in robotic applications: A review," *Sensors Journal, IEEE*, vol. 12, no. 11, pp. 3163–3173, 2012.

- [45] R. M. Macnab and D. Koshland, "The gradient-sensing mechanism in bacterial chemotaxis," *Proceedings of the National Academy of Sciences*, vol. 69, no. 9, pp. 2509–2512, 1972.
- [46] T. Jin, "Gradient sensing during chemotaxis," *Current opinion in cell biology*, vol. 25, no. 5, pp. 532–537, 2013.
- [47] P. H. Dahl, J. H. Miller, D. H. Cato, and R. K. Andrew, "Underwater ambient noise," *Acoustics Today*, vol. 3, no. 1, pp. 23–33, 2007.
- [48] M. Rubenstein, C. Ahler, and R. Nagpal, "Kilobot: A low cost scalable robot system for collective behaviors," in *Robotics and Automation (ICRA), 2012 IEEE International Conference on*. IEEE, 2012, pp. 3293–3298.
- [49] C. Blum and R. Groß, "Swarm intelligence in optimization and robotics," *Springer Handbook of Computational Intelligence*, pp. 1291–1309, 2015.
- [50] G. Beni, "From swarm intelligence to swarm robotics," in *Swarm robotics*. Springer, 2005, pp. 1–9.
- [51] X. Cui, C. T. Hardin, R. K. Ragade, and A. S. Elmaghraby, "A swarm approach for emission sources localization," in *Tools with Artificial Intelligence, 2004. ICTAI 2004. 16th IEEE International Conference on*. IEEE, 2004, pp. 424–430.
- [52] G. Ferri, E. Caselli, V. Mattoli, A. Mondini, B. Mazzolai, and P. Dario, "Spiral: A novel biologically-inspired algorithm for gas/odor source localization in an indoor environment with no strong airflow," *Robotics and Autonomous Systems*, vol. 57, no. 4, pp. 393–402, 2009.
- [53] K. Krishnanand and D. Ghose, "A glowworm swarm optimization based multi-robot system for signal source localization," in *Design and control of intelligent robotic systems*. Springer, 2009, pp. 49–68.
- [54] M. Shaukat, M. Chitre, and S. H. Ong, "A bio-inspired distributed approach for searching underwater acoustic source using a team of auvs," in *OCEANS 2013, Bergen*, 2013.
- [55] J. Kennedy, "Zigzagging and casting as a programmed response to wind-borne odour: a review," *Physiological Entomology*, vol. 8, no. 2, pp. 109–120, 1983.
- [56] A. Berdahl, C. J. Torney, C. C. Ioannou, J. J. Faria, and I. D. Couzin, "Emergent sensing of complex environments by mobile animal groups," *Science*, vol. 339, no. 6119, pp. 574–576, 2013.
- [57] Y. Tian, W. Li, and A.-q. Zhang, "A lagrangian particle random walk model for simulating a deep-sea hydrothermal plume with both buoyant and non-buoyant features," *China Ocean Engineering*, vol. 27, no. 2, pp. 215–230, 2013. [Online]. Available: <http://dx.doi.org/10.1007/s13344-013-0019-7>
- [58] D. Sutantyó, S. Kernbach, P. Levi, and V. Nepomnyashchikh, "Multi-robot searching algorithm using lévy flight and artificial potential field," in *Safety Security and Rescue Robotics (SSRR), 2010 IEEE International Workshop on*, July 2010, pp. 1–6.
- [59] E. A. Codling, M. J. Plank, and S. Benhamou, "Random walk models in biology," *Journal of the Royal Society Interface*, vol. 5, no. 25, pp. 813–834, 2008.
- [60] F. Bartumeus, M. G. E. da Luz, G. Viswanathan, and J. Catalan, "Animal search strategies: a quantitative random-walk analysis," *Ecology*, vol. 86, no. 11, pp. 3078–3087, 2005.

- [61] J. A. Farrell, S. Pang, W. Li, and R. Arrieta, "Chemical plume tracing experimental results with a remus auv," in *OCEANS 2003. Proceedings*, vol. 2. IEEE, 2003, pp. 962–968.
- [62] W. Li, J. Farrell, S. Pang, and R. Arrieta, "Moth-inspired chemical plume tracing on an autonomous underwater vehicle," *Robotics, IEEE Transactions on*, vol. 22, no. 2, pp. 292–307, 2006.
- [63] C. David, J. Kennedy, and A. Ludlow, "Finding of a sex pheromone source by gypsy moths released in the field," 1983.
- [64] R. Kanzaki, N. Sugi, and T. Shibuya, "Self-generated zigzag turning of bombyx mori males during pheromone-mediated upwind walking (physiology)," *Zoological science*, vol. 9, no. 3, pp. 515–527, 1992.
- [65] N. J. Vickers, "Winging it: moth flight behavior and responses of olfactory neurons are shaped by pheromone plume dynamics," *Chemical senses*, vol. 31, no. 2, pp. 155–166, 2006.
- [66] D. Burkhardt, W. Schleidt, and H. Altner, "Signals in the animal world," 1967.
- [67] R. A. Russell, A. Bab-Hadiashar, R. L. Shepherd, and G. G. Wallace, "A comparison of reactive robot chemotaxis algorithms," *Robotics and Autonomous Systems*, vol. 45, no. 2, pp. 83–97, 2003.
- [68] V. Braitenberg, "Taxis, kinesis and decussation," *Progress in brain research*, vol. 17, pp. 210–222, 1965.
- [69] S. Kazadi, R. Goodman, D. Tsikata, D. Green, and H. Lin, "An autonomous water vapor plume tracking robot using passive resistive polymer sensors," *Autonomous robots*, vol. 9, no. 2, pp. 175–188, 2000.
- [70] A. Lilienthal and T. Duckett, "Experimental analysis of smelling braitenberg vehicles," *environment*, vol. 5, p. 10, 2003.
- [71] P. Maes, M. Mataric, J. Meyer, J. Pollack, and S. Wilson, *Some adaptive movements of animats with single symmetrical sensors*. MIT Press, 1996, pp. 55–64. [Online]. Available: <http://ieeexplore.ieee.org.libproxy1.nus.edu.sg/xpl/articleDetails.jsp?arnumber=6291865>
- [72] P. Maes, *From animals to animats 4: Proceedings of the fourth international conference on simulation of adaptive behavior*. MIT Press, 1996, vol. 4.
- [73] S. L. Porter, G. H. Wadhams, and J. P. Armitage, "Signal processing in complex chemotaxis pathways," *Nature Reviews Microbiology*, vol. 9, no. 3, pp. 153–165, 2011.
- [74] W. J. Bell and T. R. Tobin, "Chemo-orientation," *Biological Reviews*, vol. 57, no. 2, pp. 219–260, 1982.
- [75] M. Shaukat and M. Chitre, "Bio-inspired practicalities: Collective behaviour using passive neighbourhood sensing," in *Autonomous Agents & Multi-Agent Systems (AAMAS)*, 2015.
- [76] —, "Adaptive sampling and collective behaviour in a small team of auvs for a source localization problem," in *MTS/IEEE OCEANS*, 2015a.
- [77] H. C. Berg, D. A. Brown *et al.*, "Chemotaxis in escherichia coli analysed by three-dimensional tracking," *Nature*, vol. 239, no. 5374, pp. 500–504, 1972.

- [78] D. Sutanty, P. Levi, C. Moslinger, and M. Read, "Collective-adaptive lévy flight for underwater multi-robot exploration," in *Mechatronics and Automation (ICMA), 2013 IEEE International Conference on*. IEEE, 2013, pp. 456–462.
- [79] T. U. of Graz, "Cocoro: Collective cognitive robotics," <http://cocoro.uni-graz.at/drupal/>, 2014, [Online; accessed 29-Jun-2014].
- [80] Y. Katz, K. Tunstrøm, C. Ioannou, C. Huepe, and I. Couzin, "Inferring the structure and dynamics of interactions in schooling fish," *Proceedings of the National Academy of Sciences*, vol. 108, no. 46, pp. 18 720–18 725, 2011.
- [81] P. Ogren, E. Fiorelli, and N. Leonard, "Cooperative control of mobile sensor networks:adaptive gradient climbing in a distributed environment," *Automatic Control, IEEE Transactions on*, vol. 49, no. 8, pp. 1292–1302, Aug 2004.
- [82] R. Bachmayer and N. E. Leonard, "Vehicle networks for gradient descent in a sampled environment," in *Decision and Control, 2002, Proceedings of the 41st IEEE Conference on*, vol. 1. IEEE, 2002, pp. 112–117.
- [83] F. Li, Q.-H. Meng, S. Bai, J.-G. Li, and D. Popescu, "Probability-pso algorithm for multi-robot based odor source localization in ventilated indoor environments," *Intelligent Robotics and Applications*, pp. 1206–1215, 2008.
- [84] A. Marjovi, J. Nunes, P. Sousa, R. Faria, and L. Marques, "An olfactory-based robot swarm navigation method," in *Robotics and Automation (ICRA), 2010 IEEE International Conference on*. IEEE, 2010, pp. 4958–4963.
- [85] R. Devez, D. Thiel, A. Russell, and A. Mackay-Sim, "Odor sensing for robot guidance," *The International Journal of Robotics Research*, vol. 13, no. 3, pp. 232–239, 1994.
- [86] R. A. Russell, *Odour detection by mobile robots*. World Scientific, 1999, vol. 22.
- [87] Y. Kuniyoshi, N. Kita, S. Rougeaux, S. Sakane, M. Ishii, and M. Kakikua, "Cooperation by observation: the framework and basic task patterns," in *Robotics and Automation, 1994. Proceedings., 1994 IEEE International Conference on*. IEEE, 1994, pp. 767–774.
- [88] R. Lukeman, Y. Li, and L. Edelstein-Keshet, "Inferring individual rules from collective behavior," *Proceedings of the National Academy of Sciences*, vol. 107, no. 28, pp. 12 576–12 580, 2010.
- [89] C. K. Hemelrijk and H. Hildenbrandt, "Schools of fish and flocks of birds: their shape and internal structure by self-organization," *Interface Focus*, p. rsfs20120025, 2012.
- [90] I. D. Couzin, J. Krause, R. James, G. D. Ruxton, and N. R. Franks, "Collective memory and spatial sorting in animal groups," *Journal of theoretical biology*, vol. 218, no. 1, pp. 1–11, 2002.
- [91] I. Aoki, "A simulation study on the schooling mechanism in fish," *Bull. Japan. Soc. Sci. Fish.*, vol. 48, 1982.
- [92] A. Huth and C. Wissel, "The simulation of the movement of fish schools," *Journal of theoretical biology*, vol. 156, no. 3, pp. 365–385, 1992.
- [93] C. W. Reynolds, "Flocks, herds and schools: A distributed behavioral model," *ACM SIGGRAPH Computer Graphics*, vol. 21, no. 4, pp. 25–34, 1987.

- [94] C. K. Hemelrijk and H. Hildenbrandt, "Self-organized shape and frontal density of fish schools," *Ethology*, vol. 114, no. 3, pp. 245–254, 2008.
- [95] M. Ballerini, N. Cabibbo, R. Candelier, A. Cavagna, E. Cisbani, I. Giardina, V. Lecomte, A. Orlandi, G. Parisi, A. Procaccini *et al.*, "Interaction ruling animal collective behavior depends on topological rather than metric distance: Evidence from a field study," *Proceedings of the National Academy of Sciences*, vol. 105, no. 4, pp. 1232–1237, 2008.
- [96] A. Flack, Z. Ákos, M. Nagy, T. Vicsek, and D. Biro, "Robustness of flight leadership relations in pigeons," *Animal Behaviour*, vol. 86, no. 4, pp. 723–732, 2013.
- [97] N. W. Bode, D. W. Franks, and A. J. Wood, "Limited interactions in flocks: relating model simulations to empirical data," *Journal of The Royal Society Interface*, vol. 8, no. 55, pp. 301–304, 2011.
- [98] J. G. Balchen, "Mathematical modelling of fish behaviour. principles and applications," *Proc. IFAC 6th World Congr., Boston/Cambridge*, 1975.
- [99] S. Focardi and S. Toso, "Foraging and social behaviour of ungulates: proposals for a mathematical model," in *Cognitive processes and spatial orientation in animal and man*. Springer, 1987, pp. 295–304.
- [100] W. D. Hamilton, "Geometry for the selfish herd," *Journal of theoretical Biology*, vol. 31, no. 2, pp. 295–311, 1971.
- [101] J. K. Parrish, "Re-examining the selfish herd: are central fish safer?" *Animal Behaviour*, vol. 38, no. 6, pp. 1048–1053, 1989.
- [102] J. Potter and M. Chitre, "Do fish fry use emergent behaviour in schools to find coral reefs by sound," in *AGU Ocean Sciences Meeting, Honolulu, Hawaii*, 2006.
- [103] A. Okubo, "Dynamical aspects of animal grouping: swarms, schools, flocks, and herds," *Advances in biophysics*, vol. 22, pp. 1–94, 1986.
- [104] J. C. Kinsey, R. M. Eustice, and L. L. Whitcomb, "A survey of underwater vehicle navigation: Recent advances and new challenges," in *IFAC Conference of Manoeuvring and Control of Marine Craft*, 2006.
- [105] J. W. Bales and C. Chrissostomidis, "High-bandwidth, low-power, short-range optical communication underwater," in *International Symposium on Unmanned Untethered Submersible Technology*. UNIVERSITY OF NEW HAMPSHIRE-MARINE SYSTEMS, 1995, pp. 406–415.
- [106] J. Joe and S. Toh, "Digital underwater communication using electric current method," in *OCEANS 2007-Europe*. IEEE, 2007, pp. 1–4.
- [107] T. Pitcher, A. Magurran, and I. Winfield, "Fish in larger shoals find food faster," *Behavioral Ecology and Sociobiology*, vol. 10, no. 2, pp. 149–151, 1982.
- [108] A. B. Kao and I. D. Couzin, "Decision accuracy in complex environments is often maximized by small group sizes," *Proceedings of the Royal Society B: Biological Sciences*, vol. 281, no. 1784, p. 20133305, 2014.
- [109] O. A. Misund, "Dynamics of moving masses: variability in packing density, shape, and size among herring, sprat, and saithe schools," *ICES Journal of Marine Science: Journal du Conseil*, vol. 50, no. 2, pp. 145–160, 1993.

- [110] N. C. Makris, P. Ratilal, D. T. Symonds, S. Jagannathan, S. Lee, and R. W. Nero, "Fish population and behavior revealed by instantaneous continental shelf-scale imaging," *Science*, vol. 311, no. 5761, pp. 660–663, 2006.
- [111] I. Aoki, "Internal dynamics of fish schools in relation to inter-fish distance," *Bulletin of the Japanese Society of Scientific Fisheries*, 1984.
- [112] A. Huth and C. Wissel, "The movement of fish schools: a simulation model," in *Biological Motion*. Springer, 1990, pp. 577–595.
- [113] —, "The simulation of fish schools in comparison with experimental data," *Ecological modelling*, vol. 75, pp. 135–146, 1994.
- [114] T. Vicsek, A. Czirók, E. Ben-Jacob, I. Cohen, and O. Shochet, "Novel type of phase transition in a system of self-driven particles," *Physical review letters*, vol. 75, no. 6, p. 1226, 1995.
- [115] A. Czirók, M. Vicsek, and T. Vicsek, "Collective motion of organisms in three dimensions," *Physica A: Statistical Mechanics and its Applications*, vol. 264, no. 1, pp. 299–304, 1999.
- [116] J. Buhl, D. Sumpter, I. Couzin, J. Hale, E. Despland, E. Miller, and S. Simpson, "From disorder to order in marching locusts," *Science*, vol. 312, no. 5778, pp. 1402–1406, 2006.
- [117] C. Becco, N. Vandewalle, J. Delcourt, and P. Poncin, "Experimental evidences of a structural and dynamical transition in fish school," *Physica A: Statistical Mechanics and its Applications*, vol. 367, pp. 487–493, 2006.
- [118] M. Shaukat and M. Chitre, "On social behaviours and sampling times in multi-agent source localization," in *The First International Symposium on Swarm Behavior and Bio-inspired Robotics (SWARM 2015)*, 2015.
- [119] A. E. Turgut, H. Çelikkanat, F. Gökçe, and E. Şahin, "Self-organized flocking in mobile robot swarms," *Swarm Intelligence*, vol. 2, no. 2-4, pp. 97–120, 2008.
- [120] R. J. Urick, "Ambient noise in the sea," DTIC Document, Tech. Rep., 1984.
- [121] M. Calderon, "Probability density analysis of ocean ambient and ship noise." DTIC Document, Tech. Rep., 1964.
- [122] G. Griffiths, P. Enoch, and N. W. Millard, "On the radiated noise of the autosub autonomous underwater vehicle," *ICES Journal of Marine Science: Journal du Conseil*, vol. 58, no. 6, pp. 1195–1200, 2001.
- [123] M. Cai, I. M. Sou, C. Layman, B. Bingham, and J. Allen, "Characterization of the acoustic signature of a small remotely operated vehicle for detection," in *OCEANS 2010*. IEEE, 2010, pp. 1–7.
- [124] R. P. DK-180, "Dk-180 airframe locator beacon," <http://www.radiantpowercorp.com/product-families/instruments-sensors/dukane-seacom-locator-beacons/dk-180-airframe-locator-beacon/>, [Online; accessed 19-Jun-2014].
- [125] W. H. Thorp, "Analytic description of the low-frequency attenuation coefficient," *The Journal of the Acoustical Society of America*, vol. 42, no. 1, pp. 270–270, 1967.
- [126] M. Stojanovic, "Acoustic (underwater) communications," *Encyclopedia of Telecommunications*, 2003.

- [127] K.-F. Man, K. S. TANG, and S. Kwong, *Genetic Algorithms: Concepts and Designs, Avec disquette*. Springer, 1999, vol. 1.
- [128] NVIDIA, "What is cuda?" http://www.nvidia.com/object/cuda_home_new.html, [Online; accessed 05-Jul-2014].
- [129] —, "Geforce gtx 680," <http://www.geforce.com/hardware/desktop-gpus/geforce-gtx-680>, [Online; accessed 05-Jul-2014].
- [130] A. Vargha and H. D. Delaney, "A critique and improvement of the cl common language effect size statistics of mcgraw and wong," *Journal of Educational and Behavioral Statistics*, vol. 25, no. 2, pp. 101–132, 2000.
- [131] J. Bird and P. Layzell, "The evolved radio and its implications for modelling the evolution of novel sensors," in *Evolutionary Computation, 2002. CEC'02. Proceedings of the 2002 Congress on*, vol. 2. IEEE, 2002, pp. 1836–1841.
- [132] D. B. West *et al.*, *Introduction to graph theory*. Prentice hall Upper Saddle River, 2001, vol. 2.
- [133] H. Hamann, "Towards swarm calculus: universal properties of swarm performance and collective decisions," in *Swarm intelligence*. Springer, 2012, pp. 168–179.
- [134] L. Kuenen and R. T. Carde, "Strategies for recontacting a lost pheromone plume: Casting and upwind flight in the male gypsy moth," *Physiological Entomology*, vol. 19, no. 1, pp. 15–29, 1994.
- [135] S. T. Kazadi, "Swarm engineering," Ph.D. dissertation, California Institute of Technology, 2000.
- [136] J. Board, "Robot swans bring new advanced technology to water testing," Jul. 2015, [Online; accessed 13-Sep-2015]. [Online]. Available: <http://www.channelnewsasia.com/news/singapore/robot-swans-bring-new/1958380.html>
- [137] H. Çelikkanat and E. Şahin, "Steering self-organized robot flocks through externally guided individuals," *Neural Computing and Applications*, vol. 19, no. 6, pp. 849–865, 2010.
- [138] R. J. Urick, "Sound propagation in the sea," DTIC Document, Tech. Rep., 1979.
- [139] L. M. Rios and N. V. Sahinidis, "Derivative-free optimization: A review of algorithms and comparison of software implementations," *Journal of Global Optimization*, vol. 56, no. 3, pp. 1247–1293, 2013.
- [140] D. Whitley, S. Rana, J. Dzubera, and K. E. Mathias, "Evaluating evolutionary algorithms," *Artificial intelligence*, vol. 85, no. 1, pp. 245–276, 1996.
- [141] K. Deb, "Multi-objective optimization," in *Search methodologies*. Springer, 2014, pp. 403–449.
- [142] D. E. Goldberg and K. Deb, "A comparative analysis of selection schemes used in genetic algorithms," *Urbana*, vol. 51, pp. 61 801–2996, 1991.
- [143] D. Schlierkamp-Voosen and H. Mühlenbein, "Predictive models for the breeder genetic algorithm," *Evolutionary Computation*, vol. 1, no. 1, pp. 25–49, 1993.
- [144] T. Bäck and F. Hoffmeister, "Extended selection mechanisms in genetic algorithms," 1991.

- [145] D. Thierens, "Selection schemes, elitist recombination, and selection intensity," in *ICGA*, 1997, pp. 152–159.
- [146] K. O. McGraw and S. Wong, "A common language effect size statistic." *Psychological bulletin*, vol. 111, no. 2, p. 361, 1992.
- [147] K. Alden, M. Read, J. Timmis, P. S. Andrews, H. Veiga-Fernandes, and M. Coles, "Spartan: A comprehensive tool for understanding uncertainty in simulations of biological systems," *PLoS computational biology*, vol. 9, no. 2, p. e1002916, 2013.